THERMODYNAMIC ASSESSMENT OF THE ENTROPY ACCUMULATION AND EXERGY DESTRUCTION IN MUSCLE AND NEURON CELLS

by
Bahar Hazal Yalçınkaya

Submitted to Graduate School of Natural and Applied Sciences
in Partial Fulfillment of the Requirements
for the Degree of Doctor of Philosophy in
Biotechnology

Yeditepe University
2019

THERMODYNAMIC ASSESSMENT OF THE ENTROPY ACCUMULATION AND EXERGY DESTRUCTION IN MUSCLE AND NEURON CELLS

APPROVED BY:

Prof. Dr. Mustafa Özilgen ..... 
(Thesis Supervisor)
(Yeditepe University)

Prof. Dr. Zeynep Petek Çakar .....
(Istanbul Technical University)

Assoc. Prof. Dr. Ali Bahadır Olcay .....
(Yeditepe University)

Assoc. Prof. Dr. Ali Özhan Aytekin .....
(Yeditepe University)

Assist. Prof. Dr. Canan Acar .....
(Bahçeşehir University)

DATE OF APPROVAL: ..../..../2019

To my beloved family…

ACKNOWLEDGMENTS

First of all, I would like to express my sincere gratitude to my supervisor Prof. Mustafa Özilgen who shares his endless patience, motivation and immense knowledge with me. His guidance has helped me through the Ph.D. period.

Beside my advisor, I would like to thank Assoc. Prof. Dr. Esra Sorgüven for her insightful comments and encouragement which led me to expand my research from various perspectives in the first years of my Ph.D.

My sincere thanks also go to Assoc. Prof. Dr. Ali Bahadır Olcay, Prof. Bayram Yılmaz who never spare their immense knowledge from me.

I wish to thank the members of my dissertation committee: Prof. Dr. Zeynep Petek Çakar, Assoc. Prof. Dr. Ali Özhan Aytekin and Assist. Prof. Dr. Canan Acar offering their time, support, guidance, and goodwill throughout the preparation and review of this thesis. I thank my dear colleagues who are always good friends on this journey Gizem Özan, Çağla Uysal, Neslihan Kayra, Begüm Okutan, Jale Çatak, and Duygu Kıbıcı.

I would especially like to thank Ph.D. Alain Destexhe, Ph.D. Jennifer Sarah Goldman and Ph.D. Student Trang-Anh Nghiem who provided me an opportunity to join their team as an intern, and who share me their knowledge.

I am profoundly grateful to Yeditepe University Food Engineering department.

Last but not least, I am grateful to my beloved family, Yılmaz Yalçınkaya, F. Günseli Yalçınkaya and Nehir Naz Genç for supporting to me and their continuous support every step I took. Words are not enough to thank them.

ABSTRACT

THERMODYNAMIC ASSESSMENT OF THE ENTROPY ACCUMULATION AND EXERGY DESTRUCTION IN MUSCLE AND NEURON CELLS

All living species can be treated as open systems that are in continuous exchange matter and energy to its subsystems and surroundings. The transduction of energy always obeys the laws of physics. Thermodynamic laws are great tools to demonstrate the significance of the feasibility of transduction of energy. The energy exchange for work done by biological systems is highly efficient. The energy production path starts with glycolysis in the cytoplasm of the cell while bulk production of energy is produced in mitochondria that are the "powerhouse" of the cells, where more than 90 percent of the cellular energy is produced. Functions of the body, like muscle work performance and signal transmission along the nervous system, are achieved by utilizing the energy generated in the mitochondria. The entropy and exergy thermodynamic terms provide an opportunity to interpret the efficiencies of biological systems and give the ability to compare calculated efficiencies with theoretical values. The thesis represents a comprehensive thermodynamic investigation on squid mantle muscles during different swimming behavior, the global warming effect of squid giant axon action potential cost and, pig cardiac muscles during basal metabolism and active state of the body. Thermodynamic analysis showed that during slow swimming, 3.82 J/(kg s) of chemical exergy was consumed, and a total muscle work of 0.28 J/(kg s) was produced while the jet escape consumes an exergy of 9.97 J/(kg s) and produces a muscle work of 0.16 J/(kg s). Thermodynamic analyses to determine the effects of the global warming on information transmittance in the giant squid neuron via Hodgkin and Huxley model showed that as temperature increases from 6.3 to 18.5 ^{o}C entropy generation was estimated to decrease by half, implying that living becomes easier for the squid as temperature increases. Thermodynamic analysis shows that a pig's heart consumed 0.63 J/kg s of exergy at rest and produced 0.033 J/kg s of muscle contraction work. In the active state, the heart consumed 1.31 J/kg s of exergy and produces 0.065 J/kg s of muscle work. The calculations of conversion of consumed chemical exergy into energy-rich compounds revealed that the active state of cardiac muscle is exergetically more efficient than that of the basal resting state.

ÖZET

KAS VE SİNİR HÜCRELERİNDE ENTROPİ KAZANIMI VE EKSERJİ YIKIMININ TERMODİNAMİKSEL DEĞERLENDİRMESİ

Tüm canlı türleri, alt sistemlerine ve çevresine sürekli alışveriş yapan ve enerji veren açık sistemler olarak ele alınabilir. Enerjinin dönüştürülmesi her zaman fizik yasalarına uyar. Termodinamik yasalar, enerjinin iletilmesinin fizibilitesinin önemini göstermek için harika araçlardır. Biyolojik sistemler tarafından yapılan işlerde enerji alışverişi oldukça verimlidir. Enerji üretim yolu, hücre sitoplazmasında glikolizle başlarken, enerji üretiminin yüzde 90'dan fazla olduğu hücrelerin "elektrik santrali" olan mitokondride toplu enerji üretimi yapılır. Vücudun fonksiyonları, kas çalışma performansı ve sinir sistemi boyunca sinyal iletimi gibi mitokondride üretilen enerji kullanılarak elde edilir. Entropi ve ekserji termodinamik terimleri, biyolojik sistemlerin verimlerini yorumlama ve hesaplanan verimleri teorik değerlerle karşılaştırma becerisi sunar. Bu tez, farklı yüzme davranışları sırasında kalamar manto kasları, kalamar devi akson aksiyon potansiyel maliyetinin küresel ısınma etkisi ve bazal metabolizma ve vücudun aktif durumu sırasında domuz kardiyak kasları üzerine kapsamlı bir termodinamik incelemeyi temsil etmektedir. Termodinamik analiz, yavaş yüzme sırasında 3.82 J / (kg s) kimyasal ekserji tüketildiğini ve 0.28 J / (kg s) kas çalışması ürettiğini göstermektedir. Jet kaçışının 9.97 J / (kg s) bir ekserji tüketirken, 0.16 J / (kg s) 'lik bir kas çalışması üretir. Küresel ısınmanın dev kalamar nöronunda bilgi aktarımı üzerindeki etkilerini belirlemek için yapılan termodinamik analizler, sıcaklığın 6.3 ila 18.5ºC entropi üretiminin yarı yarıya azaldığını göstermiştir. Bu sonuç sıcaklık arttıkça kalamar için yaşamın kolaylaştığını ima edebilir. Termodinamik analiz, bir domuzun kalbinin istirahatta 0,63 J / kg s ekserji tükettiğini ve 0,033 J / kg s kas kasılma çalışması ürettiğini göstermektedir. Aktif durumda, kalp 1.31 J / kg s ekserji tüketir ve 0.065 J / kg s kas çalışması üretir. Tüketilen kimyasal ekserji enerjisini zengin bileşiklere dönüştürmenin hesaplamaları, kalp kası aktif durumunun ekserjik olarak bazal dinlenme durumundan daha etkin olduğunu ortaya koymaktadır.

TABLE OF CONTENTS

LIST OF FIGURES

LIST OF TABLES

LIST OF SYMBOLS/ABBREVIATIONS

η	Efficiency
ϕ	Temperature Coefficient
λ	Characteristic length of dendrites
ADP	Adonesine di phosphate
AKG	α-ketoglutarate
ASP	Aspartate
ATP	Adonesine tri phosphate
BBB	Blood brain barrier
B	Empirical constant in the extended Debye-Hückel equation
CIT	Citrate
CMP	Centrally-located mitochondria-poor fibers
ETC	Electron transport chain
CNS	Central nervous system
CO_2	Carbon dioxide
COASH	Coenzyme A
COQ	Coenzyme Q
E	Energy
E_{subs}	Potential
Ex	Exergy
F	Force
$FADH_2$	Flavin adenine dinucleotide
FUM	Fumarate
G6P	Glucose-6-phosphate
GDP	Guanosine-5'-diphosphate
GLC	Glucose
GLU	Glutamate
GTP	Guanosine-5'-diphosphate
H	Enthalpy
c	Concentration

P	Pressure
H_2O	Water
I	Ionic strength
ICIT	Isocitrate
I_{subs}	Current
k_b	Boltzmann constant
L	Length
m	Mass
J	Flux
MAL	Malate
NAD	Nicotinamide adenine dinucleotide
NADPH	Nicotinamide adenine dinucleotide phosphate
G	Gibbs free energy
O_2	Oxygen
OAA	Oxaloacetate
Pi	Phosphate
PYR	Pyruvate
Q	Heat
QH_2	Ubiquinol
S	Entropy
Ex	Exergy
SCOA	Extracellular matrix
ACCOA	Acetyl-CoA
SMR	Superficial mitochondria-rich
SUC	Succinate
SV	Stroke volume
T	Temperature
t	Time
TCA	Tricarboxylic cycle
W	Work
X_{dest}	Exergy destroyed
z	Valence
R	Resistance

1. INTRODUCTION

Matter and energy transfer are used to develop devices in many centuries that we encounter our daily life e.g. power plants, automobiles, hydroelectric power systems, steam engines, and refrigeration systems, etc. Like devices, biological systems also are in continuous exchange of matter and energy. The human body is a familiar example of a biological phenomenon where chemical energy coming from nutrients transformed into different forms of energy as useful power output and heat. Biological systems are an organizational and thermodynamic system which always tends towards to reach a maximum conversion of available energy. Even in a steady state, cells produce or consumes metabolites via biochemical reactions and exchange produced energy and matter through their cell membranes. To investigate this conversion energy and matter in biological network helping scientist to understand the feasibility of biological systems.

In the U.S., 635.260 people died in 2016 due to heart diseases [1]. One of the major causes of this is the decline of muscle efficiency [2–4]. People lose approximately 20 to 30 percent of their muscles between the ages of 20 and 80 [5,6]; the age-related loss of muscles is related with the mitochondrial functioning and the cellular energetics [6] and accompanied with the loss of the efficiency. The decrease in muscle efficiency is also among the causes of fatigue. Estimating the theoretical maximum muscle efficiency may help us to assess a patient's actual muscle performance, the degree of muscle loss and how close they are to experience a heart problem if the in vivo muscle efficiency can be determined via appropriate measurements.

Greenhouse gases (GHG), such as carbon dioxide, water vapor, ozone, methane, and nitrous oxide, increase in the atmosphere via anthropogenic activities [7]. They absorb heat radiated from the lower levels of the atmosphere and the surface of the Earth and then reradiate the majority of it back to the surface [8]. As concentrations of the heat-trapping greenhouse gases increase in the atmosphere, they act like a thick blanket, increase the surface temperature of the Earth. Climate change alters the cloud cover and precipitation particularly over the land causes melting of ice caps and glaciers, reduces the snow cover, increases ocean temperatures, carbon dioxide absorption and acidity [9]. Global warming disturbs the balance in the ecosystem [10]. In some cases, increased CO_2 or warmer weather accelerates the growth of some species, while slowing down the others. Pests, weeds, parasites, squids,

and octopuses are among the species which thrive upon global warming. Extreme weather conditions can be destructive to farmland, crops, and livestock; and the rising sea levels can erode and salinize the croplands. NASA [11] estimates that the global surface temperature of the earth has increased by 1^{o}C between 1880 and 2016 because of global warming.

Thermodynamic analyses of energy management in a living cell has already been subject of detailed publications [12–15]. In the last decade, numerous studies are published on exergy analysis in the biological systems including assessment of the efficiency in metabolism driven processes [16–24], thermal comfort [25], physical exercise [26] and non-equilibrium thermodynamic analysis as applied to cellular systems [12,14,27].

In this study, comprehensive thermodynamic investigation discussed on squid mantle muscles during different swimming behavior, the global warming effect of squid giant axon action potential energetic cost and, pig cardiac muscles during basal metabolism and active state of the body.

2. LITERATURE REVIEW

2.1. THERMODYNAMIC ASPECT OF LIVING ORGANISMS

Development technology and science rely on the ability to understand energy and harness this energy and usage of this energy or society needs. The laws of thermodynamics have a crucial role in the analysis of systems and devices where energy transfer and transformation occur. Since the 19th century, thermodynamics has an impact on numerous fields of science including, biology, physics, chemistry, geology, and especially on process engineering disciplines like chemical engineering. Later, scientists start to focus on thermodynamics in biochemical engineering to increase the knowledge in biothermodynamics where thermodynamic analysis contributes to test the feasibility of a system in terms of energy or exergy efficiency. In real thermodynamic which is a collection of laws that describe whether the process is spontaneous or not. In nature, the conversion of energy to heat is highly efficient while another way around is not. For this purpose, to maximize heat work transfer always be the primary goal.

Thermodynamic assessment in biological systems generally used to reveal the process or reaction is beneficial for the system. The Schrödinger established the first attempt of negentropy to offer an idea about negative entropy or negentropy to reveal physiological processes lead to an increase of internal ‘order’ in living organism [28]. Another related development was the dissipative structure theory by Ilya Prigogine [29] which states that the open systems exporting entropy while importing energy continuously from the environment. The living cells considered as open systems in stationary by Ilya Prigogine. This concept of the dissipative theory provides a useful tool for the chemical, biological and mechanical engineering areas [27]. The accumulation of positive entropy eventually reaches a minimum state which is the state that the system can no longer maintain its order and organization when adaptation is concluded to the environment. The theory of dissipative structure theory starts a true understanding of the entropy of aging [30,31]. Living organisms have to maintain their high organization state [28] while entropy accumulation implies the increasing disorder [32,33].

In the lifespan of the organisms the metabolic heat and free radical formations etc. lead to a structural change of biological molecules and entropy generation. The entropy generation eventually leads to inactive state or malfunction with changing energy states of biomolecules [34,35]. Normally, genetically induced repair and replacement processes involved to reduce the change of entropy states of biomolecules but with aging, these processes cannot function properly [34]. The organisms have limitation to entropy generation when the entropy generation exceed this limit the organisms die. In most energy conversion of systems, fraction energy is lost due to the irreversibility of systems. The lost energy released as heat to the environment [36]. The non-isothermal heat transfer increases the entropy of the environment which regarded as pollution is stated by the second law of thermodynamics [37]. Bioenergetics is the exergy management in all living cells [12]. The useful energy is also known as available energy that defined as exergy that brings the system's equilibrium with the environment.

Biothermodynamics of metabolic networks has been introduced to predict of all enzymatic reaction and rates that are occurring inside living cells and of all the substances that are consumed and excreted and their rates between the cell and its corresponding environment. This metabolic network insight of thermodynamics started to yield a complete overview of the product distribution and provide the necessary knowledge of the metabolism that is needed to for biocatalysts for bio-refineries design and tailor-made in genetical basis.

2.2. ENERGY METABOLISM

The total of the metabolic pathways that store or generate metabolic energy is named as energy metabolism. The pathways that have a central role in metabolism are almost the same in diverse cellular systems and organisms. The metabolism relies on continuous uptake of organic energy sources (e.g. glucose) as a raw material from the environment

In all biological species, energy metabolism starts with glycolysis, anaerobic phases of carbohydrate catabolism reactions, in the cytosol of the cells and then followed by aerobic respiration in the mitochondria.

Glycolysis can be examined with each of its reactions (Figure 2.1.). Glycolysis starts in the cytoplasm with the conversion of glucose to glucose-6-phosphate with the utilization of two

molecules of adenosine triphosphate (ATP) and ends up with pyruvate production. The net energy production of glycolysis is two molecules of ATP.

The first five reactions, energy investment phase, sugar is metabolized through a series of phosphorylation. The second phase, energy generation phase, the produced triose phosphates in the energy investment phase metabolized further until pyruvate is produced as the end product of glycolysis. In energy investment phase, 2 moles of ATP invested while in energy generation phase 4 moles of ATP produced via substrate-level phosphorylation.

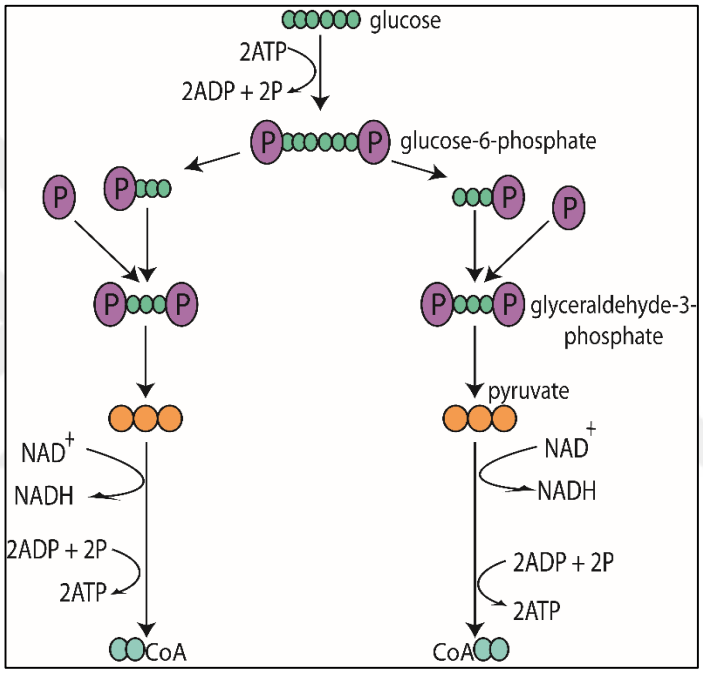

Figure 2.1. Schematic representation of glycolysis [38].

Energy production in mitochondria occurs in the form of chemiosmotic coupling where chemi refers to the chemical bond formation to generate energy and the word osmotic refers to membrane transport processes. The cellular energy is produced from the organic energy sources and delivered to the sites where it is needed in the form of ATP molecules. The ATP molecules are commonly referred to as the currency of the intracellular energy transfer. ATP is a high-energy compound, it releases energy via breakdown into its precursor's adenosine diphosphate (ADP), and organic phosphate to achieve different tasks in the cellular systems, like a contraction of the muscles, transmission of the electrical impulses along the nerves or transport of the substances through the membranes, etc. The energy-yielding chemiosmotic coupling process occurs in two stages under the control of protein complexes embedded in

the membranes. In stage 1 the energy source, e.g., the food molecules, are oxidized to yield high energy electrons and H^+ ions. The electrons are then transferred along the electron carriers embedded in the membrane. In stage 2, the H^+ ions flow depending on the electrochemical gradient and the enzyme, ATP synthase, produces ATP (Figure 2.2.).

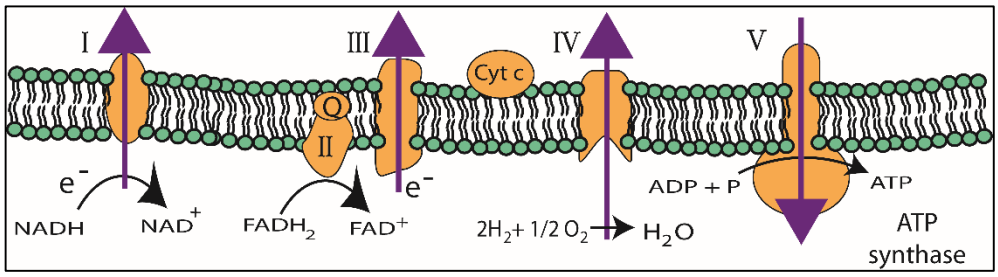

Figure 2.2. Schematic representation of the ETC [39].

This chain of electron transport in a biological system is analogous to an electrical cell that drives current through an electric pump. In a biological system, the role of conducting wires is offset with diffusible molecules (electron carriers) that have the ability to pick up and deliver electrons. In the mitochondria, the food source releases electrons while converting carbohydrate into carbon dioxide. The prior task of these electrons is to reduce oxygen to form water after transferred via the electron transport chain (ETC). Electron carriers have redox potential, they are reduced in the electron transport chain to release energy in the form of ATP via chemiosmosis. Multiprotein complex electron carriers (complex I, II, III, IV and VI) are embedded in the inner membrane. During oxidation, nicotinamide adenine dinucleotide (NADH) donates its electrons to complex I and flavin adenine dinucleotide ($FADH_2$) gives its electrons to complex II. The reduced form of coenzyme Q is oxidized by complex III and in turn, reduces cytochrome c. In the final step, oxidation of cytochrome c and reduction of oxygen to water are coupled in complex IV. These redox exergonic reactions release energy that creates a proton gradient across the inner membrane, where protons are pumped into inner membrane space. The reentering of these protons occurs through complex V. The endergonic ATP synthesis from ADP and inorganic phosphate driven by energy released by exergonic processes.

However, the whole story is not ETC, these electron carriers are products of metabolism (glycolysis and citric acid cycle also known as tricarboxylic acid (TCA cycle or *the* Krebs cycle). Glycolysis which occurs in the cytoplasm creates a precursor (pyruvate) that can

initiate the energy metabolism in mitochondria under aerobic conditions while producing two moles of ATP from one mole of glucose and two moles NADH from one mole of glucose. NADH is an electron carrier derived from nicotinamide adenine dinucleotide (NAD), a coenzyme found in all living cells which has high affinity to undergo redox potential. On the other hand, the citric acid cycle is the main metabolic process that generates high energy electrons in the mitochondria (Figure 2.3.).

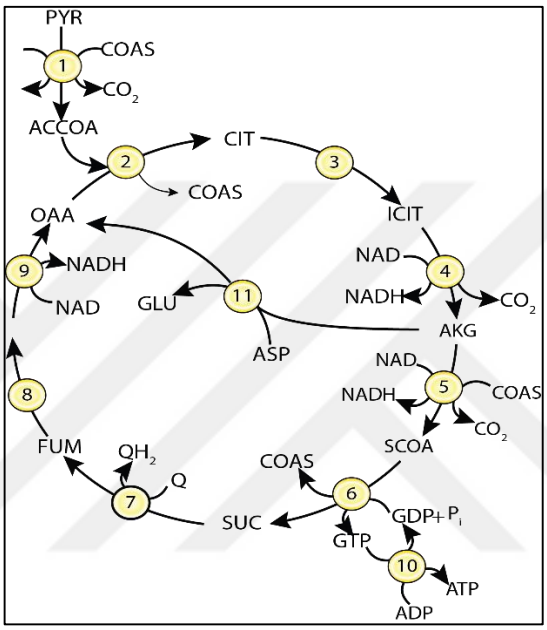

Figure 2.3. Schematic representation of TCA.

TCA cycle is fueled mainly with pyruvate produced in the glycolytic pathway from glucose or other sugars. TCA cycle also processes fatty acids coming from catabolism of fats. Both of these precursors are transported across the mitochondrial matrix and converted into acetyl-CoA, a crucial intermediate precursor of metabolism, via enzymes, pyruvate dehydrogenase complex, located in the mitochondrial matrix. Pyruvate is carboxylated rapidly into carbon dioxide and acetyl-CoA, while fatty acids from bloodstream move into mitochondria and oxidized into acetyl-CoA. Each of these processes yields electron donators. While conversion of pyruvate into acetyl-CoA yields NADH molecule, fatty acid to acetyl-CoA conversion yields NADH and $FADH_2$ molecules. Like NAD^+, $FADH_2$ come from its precursor FAD (flavin adenine dinucleotide) is a redox cofactor that donates electrons in ETC. In the TCA cycle, the acetyl group is completely oxidized into carbon dioxide and water in the mitochondria of eukaryotic cells.

In the 19th century, scientist discovered that the absence of air in the environment lead to the formation of lactic acid in muscles and ethanol in yeast. And then they hypothesized that presence of air, e.g., use of oxygen, is the major source to produce carbon dioxide and water. These findings led to the discovery of the citric acid cycle by Hans Adolf Krebs in 1937. In the cycle, two-thirds of carbonic compounds are converted into major end products. Although citric acid cycle does not use oxygen directly, it requires its presence to proceed. The cycle starts with the acetyl-CoA oxidation transferring CoA to oxaloacetate (4 carbon sugar) yielding TCA cycle which gives the subsequent reactions. The TCA cycle occurs in two phases; introduction and loss of two carbon atoms and regeneration of oxaloacetate. Eight distinct steps take place in these two phases; (1) introduction two carbon atoms to acetyl-CoA, (2) isomerization of citrate, (3) generation of carbon dioxide, (4) Generation of second carbon dioxide, (5) Substrate level phosphorylation, (6) A flavin-dependent dehydrogenation, (7) hydration of C-C double bond and (8) dehydrogenation of the formation of oxaloacetate. As an overview, the eight chain reactions end up with regeneration of oxaloacetate for the next run of the cycle are given in Table 2.1.

Table 2.1. Reactions of the citric acid cycle.

1.	$\text{Acetyl} - \text{CoA} + \text{oxaloacetate} + \text{H}_2\text{O} \rightarrow \text{citrate} + \text{CoA} - \text{SH} + \text{H}^+$
2a.	$\text{citrate} \leftrightharpoons \text{cis} - \text{aconitate} + \text{H}_2\text{O}$
2b.	$\text{cis} - \text{aconitate} + \text{H}_2\text{O} \leftrightharpoons \text{isocitrate}$
3.	$\text{isocitrate} + \text{NAD}^+ \leftrightharpoons \text{CO}_2 + \text{NADH}$
4.	$\alpha - \text{ketoglutarate} + \text{NAD}^+ + \text{CoA} - \text{SH} \leftrightharpoons \text{succinyl} - \text{CoA} + \text{CO}_2 + \text{NADH}$
5.	$\text{succinyl} - \text{CoA} + \text{Pi} + \text{GDP} \leftrightharpoons \text{succinate} + \text{GTP} + \text{CoS} - \text{SH}$
6.	$\text{succinate} + \text{FAD} \leftrightharpoons \text{fumarate} + \text{FADH}_2$
7.	$\text{fumarate} + \text{H}_2\text{O} \leftrightharpoons \text{L} - \text{malate}$
8.	$\text{L} - \text{malate} + \text{NAD}^+ \leftrightharpoons \text{oxaloacetate} + \text{NADH} + \text{H}^+$

The importance of citric acid cycle can be pointed as the production of energy-rich activated carriers; NADH and $FADH_2$ and formation of a relatively small amount of GTP (guanosine triphosphate) which is a close relative of ATP and transfers its phosphate group into ADP to form ATP in each cycle. The high energy carriers subsequently utilized to from ATP molecule via oxidative phosphorylation which is the process that requires the direct presence of oxygen. In addition, to being the site of oxidation of pyruvate and fatty acids, citric acid

cycle also oxidizes some amino acids by converting them to the same precursor, acetyl-CoA. Thus, whether it begins with sugar, fat or protein mitochondria is the location center that energy-yielding process takes place.

Every day, an average human body synthesizes enough metabolic energy in the form of ATP to carry out its daily activities. The contribution of glycolysis and the citric acid cycle is relatively small in energy generation. However, in these metabolic pathways one in glycolysis, another in pyruvate dehydrogenation and four more in citric acid cycle produce energy-rich activated carriers, NADH and $FADH_2$. The re-oxidation of these carriers take place in ETC in mitochondria during aerobic respiration with concomitant ATP production. The inner membrane of mitochondria folds to form cristae to enlarge the surface, where ETC takes place. The cristae folding rate is directly related to the respiration rate, where respiratory proteins are bound to the inner membrane. For instance, the cell which has a high respiratory rate, like heart muscle, contains highly dense cristae while the cells with a low rate of respiration have more sparsely distributed cristae.

2.3. SQUID MANTLE MUSCLE SYSTEM

In nature, million or more animal species are invertebrates all over the World. Invertebrates are animal species that cannot derive vertebral from notochord. Just 4 percent of animal species have a vertebral column in their anatomy. The absence of a vertebral column is a feature that divides animals to two categories; vertebrates and invertebrates. Squids are invertebrates; they belong to the cephalopod class and have bilateral body symmetry. Cephalopods include many marine animals which originate with prominent head, arms, and tentacles. Squid anatomy consists of one prominent head, eight arms, two tentacles, and a mantle. The mantle of a squid is made of muscles in conical shape and encloses vital organs and mantle cavity (Figure 2.4).

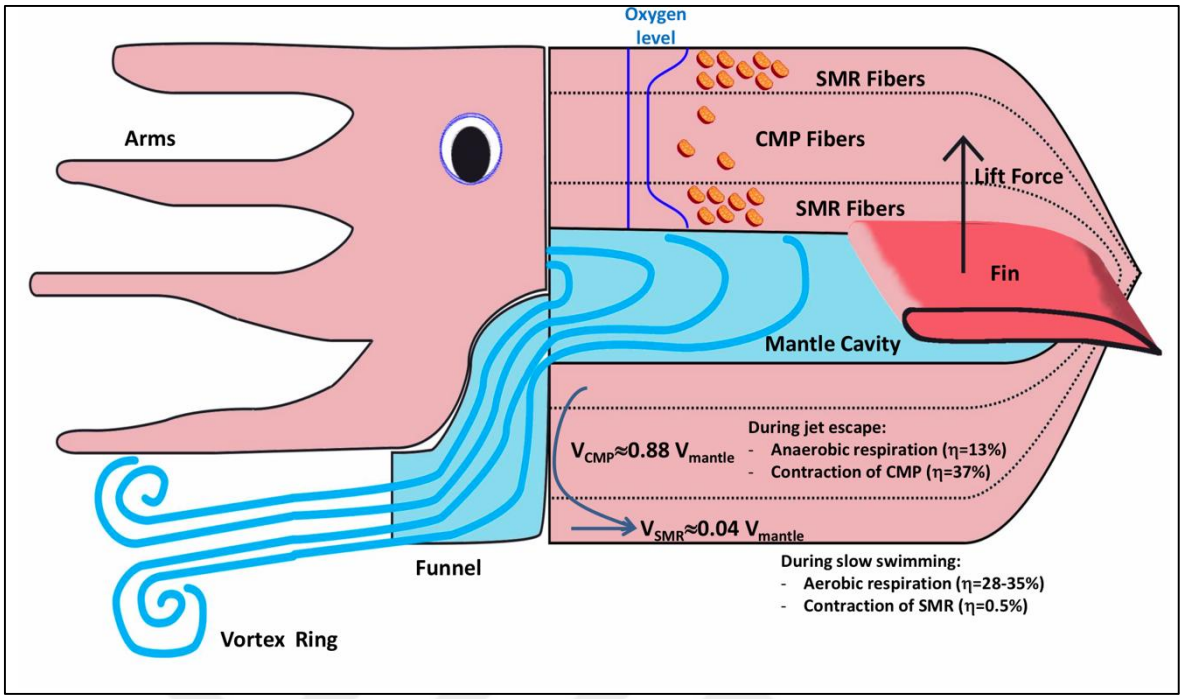

Figure 2.4. Schematic drawing of the squid [23].

Openings on each side of the prominent head are used to suck water into the mantle cavity [40], and then water is ejected from the mantle cavity via contractions of mantle muscles at different speeds to provide the squid with the necessary momentum for propulsion. Muscles of the mantle are arranged in two orientations: radial and circumferential [41]. The radial muscles are engaged to suck water into the mantle cavity [42]. Circular muscles occupy about 90 percent of the total muscle volume and provide power for contraction (Figure 2.5).

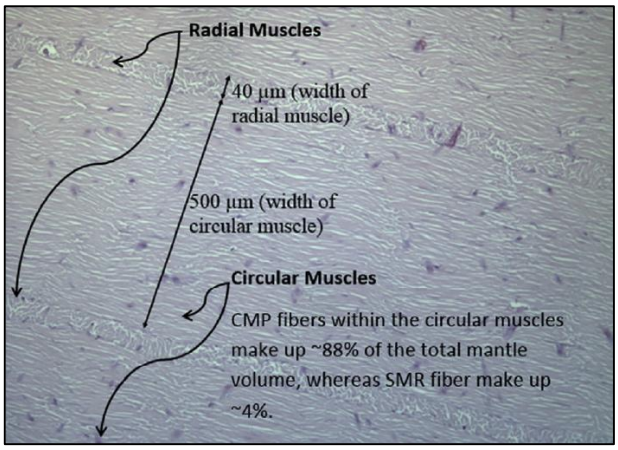

Figure 2.5. Muscles of the squid as visualized under the microscope [23].

The circumferential muscle fibers, which are located along the inner and outer surfaces of the mantle, have a large number of mitochondria (Figure 2.6).

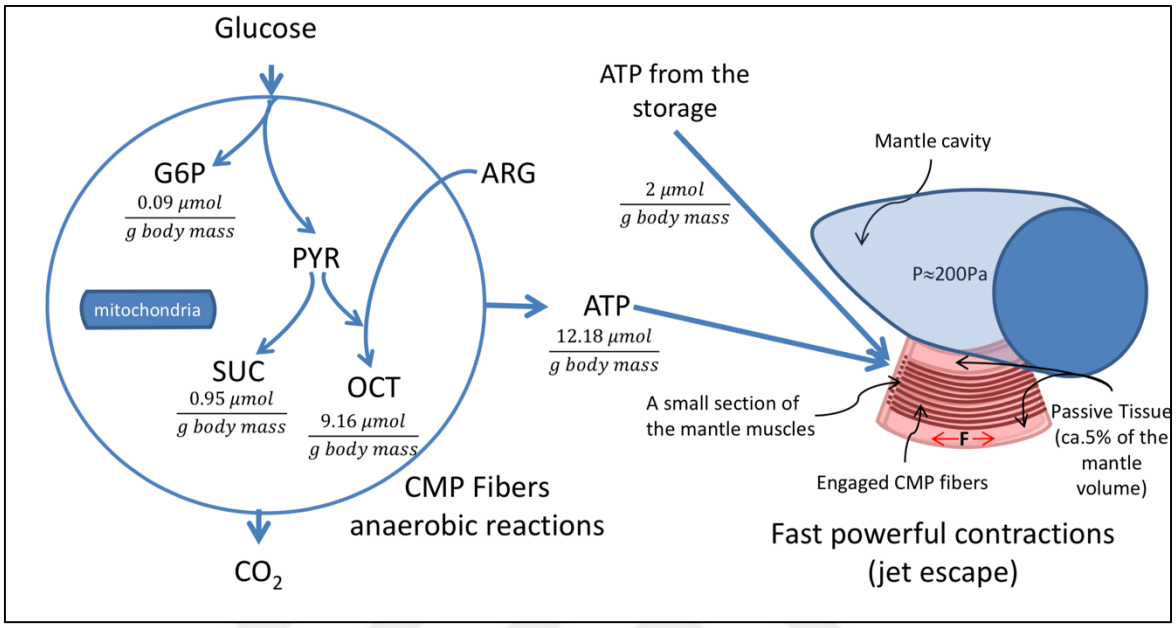

Figure 2.6. Schematic representation of the CMP fiber model. Concentration changes of the metabolites are given as measured by Finke et al. [43] during 15 min of jet escape at a speed of 3 mantle length/sec.

The squids, just like all cephalopods, cannot carry oxygen in their blood. Therefore, oxygen concentration drops as the distance to the mantle surface increases. In the center of the muscle tissue, the fibers contain only a few mitochondria. The volume occupied by the centrally-located mitochondria-poor fibers (CMP) is about 20 times larger than the superficial mitochondria-rich (SMR) fibers [44]. It is hypothesized that the CMP fibers provide the muscle power in the cases of emergency, e.g. during hunting or escape, when the squid has to swim very fast [40,45–47]. The escape jet swimming is fueled via anaerobic metabolism [48]. One evidence that supports this hypothesis is the accumulation of octopine and succinate, byproducts of the anaerobic catabolism of carbohydrate and amino acids [49] in the muscle tissue during fast motion [50]. During the jet escape, the CMP fibers contract and reduce the mantle cavity volume, then water is expelled out and create a jet flow with a high momentum. This momentum transfer accelerates the squid in the opposite direction. Maximum pressure inside the mantle cavity is about 25 kPa (gauge). During the contraction, the inner pressure of the cavity decreases about one kPa below the surroundings pressure, so

the refilling begins immediately after the minimum volume is reached. These SMR fibers (Figure 2.7) are engaged during slow, steady state swimming.

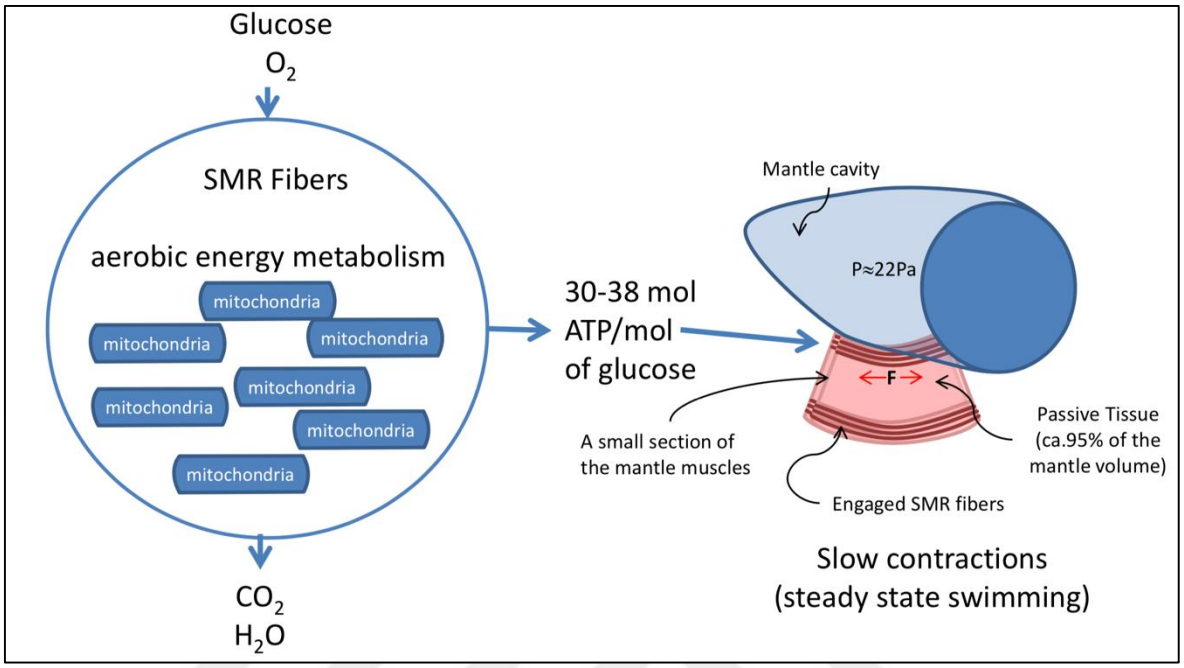

Figure 2.7. Schematic representation of the SMR fiber model [23].

It is hypothesized that, since the SMR fibers are on the surface, these can uptake oxygen from water and carry out aerobic catabolism of the nutrients to produce ATP for the muscle contraction.

2.4. THE BRAIN

The voluntary and involuntary communication within the body occurs through the nervous system. The human nervous system is composed of central and peripheral subdomains. The central nervous system (CNS) is composed of the brain and the spinal cord where the peripheral nervous system (PNS) connects the CNS to the limbs and organs. The brain is the center of the nervous system that is found in all vertebrates and invertebrates with a few exceptions. It is the most complex organ in the body. The building blocks of the nervous system are known as neuron which is an electrically excitable cell. A neuron can exhibit highly polarized activity that can create subcellular domains with different functions. A

typical neuron is composed of three morphologically distinct subcellular domains: soma (cell body), axon (nerve fiber) and dendrite (Figure 2.8).

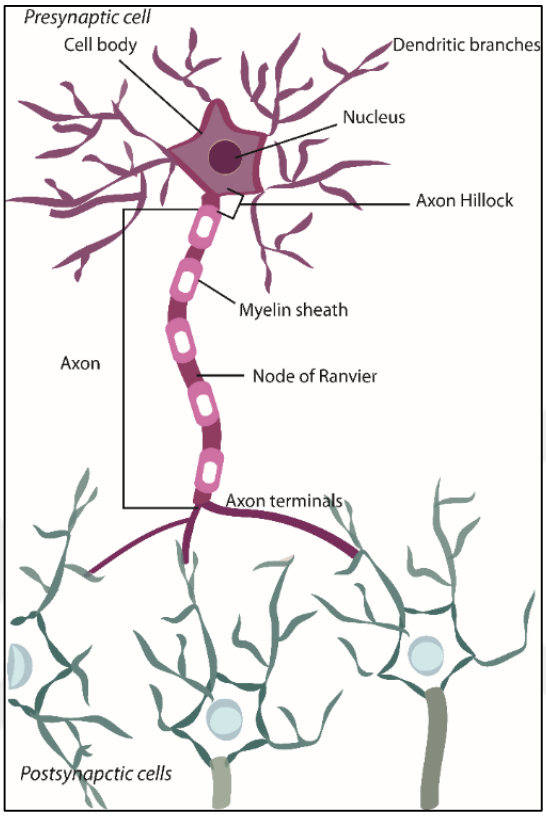

Figure 2.8. Schematic description of the neuron [39].

Basic neuron compromise of dendritic arborization, soma, and a single axon. The neurons are specialized cells that can generate and transmit information via action potentials and synaptic transmission. Cytoplasmic organelles, nucleus, dendrites, and axon on presynaptic and postsynaptic neurons are represented. The axonal length of neuron and dendritic arbor are not the same in different neurons. Most of the large neurons in vertebrates are myelinated, where the node of Ranvier permits rapid conduction of the action potential by a process termed salutatory conduction in the peripheral nervous system. The soma includes cytosol, nucleus and some cytoplasmic organelles. Its main function is transmitting electrochemical signal from the dendrites to the axons. Soma also catalyzes the metabolic activity of the neurons through enzymes in the cytosol. These enzymes synthesize proteins building blocks of the axons, dendrites and the synaptic terminals. Like all the cells in living systems, the interior of the neuron (cytosol) and its exterior (extracellular fluid) are separated by a cell

membrane which is made up of lipids and proteins. The neuronal membrane has a bilayer or sandwich of phospholipids that serve a semipermeable barrier between extracellular and intracellular fluid. Each cytoplasmic organelle located in the soma, like Golgi apparatus, endoplasmic reticulum, polyribosome, and mitochondria has different unique functions. Mitochondria supply more than 90 percent of the energy demand of the cell in the form of ATP.

In a typical neuron, a single axon originating from the axon hillock of the cell body may travel a few hundred microns to several centimeters, depending on the species and the type of neuron. Most axons are very short (20 μm or shorter) and relatively few extend longer than 1 cm in the mammalian CNS. The squid giant axon is just about 1 mm long [51]. However, sensory nerve fibers (transmitting impulses from the periphery to the CNS) and axons of motor neurons (transmitting motor signals from the CNS to the skeletal muscles) can be as much as 1 m long (although only a few micrometers in diameter). Axons are responsible to conduct information from the soma to the nerve terminal. In other words, an axon transmits an upcoming signal from a cell body to their destination axonal terminus via a series of action potentials. Both myelinated and unmyelinated axons are found in the nervous system. In the PNS, myelin sheath originates from the Schwann cells (a neuroglia in the periphery) wrapped around the plasma membrane of the axon. Myelinated axons have a discontinuous structure, separated with short gaps called the nodes of Ranvier [52]. The speed of neuronal communication depends on the velocity of conduction. The length of an axon is the limiting factor in this communication. The myelin sheath of a myelinated axon enables to transmit a signal faster compared to the unmyelinated nerve fibers. The axon membrane is equipped with ligand- and voltage-gated ion channels which have an important role in the initiation of action potentials, its conduction, and synaptic transmission. The extensive ending of axon terminals enables the nerve cell to receive more than one target neuron or muscle or another type of cell via synapses, where the signals are transmitted to the postsynaptic target cell.

Energy metabolism of the brain is highly dynamic, coupled with cerebral blood flow and oxygen supply through the blood-brain barrier (BBB). Oxygen and carbohydrate influx rises and falls together with the blood flow, in association with a coupled system to supply energy demand involving neurons, non-neuronal cells, and the endothelial cells. In brain energy metabolism, a number of substances such as mannose, lactose, and pyruvate are tested as

alternative energy sources in oxidative phosphorylation. Mannose is a six-carbon sugar monomer seems to be the only one that can go through BBB in two enzymatic steps that can sustain the normal functioning of the brain. The internalized mannose readily contributes to the glycolytic pathway from the 3rd step, but unfortunately, mannose is not normally present in brain tissue.

On the other hand, lactose and pyruvate which are the precursors of oxidative phosphorylation can sustain the normal metabolic activity of the brain only in the absence of glucose in the environment. Glucose is obligatory for brain activity and almost the only carbon source of cerebral energy metabolism. Glucose goes through the glycolytic pathway, TCA cycle, and ETC to oxidize glucose entirely to carbon dioxide and water to supply the high energy requirement of the brain.

Brain glucose metabolism as illustrated in Figure 334.2 is similar to that of the other tissues. Glycolysis is the conversion of glucose to pyruvate in the cytoplasm, where 2 molecules of ATP are produced per one mole of glucose. Under aerobic conditions, pyruvate undergoes series of chemical reactions to release energy via pyruvate oxidative decarboxylation to acetyl-CoA while producing specific electron carriers (NADH and $FADH_2$). These reducing agents go to the ETC for reduction and reach the final electron acceptor, oxygen. In ETC glucose is oxidatively phosphorylated and ATP is produced via chemiosmosis. Although in aerobic conditions glycolytic pathway, TCA and oxidative phosphorylation are the major pathways to provide energy in the form of ATP, ATP is not the only energy-rich metabolic agent. Pentose phosphate pathway is parallel to a glycolytic pathway which corresponds two phases; oxidative phase production of reducing agent (NADPH, Nicotinamide adenine dinucleotide phosphate) and non-oxidative phase production of 5-carbon sugar which is a precursor in the formation of nucleic acids and functionally essential to supply major structural elements of neurons such as plasma membrane.

On the other hand, oxidative phase directly involves metabolic activity in the brain although the contribution is relatively small if quantized. The other major role of the pentose phosphate pathway is oxidative defense. The reducing agent, NADPH, is produced in this pathway, needed for the scavenging of the reactive oxygen species (ROS) formed during oxidative phosphorylation to yield large amounts of ATP. Generation of ROS can cause damage to neurons and profound deleterious consequences in the brain such as

neurodegenerative diseases. A reducing agent, NADPH, have a role in the protection of cells from the ROS mediated damage (oxidative stress).

Although the brain weighs only 2 percent of the total body weight, its energy requirement is very high. The brain metabolism consumes about 20 percent of the total body oxygen at the resting state [53]. Availability of energy may limit the size [54], circuitry and activity of the brains in the primates [55–57]. Neuronal function and signaling in the brain are energetically and metabolically expensive. Neurons are never entirely quiescent. There is continuous and spontaneous activity in the awake or conscious state. This activity declines during sleep phase and increases when there is a sensory and motor function. Maintenance of ionic gradient across the excitable cell membrane is crucial for information transmission. A significant amount of metabolic ATP is utilized to fuel ionic pumps, maintain neurotransmitter recycle, synaptic vesicle packaging and cell structural elements production in resting state.

In the cell membranes of excitable cells, ion channels are typically closed. They open and close in response to a change in the membrane potential (voltage gating) or binding of a chemical (ligand gating). In the nervous system, the activity of ionic pumps corresponds to about 50 percent basal glucose oxidation. Studies on the rat [58] and human [59] cerebral cortex have shown that energy is needed to pump out ions to re-establish resting membrane potential after initiation and propagation of neural information.

Upcoming synaptic input activates neurons in response to stimulation and result is firing in axons as a sequence of action potential for information transmission. This neural excitation creates significant energy demand that results in immediate activation of metabolic energy production cascade. Stimulated neuron generates ATP, NAPDH as an energy source through mitochondrial oxidization in neurons and astrocytes. Energy budget of the brain has been investigated to identify processes that utilize energy [58,60,61]. In subcellular processes, energy allocation calculations in the rat cerebral cortical gray matter showed that nearly 75-80 percent of total ATP is used for the signaling activity of the brain while the remaining is used for glial based processes: production of proteins, lipids, and transportation, etc. [60,62]. Young [51] and Alan Hodgkin and Andrew Huxley [63,64] made the earliest contributions to our understanding of electrophysiological behavior of the squid giant axon. The intracellular recordings in the mammalian nervous system demonstrated that mammalian action potential mechanism is similar to that of the squid giant axon [65–67]. Hodgkin and

Huxley not only successfully achieved collecting the intracellular recordings, but also qualitatively and quantitatively explained the ionic mechanisms underlying the action potential. The initiation of action potential starts when an external stimulus comes to the initial segment of an axon, e.g., to the axon hillock. Action potential establishes first a rapid, transient and increased membrane permeability to the Na^+ ions (depolarization) and then becomes slower and then extend to the K^+ ions (repolarization) (Figure 2.9). Action potential is; (i) Resting state: the Na^+ and K^+ channels closed. (ii) Depolarization (rising phase): this upcoming stimulus opens Na^+ channels. Na^+ influx through the channels depolarizes the potential when the depolarization reaches to threshold value it initiates an action potential. (iii) Repolarization: Na^+ channels are no longer voltage sensitive and close at maximum voltage and K^+ channels fully open, outflow of K^+ ions makes voltage become negative. (iv) Undershoot: Fully open K^+ channels make voltage further negative and channels eventually turn its mostly-closed-but leaky state with establishing resting potential. (v) Resting state: the Na^+ and K^+ channels are closed.

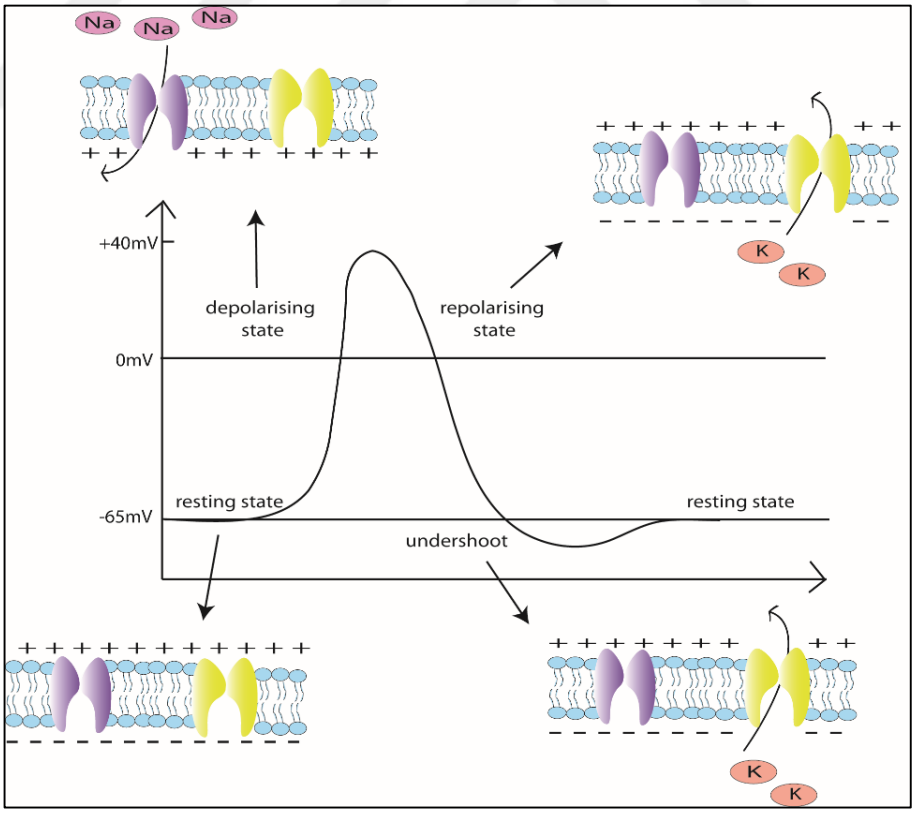

Figure 2.9. Schematic description of the action potential [39].

In the 1940s, Hodgkin and Huxley started doing experiments on the permeability of the squid giant axon membrane to Na^+ and K^+ ions during action potential to determine the rise in the amplitude (depolarization) as a function of the external Na^+ ion concentrations. These experiments showed that when a nerve cell has lower external Na^+ ion concentration the rise of the amplitude of the action potential decreases. Action potential propagates to long distances by the movement of the ions through voltage-gated ion channels embedded in the plasma membrane of the neurons. The voltage-gated ionic channels have 3 conformational states, e.g., open, closed and inactivation. The external stimulus command the voltage-gated Na^+ channels to open and Na^+ ions flux inside while depolarizing the neuron membrane. When depolarization reaches a predetermined threshold, action potential begins. At the open state, the voltage-dependent Na^+ channels make the intracellular membrane more positive than the extracellular surface of the membrane in the rising phase of the action potential and then the membrane becomes extraordinarily permeable to the Na^+ ions and keep depolarizing. Eventually, the membrane potential becomes equal to the Na^+ voltage ($E_{Na} = 58mV$). This short-lived peak point voltage-dependent Na^+ channels have enough voltage to prevent any further channel opening. As the cytoplasm becomes more positive, voltage-gated K^+ channels open and K^+ ions diffuse out of the neuron towards the extracellular space. K^+ efflux causes repolarization stage of the action potential. Then, Na^+/K^+ ATPase is activated and this enzyme energizes the Na^+/K^+ pump. In this refractory phase, the Na^+/K^+ pump binds three Na^+ ions from the inner side and two K^+ ions from the exterior of the neuron and transports them to their original compartments by primary transport mechanism that consumes 1 ATP molecule. At the end, the membrane potential reaches to its normal resting state (- 70mV). All these events occur in a fraction of a second. Although, a signal is generated and transmitted in an axon in the form of the action potential, the arrival of a signal to its destination relies on another mechanism which involves a specialized synapse. The transmission between synapses and target organs or tissues is a nerve-to-nerve signaling and all known nerve-to-muscle or gland signaling rely on the synaptic transmissions.

Electrical information transmission with action potential is an “all-or-none” event. In the 1930s, the squid giant axon was utilized as a useful tool for the experimentation of the action potential. The first studies on this subject were carried out by Marmont [68] with a non-propagating impulse. Cole and Curtis discovered that the membrane conductance increases during action potential and suggested a mechanism for the ionic of initiation and propagation

of the nerve impulse by using the voltage-clamp technique [69]. This technique made it possible to obtain recordings of the voltage across the membrane in the squid giant axon. In these experiments, two independent electrodes were inserted to the axon, one for the voltage and the other for the intracellular current. Hodgkin and Huxley proposed the pioneering action potential initiation and propagation model for the nerve axonal membrane in 1952 [70]. Later Hodgkin and Katz reported a correction for the model [71] and achieved the direct measurement of the membrane voltage [72]. The model was improved in the follow-up studies [70,73–75].

Dendrites of neurons show diversity in terms of their size, elongation, morphology, and distribution of ion channels on their membranes. This diversity and complex geometry make special neurons to different computational tasks like memory, learning, motor functions, etc. Mathematical analysis of the dendrites is fundamental to understand the brain function and neurological diseases. The complex geometry of a neuron causes voltage variations in different regions. When the ionic current flows through the cell membrane, the voltage at that region changes rapidly while the voltage at distant regions from the current flow changes slowly. Electrical signal flow changes the membrane properties by triggering cellular events until reaching the final event like muscle contraction. Electrical signals may be passive or active. When the propagating voltage does not affect the membrane conductance, the transmission is regarded as “passive” and it travels only a limited distance. The membrane conductance is a function of the voltage, can travel an unlimited distance as an active form via a series of the action potential. The passive signaling principles are derived from the basic electrical circuits, where current arises from a voltage flow through a resistor, meanwhile, change by charging a capacitor. This simple circuit derivation is for continuous geometries, where the circuit element located in the cell membrane and cytoplasm leads to a cable equation.

The electric current propagation properties over the electrotonic length of a neuron are called the “cable properties”. The cable theory for active signaling was first applied to a squid giant axon by Hodgkin and Huxley in the 1930s and 1940s. A later theory was offered by Rall for the passive signals transmitted over assistive dendritic trees [76–82]. Rall was inspired from underwater telegraph transmission cables while establishing his model and tried to understand the behavior of an actual neuron, rather than an imaginary neuron summing up all the information at one point. In the cable model, the current flow through an axon is

formulated like that of a core conductor in three-dimensional cylindrical coordinates with partial differential equations. An actual neuron has extensive dendritic trees. The voltage attenuates from the synapses and the current arrives at the soma with time delay. Cable theory regards the dendritic trees as connected cylinders of individual geometry (Figure 2.10).

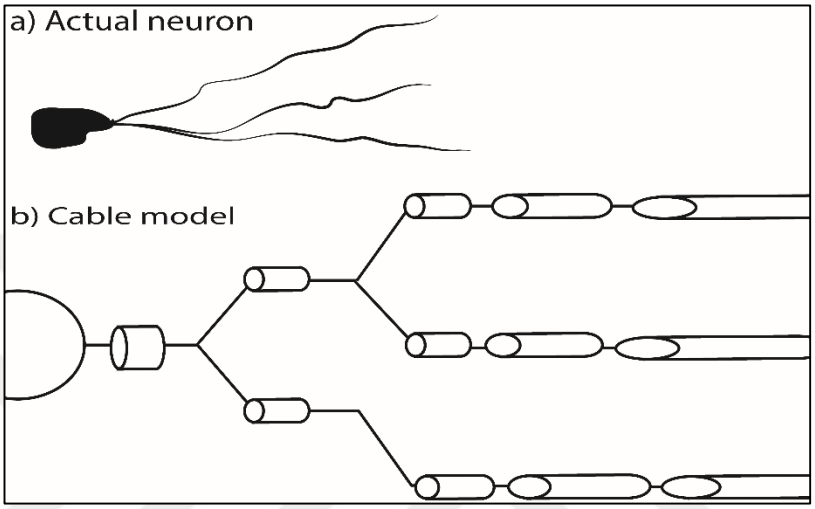

Figure 2.10. Neuronal physiology (a) and its equivalent cylinder cable model (b) [39].

An individual cylinder has a membrane with axoplasm (cytoplasm) inside. This axoplasm generates the axial resistivity. In the case of receiving the information (current) coming on the cylindrical membrane, through ionic channels, most current flows inside the cylinder and some leak from the cable. The leakage from the membrane causes voltage attenuation while current flows axially. The conduction is a passive process, not active like that of the action potential. Cable theory aims to answer the questions on how dendritic input propagate to soma or axon hillock, how individual dendrites interact with each other and the role of dendritic input in functioning.

Cable theory takes into account the electric current flowing in the axial direction. In other words, the voltage across the membrane is only a function of time (t) and distance (x) along the one-dimensional core conductor. The other assumptions of the basic cable theory can be listed as; (i) the membrane of cylinder is uniform and passive (independent of potential), (ii) extracellular fluid is isopotential, (iii) the input is in a form of current and (iv) intracellular fluid of the core conductor is Ohmic resistance with a constant cross section.

The electrotonic property of a neuron is assessed along the isotonic length of the dendritic branches. The dynamic structure of electrotonic property can change depending on the kinetics, the direction of the signals spreading along the dendritic tree and the membrane resistance to the dynamic changes. Every dendritic tree may have a different electrotonic property than the other ones of the network. Division of the (l) a the ctual length of a neuron to (λ) its characteristic length gives its electrotonic length. For sealed-end boundary cylinder as described within the context of the cable model, the electrotonic length $L = \frac{l}{\lambda}$ may be expressed in terms of τ_0, the system time constant and τ_1, e.g., the first equalization time constant, $L = \frac{\pi}{\sqrt{\tau_0/\tau_1 - 1}}$. Rall assumed all the branches end in the same electrotonic length, to enable the branches collapse into one cable. If all the branches do end in the same electrotonic length, they need to be mathematically analyzed separately.

2.5. HEART

Mammalian heart act as a very simple double pump system responsible to transfer blood from the veins to the arteries. The pumped blood meets the hematologic requirements of all type cells of the body through the entire circulation. As a pump, the heart adds enough mechanical work that creates blood flow to overcome the vascular terminal. To exert blood heart is continuously increase and decrease its pressure where contraction (systole) and relaxation (diastole) phases of muscle fiber takes place. The process of blood flow into the heart and pumped out create a unique pressure-volume diagram in one cardiac cycle. The calculation network analysis is derived from pressure-volume diagrams are primarily seen heat engine and frequently used in steam engines performance estimations to estimate work performed. Heat engine converts energy provided from heat to expand as work while the heart uses chemical exergy of nutrients to do work. As in steam engines, work done by the heart can be simply calculated from the integral of the pressure with respect to volume. During contraction of the heart, a large part of the energy in energy metabolism is converted to heat. Heart heat generation and transport arose among other heat estimation in the biological body since heat measurements were thought to be useful to assess the local rate of energy metabolism or blood flow. Pig is regarded as a feasible organ donor for the humans for heart transplantation. This consideration has led to the development of transgenic pigs with the goal of avoiding rejection caused by xenotransplantation.

Circulatory system, including heart, has been central to energy analysis in previous studies. Kameyama et al. [83] analyzed human left ventricular mechanical efficiency by correlating the pressure-volume work with myocardial oxygen consumption. Dasi et al. [84] performed energy analyses in the circulatory system after defining circulation, aortic valve and the right pulmonary artery to superior vena cava connection energy dissipation indexes to represent the full energy budget of circulation. These indexes were considered as the proper measure of the energy utilized for work performance to overcome the frictional forces. Gabr et al. [85] studied the relationship between the cardiac mechanical work performance and the energy supply to the heart and concluded that the energy supply would be sufficient for the mechanical work performance at rest, but becomes limiting at the higher activity levels so heart fails to function. Munoz-Diosdado et al. [86] while studying thermodynamic efficiency of the cardiac cycle and irreversibility in the interbeat interval time series concluded that there is a variability of cardiac efficiency along the day for both healthy and congestive heart failure patients, and there is a substantial reduction in efficiency for congestive heart failure patients. It may be possible for the heart to fail in one of those low-efficiency time periods as pointed by Gabr et al. [85]. Henriques et al. [87] and Çatak et al. [88] preferred performing engineering thermodynamics analyses for circulatory system research. Engineering thermodynamics analyses make it possible to refer to both first and the second laws of thermodynamics and discuss the effects of entropy generation and exergy destruction while assessing the system.

3. METHODOLOGY

3.1. THERMODYNAMIC BALANCE EQUATIONS

First law of thermodynamics which defines the quantity of energy in the universe states that energy can neither be created or destroyed but can be converted one to another via heat, mass and work transfer. The second law of thermodynamics, quality of energy, states that there is a natural tendency of systems goes from ordered to disordered state which results in randomness, entropy. Based on second law, the availability of useful work potential of a system defined with exergy.

Thermodynamic assessment of biological systems requires mass, energy, entropy, and exergy governing equations;

$$\frac{dm}{dt} = \sum(\dot{m})_{in} - \sum(\dot{m})_{out} \tag{3.1}$$

$$\frac{dE}{dt} = \sum(\dot{m}h)_{in} - \sum(\dot{m}h)_{out} + \dot{Q} - \dot{W} \tag{3.2}$$

$$\frac{dS}{dt} = \sum(\dot{m}s)_{in} - \sum(\dot{m}s)_{out} + \sum\frac{\dot{Q}}{T} + \dot{S}_{gen} \tag{3.3}$$

$$\frac{dEx}{dt} = \sum(\dot{m}ex)_{in} - \sum(\dot{m}ex)_{out} + \sum\left(1 - \frac{T_0}{T}\right)\dot{Q} - \dot{W} + P_0\frac{dV}{dt} - \dot{X}_{dest} \tag{3.4}$$

In Equation 3.1 the left-hand side describes mass temporal change while right-hand side difference between the sum of inflow mass flow rate and the sum of outflow mass flow rate. In Equation 3.2 left-hand side describes accumulation term, $\sum(\dot{m}h)_{in}$ the sum of the rate of energy that inflow into the system, $\sum(\dot{m}h)_{out}$ the sum of the rate of energy that outflow from the system, $\dot{Q}$ is the rate of transferred heat and $\dot{W}$ is the rate of conducted work. In Equation 3.3 left hand side describes accumulation entropy term, $\sum(\dot{m}s)_{in}$ the sum of the rate of inflow masses entropy, $\sum(\dot{m}s)_{out}$ the sum of the rate of outflow masses entropy, $\sum\frac{\dot{Q}}{T}$ is the entropy rate of all heat transfer and $\dot{S}_{gen}$ is the rate of entropy production within the system. In Equation 3.4 left hand side describes accumulation exergy term, $\sum(\dot{m}ex)_{in}$ the sum of the rate of inflow masses exergy, $\sum(\dot{m}ex)_{out}$ the sum of the rate of outflow masses

exergy, $\sum \dot{Q}\left(1-\frac{T_0}{T}\right)$ the rate of heat transferred exergy into the system, $\dot{W}+P_0(\frac{dV}{dt})$ is the rate of work conducted by the system and $\dot{X}_{dest}$ is the exergy destruction inside the system. As the first step of thermodynamic assessment in systems, the system boundaries was selected and the governing equations was applied to system.

3.2. CALCULATION OF THERMODYNAMIC PROPERTIES

Biochemical species of undergoing biochemical reactions the standard Gibbs free energy and enthalpy of formation were estimated based on a method developed by Alberty [89]. The data illustrated designed thermodynamical tables were used to calculate thermodynamic properties of various biochemical species depending on their physiological conditions; temperature, ionic strength, and pH. During these calculations extended Debye-Huckel theory and Van't Hoff equation was used. At a specific physiological condition biochemical species transformed Gibbs free energy of formation illustrated as;

$$\Delta G_{f,i}^{T}=\frac{T}{T_0}\Delta G_{f,i}^{0}+\left(1-\frac{T_0}{T}\right)\Delta H_{f,i}^{0}-\frac{RT\alpha(T)I^{\frac{1}{2}}}{1+BI^{\frac{1}{2}}}\left(z_i^2-n_{H,i}\right)-n_{H,i}\Delta G_{f,H^+}^{0}+2.303n_{H,i}RTpH \tag{3.5}$$

In some physiological conditions, some biochemical species can coexist with different valence states in the cell. For this reason, while calculating standard transformed Gibbs free energies each valence state was considered. The collective equation of standard transformed Gibbs free energies of species that have more than one valence state illustrated and the standard transformed enthalpy of formation as;

$$\Delta G_{f,j}^{T}=-\mathrm{RTln}\sum exp\left(-\frac{\Delta G_{f,i}^{T}}{RT}\right) \tag{3.6}$$

$$\Delta H_{f,j}^{T}=\Delta H_{f,j}^{0}+\frac{RT^2\beta(T)I^{\frac{1}{2}}}{1+BI^{\frac{1}{2}}}\left(z_i^2-n_{H,i}\right) \tag{3.7}$$

In each investigated model depending on their physiological condition of systems, related metabolites Standard transformed Gibbs free energies and standard transformed enthalpy of formation was computed with using Wolfram Mathematica 10.

Although the method developed by Alberty for biochemical thermodynamics is well established some complex biochemical structures may not be found. In such cases, groups in such biochemical species that contribute their overall structure can be used to estimate their standard Gibbs free energy and enthalpy of formation which is called group contribution method [90–95]. As an example of such complex biochemical structures, arginine, standard Gibbs free energy and enthalpy of formation values estimated with this method. The complex molecular structure is divided into subgroups as in the figure above.

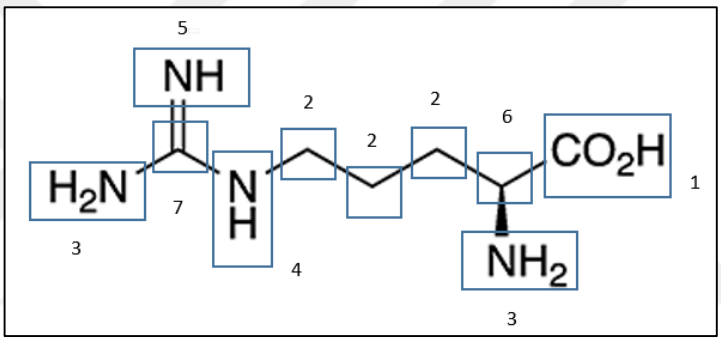

Figure 3.1. The increment groups of arginine.

Table 3.1. Group contribution of arginine.

Group no.	Increments	Number of repeat	ΔH (kJ/mol)	ΔG (kJ/mol)
1	—COOH	1	-426.72	-387.87
2	—CH_2—	3	-20.64	8.42
3	—NH_2	2	-22.02	14.07
4	—NH	1	53.47	89.39
5	=NH	1	93.70	119.66
6	—CH	1	29.89	58.36
7	=C—	1	83.99	92.36
TOTAL			-271.63	25.2

Standard Gibbs free energy and standard enthalpy of formation calculated as above;

$$\Delta G^0_{f298} = 53.88 + \sum_{i=0}^{n} Ni \times \Delta Gi \tag{3.8}$$

$$\Delta H^0_{f298} = 68.29 + \sum_{i=0}^{n} Ni \times \Delta Hi \tag{3.9}$$

The entropy of formation at specific physiological condition was calculated from;

$$\Delta G^0_{fT} = \Delta H^0_{fT} - T \times \Delta S^0_{f,T} \tag{3.10}$$

where elemental entropy calculated as;

$$\Delta S^0_{f,T} = S^0_{compound} - \sum_{i=1}^{n} Ni \times S^r_{element\ i} \tag{3.11}$$

$\Delta S^0_{f,T}$ is the entropy of formation at a defined temperature and atmospheric pressure, $S^0_{compound}$ is the ideal gas absolute entropy of the compound at a defined temperature and atmospheric pressure, *n is the* number of different elements contained in the compound, Ni is the moles of element *i* contained in one mole of compound and $S^r_{element\ i}$ is absolute entropy of element *i* in its standard state. The above table shows an example for the calculation of absolute entropy and ideal gas absolute entropy of the compound of arginine.

Table 3.2. Values of arginine for the calculation of Absolute entropy.

Element	Number of repeats	Absolute entropy (kJ/molK)
C	6	5.74
H_2	7	130.571
N_2	2	191.5
O_2	1	205.043
$S^r_{element\ i}$		1536
$S^0_{compound}$		588.8

Most elements standard chemical exergy values given by Szargut et al. [92]. Species chemical exergy at reference state is equal to um of Gibbs free energy of formation and elemental exergies;

$$Ex^{0}_{ch,j} = \Delta G^{0}_{f,j} + \sum_{i=1}^{n} Ni \times Ex^{0}_{ch,i} \tag{3.12}$$

The above table shows an example for the calculation of exergy at the reference state of the compound of arginine.

Table 3.3. Elemental values of arginine for the calculation of exergy at the reference state.

Element	Number of repeats	Exergy at reference state (kJ/mol)
C	6	410.25
H_2	7	236.10
N_2	2	0.66
O_2	1	3.97
$Ex^{0}_{ch,i}$		4119.49
$Ex^{0}_{ch,j}$		4198.57

Exergy of biochemical species function of physiological conditions such as; temperature, ionic strength, pH, elemental exergies and dilution.

$$\begin{aligned} Ex_{\text{species}}\left(T, I, pH, c_{\text{species},c}\right) = & \underbrace{\frac{T}{T_0}\Delta G^{0}_{f,\text{species}} + \left(1 - \frac{T}{T_0}\right)\Delta H^{0}_{f,\text{species}}}_{\text{effect of temperature}} \\ & \underbrace{- \frac{RT\alpha(T) I^{1/2}}{1 + BI^{1/2}}\left(z^{2}_{\text{species}} - n_{H,\text{species}}\right)}_{\text{effect of ionic strength}} \\ & \underbrace{- n_{H,\text{species}}\Delta G^{0}_{f,H^{+}} + 2.303 n_{H,\text{species}} RTpH}_{\text{effect of pH}} \\ & \underbrace{+ 6ex^{0}_{ch,C} + 6ex^{0}_{ch,H2} + 3ex^{0}_{ch,O2} + \ldots}_{\text{chemical exergy of elements}} \\ & \underbrace{+ RT\ln(c_{\text{species},c})}_{\text{effect of dilution}} \end{aligned} \tag{3.13}$$

where, ΔG_{fT}^{0} and ΔH_{fT}^{0} are standard Gibbs energy of formation, and standard enthalpy of formation of biochemical species, respectively. T is the temperature in the system, T_o is the environmental temperature, B is an empirical constant (1.6 $L^{½}mol^{-1/2}$), I is ionic strength, α is a coefficient in the Debye-Huckel equation, z is the valence of isomer, n and n are the stoichiometric constants and c is the concentration of the chemical species under consideration.

3.3. THERMODYNAMIC ANALYSIS OF THE SQUID MANTLE MUSCLES

In the thermodynamic investigation of squid mantle muscle metabolism study, two muscle fiber types, SMR, and CMP fiber models were considered. In both models energy, in the form of ATP produced via muscle metabolism due to catabolized nutrients, and utilized in the consequent contraction of muscle fibers. Squids gain momentum via eject water from the mantle cavity with the contraction of fibers. For both muscle models, the thermodynamic assessment was performed with analytical solving of mass, energy and exergy equations (Equations 3.1-4). However, before the governing equations analysis, each metabolite that contributes to muscle model systems was calculated depending on Alberty and in special cases of octopine, arginine and succinate group contribution contributed with following Alberty method [89]. In this study motion of squid, muscle was regarded as a periodical contraction with the same intensity and period. As a consequence of this assumption cyclic integral was taken over one period in the governing equations;

$$\oint \frac{dm}{dt} = \oint \sum (\dot{m})_{in} - \oint \sum (\dot{m})_{out} \tag{3.14}$$

$$\oint \frac{dE}{dt} = \oint \sum (\dot{m}h)_{in} - \oint \sum (\dot{m}h)_{out} + \oint \dot{Q} - \oint \dot{W} \tag{3.15}$$

$$\oint \frac{dEx}{dt} = \oint \sum (\dot{m}ex)_{in} - \oint \sum (\dot{m}ex)_{in} + \oint \dot{Q} \sum \left(1 - \frac{T_0}{T}\right) - \oint \dot{W} + \oint P_0 \frac{dV}{dt} - \oint \dot{X}_{dest} \tag{3.16}$$

During sustained slow swimming, steady state, ATP produced via aerobic metabolism which is engaged with SMR fibers. The nutrient, glucose, oxidized entirely into its final products,

CO_2 and H_2O. The final products are transferred to the intracellular region without any accumulation within the system boundaries. In the governing equations, the accumulation terms (i.e. left-hand side of the equal sign) become zero. Due to periodic volume change, the surrounding work term $\oint P_0 \frac{dV}{dt}$ becomes also zero. In the model, boundary temperature and dead state temperature assumed to be same the throughout the whole cycle leaving $\oint \dot{Q} \sum \left(1 - \frac{T_0}{T}\right)$ also equal to zero.

During jet escape where mainly CMP fibers engaged, the energy that fuels the contraction of fibers produced by switching metabolism into anaerobic reactions. Metabolic contraction measurements during jet escape mode showed that three biochemical species, octopine, arginine, and glucose6phosphate, accumulates within the system boundaries which makes accumulation terms non-zero in the governing equations but still surrounding work term $\oint P_0 \frac{dV}{dt}$ and $\oint \dot{Q} \sum \left(1 - \frac{T_0}{T}\right)$ terms zero.

3.3.1. Squid Mantle Muscles Work Analysis

Squids are negatively buoyant, they have to generate vertical and horizontal force during swimming. Horizontal direction water eject with a high momentum produce horizontal force where squid mantle cavity act as a pressure vessel. Water inside the mantle cavity ejected to surrounding through funnel due to contraction. This cavity contraction changes both pressure and volume. Mechanical work applied to water was calculated as;

$$W = \int P dV \tag{3.17}$$

where P is water pressure and dV corresponds to the volume change of mantle. Mantle cavity volume calculated with using $V = \pi r^2 L$ where r is the radius of mantle cavity at any location and L is the length along squid's mantle dorsal length. Squid mantle cavity volume change estimated as;

$$V = \int \pi \left[\sin\left(\frac{x\pi}{2L}\right) r_{max}\right]^2 dx \tag{3.18}$$

where radius (r) diversifies along the length of the dorsal mantle (L).

Work of muscle contraction was calculated with using force and displacement measurements via electromyography data.

$$W = \int F dl \tag{3.19}$$

Basically, for the calculation of the segmented thickness of muscle, the muscle was divided into 150 parts which have an equal thickness and length. For each fiber group force, the area was calculated via multiplying muscle segment length with a thickness which further multiplied by average stress. These two illustrated detailed muscle work analyses contributed to both of muscle models, SMR and CMP.

3.4. THERMODYNAMIC ANALYSIS OF THE SQUID ACTION POTENTIAL

Biological excitable membrane studied in analogy with electric circuits (Figure 3.2). The axonal membrane of a neuron can be modeled by an equivalent electrical circuit for the Hodgkin–Huxley model of the action potential with three ions where Na^+, K^+, and CI^- each has conductance, currents, and equilibrium potentials and also single constant capacitance. The C_m represents the capacitance of the membrane I_m and V_m represent the current through, and the voltage across the membrane, respectively.

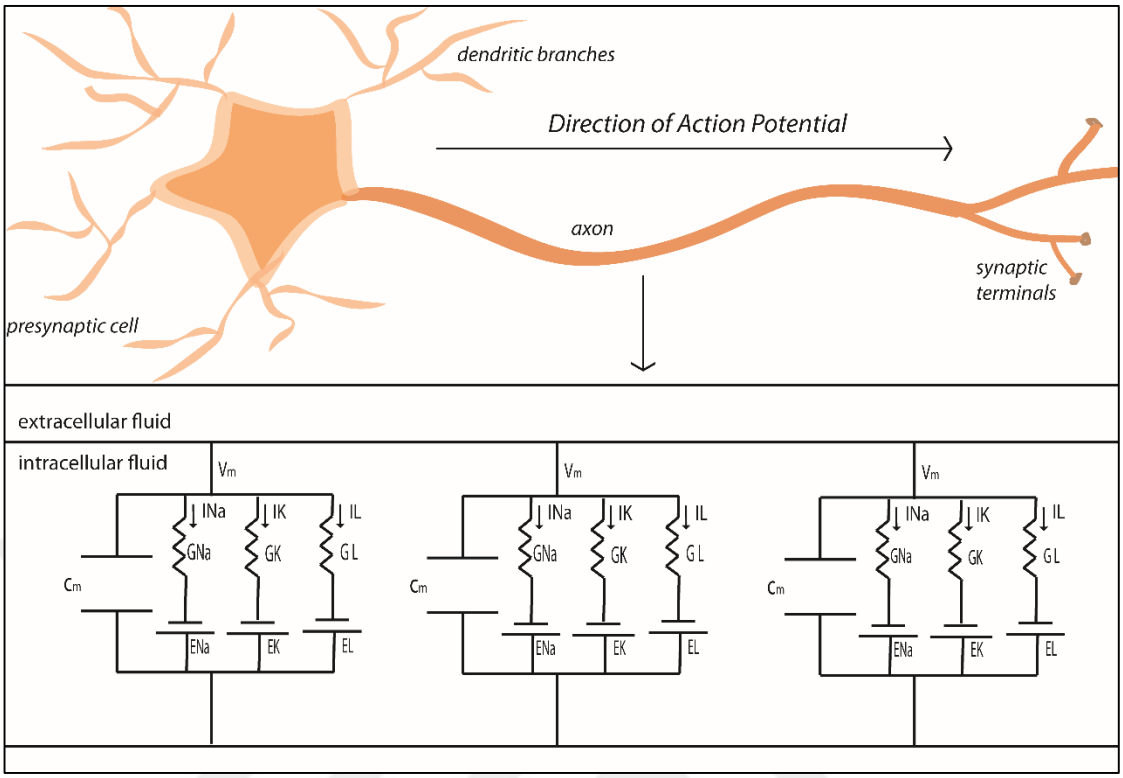

Figure 3.2. Actual neuron vs. equivalent electrical circuits along axonal membrane [39].

Depending on the process that cell undergoes the plasma membrane can act as a capacitor or resistor. The nerve membrane can store, transmit and release electrical energy without owning metallic conductors which is substitute by intracellular and extracellular fluids in the cell plasma membrane. The membrane also acts as a non-conducting material between intracellular and extracellular fluid. When the current pass across the plasma membrane, the membrane act as a resistor. In the plasma membrane, ionic channels responsible to the permeability of ions and each channel represent small resistor in parallel. The membrane resistance is the flow of ions thru these channels. The membrane capacitance not function of time and voltage and specific and constant in most of the cell.

Current $i = C_m \frac{dV}{dt}$ is through the membrane capacitance (C_m) is the product of time derivative of the voltage $\left(\frac{dV}{dt}\right)$ and capacitance. The excitable cell electrical signals primarily controlled by membrane conductance which is a function of time and voltage. The equivalent circuit and Kirchhoff's law adaptation gives;

$$I_m = I_C + I_i = C_m \frac{dV}{dt} + \frac{V_m - E_{ion}}{R_m} = C_m \frac{dV}{dt} + G_m(V_m - E_{ion}) \quad (3.20)$$

where I_m is the total membrane is current, I_C is the sum of capacitive current, I_i is the ionic current, G_m is the total membrane conductance, R_m is the membrane resistance and E_{ion} is the ions reversal potential (Nernst potential). The driving force of the ionic current (V) is the difference between membrane potential (V_m) and reversal potential of ion (E_{ion}).
Electrical properties of the biological electrical membranes give the ability to characterize the membrane like an electric circuit where dielectric property give rise to capacitance, ionic channels represented as conductance. This unique characteristic of excitable neuronal membrane gives rise to many modeling to understand the function of the neuron under the voltage.

Quantitative analysis and biophysics of excitable membranes are very important phenomena. The action potential is an electrical information transmission which is an all-or-none event modeled with Hodgkin and Huxley parallel conductance model of the biological membrane which contains parallel Na^+, K^+ and CI^- conductances (g_{Na}, g_K, g_{CI}), constant capacitance (C_m), ionic current composed of Na^+, K^+ and CI^- ions; sodium current (I_{Na}), potassium current (I_K) and small leakage current (I_I) and equilibrium potentials of ions (E_{Na}, E_K, E_{CI}). The total membrane current is the sum of the individual ionic currents (sodium, potassium and leakage) which are determined by a driving force represented as;

$$I_m = I_C + I_{Na} + I_{CI} + I_K \quad (3.21)$$

For a given ion species the ion current is the product of conductance of the ion and the driving force (voltage difference between membrane potential and Nernst potential of ion) expressed as;

$$I_{ion}(V,t) = g_{ion}(V_m,t)(V_m - E_{ion}) \quad (3.22)$$

The experiments suggested that current and conductance is a function of time and potential where Nernst potential, the capacitance of ions and leakage conductance are constant over time and potential. Thus the conventional and simplified versions and for more practical use Hodgkin and Huxley suggested a more simplified version expressed as;

$$I_{Na}(V_m, t) = g_{Na}(V_m, t)(V_m - E_{Na}) \tag{3.23}$$

$$I_{Na} = g_{Na}(V_m - E_{Na}) \tag{3.24}$$

$$I_{Na} = g_{Na}(V_m - V_{Na}) \tag{3.25}$$

$$I_K(V_m, t) = g_K(V_m, t)(V_m - E_K) \tag{3.26}$$

$$I_K = g_K(V_m - E_K) \tag{3.27}$$

$$I_K = g_K(V_m - V_K) \tag{3.28}$$

$$I_{CI} = \overline{g_{CI}}(V_m - E_{CI}) \tag{3.29}$$

$$I_{CI} = \overline{g_{CI}}(V_m - E_{CI}) \tag{3.30}$$

$$I_{CI} = \overline{g_{CI}}(V_m - V_{CI}) \tag{3.31}$$

where V,V_{Na}, V_K, V_{CI} are displacements from resting potential and directly derivable from extraction absolute value of resting potential (E_r) from the ionic potentials (E_{Na}, E_K, E_{CI}). The total membrane current can be expressed as;

$$I_m = C_m \frac{dV}{dt} + g_{Na}(V_m - E_{Na}) + g_K(V_m - E_K) + \overline{g_{CI}}(V_m - E_{CI}) \tag{3.32}$$

If the cell at rest which mean steady-state total membrane current ($I_m = 0$) and the voltage change over time ($\frac{dV}{dt} = 0$) also became equal to zero and V becames as;

$$V = \frac{g_{Na}E_{Na} + g_K E_K + \overline{g_{CI}}E_{CI}}{g_{Na} + g_K + \overline{g}_I} \tag{3.33}$$

The model proposed that there is a number of gates to allow or prevent ion passage and each has to bear upon to control of a number of independent gating particles. Also, the gating particles can be either open or closed, changing their state depending on membrane potential. The forthcoming will focus on the ion permeability of gates and gating particles.

Potassium gates gating variable 'n' is formally assumed the probability of the gate is open. This gates are independently acting and 'n^x' refers to the sum of all potassium gates are being open where 'x' represents gating particles in a gate. Potassium conductance became as;

$$g_K = \overline{g_K} n^4 \tag{3.35}$$

where $\overline{g_K}$ is the maximum conductance of potassium which is a dimension of conductance per cm^2. The transition rates between open (n) or closed $(1-n)$ state of gates described by α, β variables. α refers to time passed that gates go from closed to open state where β is exact opposite time passing. The variables α_n and β_n is the rate coefficients which depend on membrane potential. First order kinetic equations applied and represented as;

$$\frac{dn}{dt} = \alpha_n(1-n) - \beta_n(n) \tag{3.36}$$

The probability of the gate is open can respond to positive voltage in the time course, it can be squared, cubed or power four. However, it has to give inflection in the curve and best fit established in the Hodgkin and Huxley model with raising the power of probability to four. It clearly means that each gate has four gating particles. As mentioned earlier, 'n' response to voltage step in time course and represented as;

$$n(t) = n_\infty(V) - (n_\infty(V) - n_0)\exp(-\frac{t}{\tau_n(V)}) \tag{3.37}$$

where n_0 is starting value of n under voltage step, the steady state activation ($n_\infty = \frac{\alpha_n}{\alpha_n+\beta_n}$) and time constant ($\tau_n = \frac{1}{\alpha_n+\beta_n}$). The best fit of experimental data of rate constants is established with the following constants;

$$\alpha_n = \frac{0.01(V+10)}{exp\left[\frac{V+10}{10} - 1\right]} \tag{3.38}$$

$$\beta_n = 0.125exp\left(\frac{V}{80}\right) \tag{3.39}$$

For squid giant axon (where V is the displacement voltage from its resting state value). The rate coefficients represented reciprocal of msec. The amount of potassium current that pass thru open channels represented as;

$$I_K = \overline{g_K}n^4(V_m - V_K) \tag{3.40}$$

In the same manner with K^+ conductance, the Na^+ conductance was calculated over voltage clap sets. Hodgkin and Huxley proposed two different methods for sodium conductance where the first method obeys second-order differential equation while the second one obeys first order differential equation with two gating particles in both methods. The first order differential equation showed more correlation with experimental results. In this approach, the model introduce another gating particle rather than activation which is 'h' that represents the level of inactivation. The first order kinetic equation represented as;

$$\frac{dh}{dt} = \alpha_h(1-h) - \beta_h(h) \tag{3.41}$$

As like potassium conductance α_h and β_h voltage dependent rate coefficients for inactivation of the gate and can be written depending on the time constant and limiting value. The other gating particle behaves like 'n' gating particle variable (potassium gating particle) and donated with letter 'm', which represents the inside proportion of activating molecules and where '$1-m$' is an outside proportion (same manner with 'h'). The first order kinetic equation for 'm' represented as;

$$\frac{dm}{dt} = \alpha_m(1-m) - \beta_m(m) \tag{3.42}$$

The steady-state activation, inactivation and time constants where are satisfies boundary conditions $m = m_0$ and $h = h_0$ at $t = 0$ expressed as;

$$m = m_\infty - (m_\infty - m_0)\exp(-\frac{t}{\tau_m}) \tag{3.43}$$

$$h = h_\infty - (h_\infty - h_0)\exp(-\frac{t}{\tau_h}) \tag{3.44}$$

where;

$$m_\infty = \frac{\alpha_m}{(\alpha_m + \beta_m)}, \qquad \tau_m = \frac{1}{(\alpha_m + \beta_m)} \tag{3.45}$$

$$h_\infty = \frac{\alpha_h}{(\alpha_h + \beta_h)}, \qquad \tau_h = \frac{1}{(\alpha_h + \beta_h)} \tag{3.46}$$

The model of sodium conductance showed satisfaction with experimental data when there is three 'm' and one 'h' gating particles available. The sodium conductance became as;

$$g_{Na} = \overline{g_{Na}} m^3 h \tag{3.47}$$

where $\overline{g_{Na}}$ maximum conductance of sodium. The best fit with experimental data in squid giant axon provided by;

$$\alpha_m = \frac{0.1(V+25)}{exp\left[\frac{V+25}{10} - 1\right]}, \qquad \beta_h = 4exp\left(\frac{V}{18}\right) \tag{3.48}$$

$$\alpha_h = 0.07exp\left(\frac{V}{20}\right), \qquad \beta_h = \frac{1}{exp\left[\frac{V+30}{10} + 1\right]} \tag{3.49}$$

The amount of sodium current that pass thru the open channels in the plasma membrane expressed as;

$$I_{Na} = \overline{g_{Na}} m^3 h (V_m - V_K) \tag{3.50}$$

Hodgkin and Huxley found that some currents flow when potassium equilibrium potential reached where the flow is not sodium current. This non-sodium current occurs also independently from potassium ions because of the driving force $V - E_K$ is equals to zero at equilibrium potential. But, the cell plasma membrane is permeable to chloride ions and they leak thru membrane independently from membrane potential. The leak current represented as;

$$I_{CI} = \overline{g_{CI}} (V_m - E_{CI}) \tag{3.51}$$

Hodgkin and Huxley tried to gain mathematical understanding to structural and functional properties of ion channels and their propagation under voltage difference with using electrophysiological experiments on squid giant axon. The overall summary of membrane potential change over time is illustrated as;

$$C_m \frac{dV}{dt} = \overline{g_K} n^4 (V_m - V_K) + \overline{g_{Na}} m^3 h (V_m - V_K) + \overline{g_{CI}} (V_m - E_{CI}) - I \quad (3.52)$$

where I is the total membrane current (local circuit current) which is a function of time and voltage.

From 1952 to up to now Hodgkin and Huxley cable model not only a very successful model in squid giant axon it also very useful model for mammalian neuron models. But the model all data set collected at the same temperature which is different from the physiological temperature of the systems. The model shows a strong temperature effect on gating variable coefficients. For different temperature, the channel rate transfer can be normalized by an additional temperature compensating factor (ϕ). In the case of either increase or decrease of gating variable rate coefficient temperature from the model temperature compensating factor represented as;

$$\phi = Q_{10}{}^{(T-T_0)/10} \quad (3.53)$$

where, T_0 is the original temperature of the model, T is the temperature of simulation and, Q_{10} constant for gating variable Q_{10} is also a function of the temperature and this can be comprehended by transition state theory.

The maximal conductance, reversal potentials and, capacitance were the original model parameters established as; $\overline{g}_{Na} = 120\, ms/cm^2$, $\bar{g}_K = 36\, ms/cm^2$, $\bar{g}_L = 0.3\, ms/cm^2$,$E_{Na}50\, mV$, $E_K = -77\, mV$, $E_L = -54.4\, mV$ and $C_m = 1\ \mu F/cm^2$.

Analogies of the electrical circuit can be useful to understand to work, heat, entropy and exergy concepts in the squid giant axon. In the electrical circuit analogy model, the energy stored in the capacitor was calculated for constant capacitance between the electrodes, where the voltage difference was; $En = \frac{1}{2} C_m V^2$ [96] while during the charging of the capacitor the current generates heat as expressed in terms of the constant capacitance C_m and the final voltage V_0 [97] as; $Q = \frac{1}{2} C_m {V_0}^2$. Temperature effects on the time constants of the gating variables were represented in the model by multiplying parameters α and β with parameter $\phi(T) = Q_{10}{}^{\frac{(T-6.3^0C)}{10^0C}}$, where $Q_{10} = 3.0$.

Governing equations of the first (Equation 3.2) and the second (Equation 3.4) laws of thermodynamics may be expressed as;

$$\sum_{in}[\dot{m}\,(h+\,e_p+e_k)]_{in}-\sum_{out}[\dot{m}\,(h+\,e_p+e_k)]_{out}+\sum_{i}\dot{Q}_i$$
$$-W=\frac{d\left[m(u+\dot{}\,e_p+e_k)\right]_{system}}{dt} \tag{3.54}$$

$$\sum_{in}[\dot{m}\,ex]_{in}-\sum_{out}[\dot{m}\,ex]_{out}+\sum_{i}[1-\frac{T_0}{T_{b,i}}]\,\dot{Q}_i-W-\dot{E}x_{dest}=\frac{d[m\,ex]_{system}}{dt} \tag{3.55}$$

where, $\dot{m_{in}}$ and $\dot{m_{out}}$ describes the mass input and output through the system boundaries. When we apply these equations to a single spot in Figure 3.3. $\dot{m_{in}}$, a neuronal signal entering through the system boundary may establish an analogy with $\dot{m_{in}}$, and the signal leaving through the system boundary may establish an analogy with $\dot{m_{out}}$. In equation (10), $\dot{W}$ is the work done within system boundaries and $\dot{Q}$ is the heat generation.

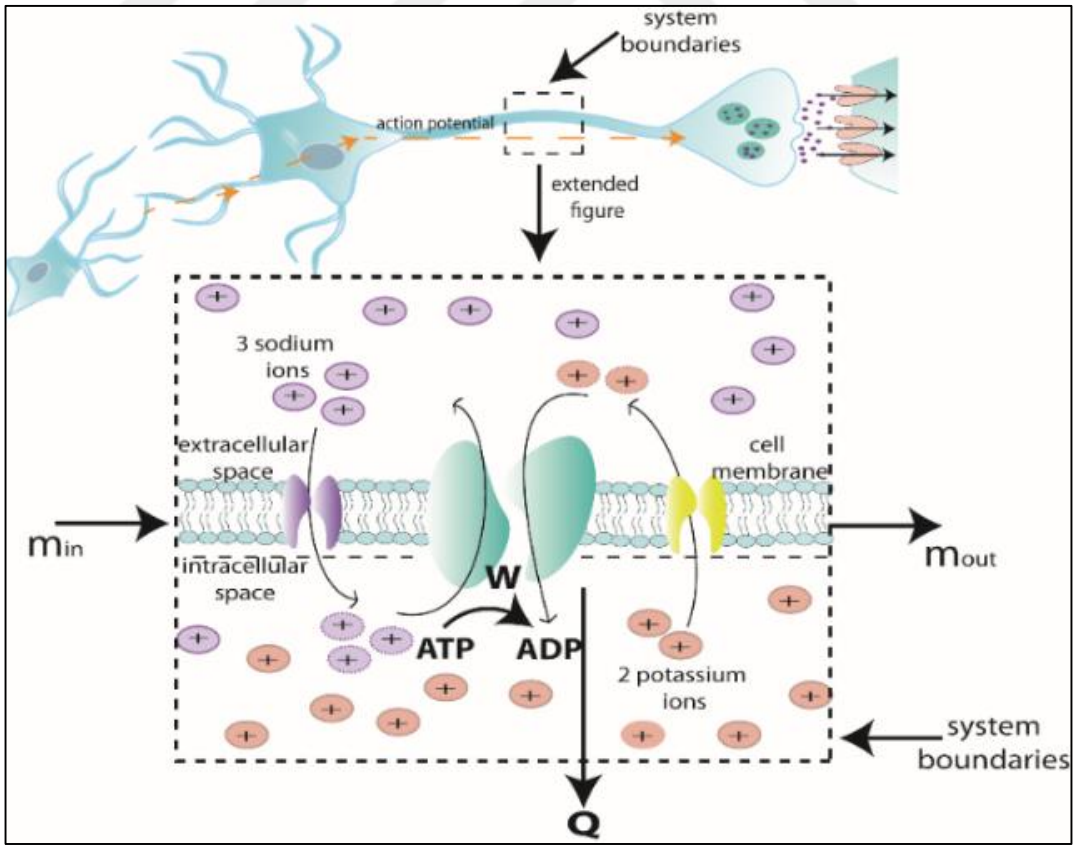

Figure 3.3. Schematic drawing of the axonal model.

The standard Gibbs energy and the enthalpy of formation of the chemical species involving in the biochemical reaction were calculated based on the method developed by Alberty [89] similarly as Genc et al. [21] and Yalçınkaya et al. [23].

Gibbs free energy and exergy of the metabolites are listed in Table B.1 for the prevailing physiological conditions. Exergy destruction of the ATP hydrolysis process and ATP production during aerobic respiration of the squid giant axon were computed as:

$$Ex_{destr} = Ex_{ATP} - Ex_{P,} - Ex_{ADP} + Ex_{H_2O} \tag{3.56}$$

$$Ex_{destr} = Ex_{GLU} + 6Ex_{O_2} - 6Ex_{H_2O} - 6Ex_{CO_2} \tag{3.57}$$

Entropy generation was derived from the sum of the exergy destruction calculated in equations (8) and (9) as;

$$S_{gen} = Ex_{destr}/T \tag{3.58}$$

Thermodynamic analysis of the energy allocation for an action potential was contributed. Energy supplied for action potential was calculated by referring to the Hodgkin and Huxley theory based on the Na^+ kinetics [70]. The total Na^+ ion load of the action potential over the entire process was estimated for squid giant axon with the same procedure as Sengupta et al. [98]. The Na^+ ion loads were multiplied with $N_A/3F$ (N_A is the Avogadro's number and F is the Faraday's constant) to calculate the energy coming from ATP to maintain action potential.

Energy supplied to a neuron was estimated directly from the amount of metabolic energy cost for the ion pumping [99]. Metabolic energy released by dissociation of ATP is the direct energy source for the neuron, where, each mole of ATP may release 46 to 62 kJ of free energy [100]. Thus, entropy generation and exergy destruction can be calculated from the membrane and Nernst potentials and the ion current. As a result, exergy destruction, Ex_{destr}, and entropy generation, S_{gen}, which is a consequence of ATP hydrolysis, $En_{ATP \rightarrow ADP}$, were calculated based on the Hodgkin and Huxley model as;

$$En = \frac{en}{eN_A} \int_t g_{Na} m^3 h (E_{Na} - V) \tag{3.59}$$

$$Ex = \frac{ex}{eN_A}\int_t \; g_{Na}m^3h(E_{Na} - V) \tag{3.60}$$

$$S_{generation} = \frac{s}{eN_A}\int_t \; g_{Na}m^3h(E_{Na} - V) \tag{3.61}$$

where En is energy release, Ex is exergy destruction, S is entropy generation during hydrolysis of 1 mole of ATP and e is an elementary charge of ion, e.g., $1.6x10^{-19}$ Coulombs.

3.5. THERMODYNAMIC ANALYSIS DENDRITIC DISSIPATION

For the Dendritic dissipation, entropy generation and exergy analysis Rinzel and Rall model was used. A cell with other geometries like nerve cell bifurcates extensive massive branching of dendritic trees are more complicated to model requires some assumptions;

i. the neurons are dendritic trees including a cylindrical trunk and other branch components,
ii. membrane electrical properties are uniform over the entire soma-dendritic surface,
iii. external fluid is isopotential and the internal surface of the soma have constant electrical potential,
iv. all the dendritic branching and junctions have continuous internal potential and current,
v. inside the cylinder, the electric current flows axially through an ohmic Resistance offered the "trees equivalent cylinder" approximation which assumed to have M order symmetrical branching in N order identical trees.

Each branch symmetrically bifurcates with satisfying 3/2 power law in an infinitely long cylinder with usual core conductor assumptions and the membrane potential is conserved at all the branching points of the core conductor. The $3/2$ power law, which is employed with this model states that the $3/2$ power of the parent branch is the sum of $3/2$ of two daughter branches (d_1 and d_2):

$$P^{3/2} = {d_1}^{3/2} + {d_2}^{3/2} \tag{3.62}$$

The assumptions of the Rinzel-Rall's [101] model are valid in the present dendritic dissipation, entropy generation and exergy analyses at the input (BI), sister (BS) and two cousins (BC-1and BC-2) branches (Figure 3.4). BI is input branch, BS is sister branch, P and GP is their parent and grandparent branch points and BC-1 and BC-2 are first and the second cousin branches an OT is other trees of the model. In the model N=6, M=3 and L=1.

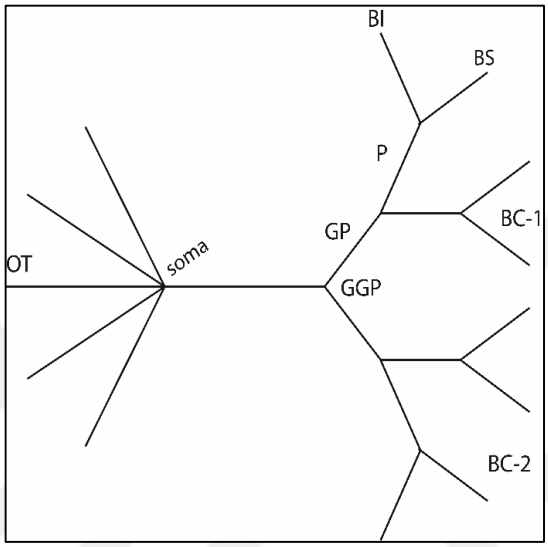

Figure 3.4. Schematic description of branching diagram of a dendritic tree.

The membrane resistivity R_m, neuron input resistance, R_n, intracellular resistivity, R_i, membrane capacitance, C_m, diameter of membrane cylinder, d, and dimensionless conductance ratio, ρ, were the parameters of the analyses carried out with two cat spinal motoneurons (CA-1) [102] and (CA-2) [82], guinea pig vogal motoneuron (GP) [103] and squid giant axon (SA) [82] (Table B.2).

The input current I(T) was simulated with eq (1), where α = 20, electronic length of cable = L and T = the dimensionless time. An individual transient was simulated as an alpha function, its peak transient current $I_p = 10^{-6}$ mA and the rise time = 0.5 ms:

$$I(T) = I_p \propto Te^{(1-\alpha T)} \tag{3.63}$$

Work done by mowing a charge in an electric field was;

$$\dot{W} = Vq \tag{3.64}$$

The semi-log plots for the BI, BS, BC-1and BC-2 nodes along the mainline from BI to the soma of transient membrane potential versus T were drawn by referring to the convolution of I(t) with K(X, T; L) and compared with Rinzel and Rall's model. After the verification of the model, the convolution times, T, was replaced with the dimensionless time. Dissipation, entropy generation and exergy loss at each branch were calculated with respect to the position for all times.

3.6. DEFINITION OF PIG HEART SYSTEM AND KINETIC SIMULATION

Kinetic and thermodynamic investigation of pig isolated heart metabolism during resting and active state TCA cycle, oxidative phosphorylation and metabolic transport considered with using data sets published by Bose et al. [104], respectively. In both systems, ATP produced via aerobic metabolism where pyruvate is a substrate, utilized in the consequent muscle contraction that drives blood flow through the entire body. The whole systems, heart divided into three subsystem spaces, compartments, cytoplasm, mitochondrial intermembrane space and mitochondrial matrix donated with c, i and x, respectively. In total, 61 state variable considered where 39 flux expression included, TCA cycle, oxidative phosphorylation, substrate & cation transport and passive permeation fluxes (Table C.1).

During contraction and relaxation period kinetic mechanisms of metabolic activity, TCA cycle, oxidative phosphorylation, and metabolic transport reactions simulated work provided by Wu et. al [105]. All initial concentration values of biochemical reactants and model parameters enzyme maximal fluxes are driven by Wu et al. [105] is work. It is nearly impossible to measure all metabolite concentration in each time step in experimental setup and thermodynamic behavior of cell highly dependent on those concentration levels. Consequently, a general mathematical model approach was used to simulate the metabolite concentration gradient in time in the heart.

Kinetic analysis of basal and active energy metabolism was simulated under unsteady-state conditions with using COPASI 4.4.24 modeling platform with Deterministic Livermore solver of ordinary differential equation method in a time course regime. Simulations of states pig heart were performed 30s with the 0.5-time step where concentration variation of

metabolites, reaction fluxes, overall exergy destruction, and work potential with time were generated.

The model assumptions were as follows:

i. The heart system of pig works under unsteady-state with moving boundaries,
ii. There is no anaerobic metabolism involved only aerobic respiration takes place
iii. Pyruvate is selected as a substrate the subsystem under investigation selected as a mitochondrial matrix.
iv. Temperature (T=37^0C) is taken as distributed uniformly throughout the subsystems.

3.6.1. Pig Heart Work Analysis

The heart is an open system with moving boundaries where pressure and volume of ventricles changing throughout heartbeat that increase with the level of exercise. Mammalian heart has two parts right and left, where venous blood received from the right ventricle through thevenae cavae which pumped after by the pulmonary artery to the lungs. The blood is circulated in the respiratory system for gas exchange, oxygenation that flows thru pulmonary veins to the left part of the heart. The blood is circulated to the whole body, organs which will initiate another cardiac cycle. In one cardiac cycle, two phases occur; systole phase occurs when heart contracts to pump out the blood and diastole occurs when relaxed after contraction.

Although, various type of work done by heart negligibly small [106] work consumed for pumping blood is not. Since heart two sides considered as two pumps the total work done by the system is calculated with approximating work done by the left and right ventricles. The work was done by left ventricle in a cardiac cycle was calculated via;

$$W_L = SVxP_{ss} \tag{3.65}$$

where SV is stroke volume and P_{SS} is systematic systolic blood pressure. Also can be calculated from PV diagram with trapezoidal rule. Thus, work done by the right ventricle in a cardiac cycle was calculated with the same method illustrated as;

$$W_R = SVxP_{ps} \tag{3.66}$$

where P_{ps} pulmonary systolic pressure and the total work done by the system was calculated as;

$$W_H = W_L + W_R = SVx(P_{ps} + \ P_{ss}) \tag{3.67}$$

3.6.2. Pig Heart Thermodynamic Analysis

The system boundaries correspond control volume which is permeable to mass and energy transfer. A thermodynamic analysis was performed with analytical solving of mass and energy Equations 3.1-3.

Maximum work that can be extracted is equal to exergy of a substance when the system is in the thermal, mechanical and chemical equilibrium state with its surroundings due to reversible processes. Unsteady flow systems exergy balance is given in Equation 3.4.

The system investigated for both resting and active state under unsteady state conditions. In the governing equations, left-hand side of equal sign states the exergy change with respect to time in a control volume. $\sum(\dot{mex})_{in} - \sum(\dot{mex})_{out}$ terms denotes mass inflow and outflow exergies, $\dot{W} + P_0 \frac{dV}{dt}$ terms denotes surrounding work term and $\dot{X}_{dest}$ denotes exergy destruction rate in the control volume. In the model, $\oint \dot{Q} \sum \left(1 - \frac{T_0}{T}\right)$ denotes exergy transfer due to heat transfer.

Biological systems exergy of reactants can be calculated considering its chemical and physical exergy. The biomolecules considered in the system and subsystems are at the mammalian body temperature and pressure. In the system, inflow and outflow streams have different compositions which make difference between the entropy of a substance under this specific physiological and its entropy at the dead state. Therefore, exergy of the metabolite is the sum of its chemical exergy, the transformed Gibbs energy of formation and exergy change of species due to its concentration where R is the universal gas constant and c_j is the

concentration of the j^{th} biomolecule in the solution. In the unsteady state system, exergy of system or subsystem at a specific time step is the sum of its chemical and physical exergies at that time step. Metabolites standard Gibbs free energy and enthalpy of formation were estimated under the physiological conditions where pH=7.27, T=310.15 K and I=0.14 M illustrated at Table C.2.

4. RESULTS AND DISCUSSION

4.1. THERMODYNAMIC ANALYSIS OF SQUID MANTLE MUSCLE

Enthalpy, Gibbs free energy and exergy of the metabolites under physiological conditions in squid muscle cell in (pH=7, T=298.15K, and I=0.25M) illustrated in Table A.1. Thermodynamical data for two metabolites, arginine and octopine could not be found in the literature, therefore estimated with the group contribution method. Thermodynamic calculations were conduct based on method, Table 4.1 lists the glucose oxidization and ATP formation reactions, and the changes of their enthalpy, Δh_{rxn}, and Gibbs free energy, Δg_{rxn}.

Table 4.1. Metabolic reactions occurring during the slow swimming mode in the SMR fibers and during the jet escape in the CMP fibers [23].

Slow Swimming Mode: ➢ ATP produced through aerobic energy metabolism. ➢ SMR fibers are engaged.				
		Reaction Rate (μmol/(gs))	ΔH_{rxn} (kJ/mol)	ΔG_{rxn} (kJ/mol)
SMR1	$Glu + 6\ O_2 \Rightarrow 6CO_2 + 6\ H_2O$	$6.48x10^{-4} – 1.85x10^{-3}$*	-4540.34	-3930.39
SMR2	$ADP + P_i \Rightarrow ATP + H_2O$	$1.94x10^{-2} – 7.04x10^{-2}$ **	-22.93	-36.31
Jet Escape Mode: ➢ ATP produced both through aerobic and anaerobic energy metabolisms. ➢ Mostly CMP fibers are engaged.				
		Reaction rate (μmol/(gs))	ΔH_{rxn} (kJ/mol)	ΔG_{rxn} (kJ/mol)
CMP1	$Glu + ATP \Rightarrow G6P + ADP$	$1.00\ x10^{-4}$	-22.50	-21.00
CMP2	$Glu + 2\ NAD + 2\ ADP + 2\ P_i \Rightarrow 2\ PYR + 2\ NADH + 2ATP + 2\ H_2O$	$6.14x10^{-3}$	182.04	-381.73
CMP3	$PYR + ARG + NADH \Rightarrow OCT + NAD + H_2O$	$1.02x10^{-2}$	-52.42	-18.19
CMP4	$2\ PYR + 2\ H_2O + 3\ NAD \Rightarrow SUC + 2\ CO_2 + 3\ NADH$	$1.06x10^{-3}$	-432.13	-779.68

In the Table * sign refers to reaction rate depends on various parameters, such as the swimming velocity, mass of the squid, tail- or arms- first positioning, angle of attack. In this

study, calculations for the slow swimming mode has been performed assuming a swimming velocity of 0.5 mantle length/s and a corresponding O_2 consumption of $9.72x10^{-4}$ μmol/(gs). For the jet escape, swimming velocity is taken as 3 mantle length/s and the O_2 consumption as $16.67x10^{-4}$ μmol/(gs). These values correspond to the measurements of Finke et al. [43]. ** sign is the number of ATP produced through an aerobic pathway varies between 30 and 38 moles of ATP per mole of glucose.

These results showed that if the squid muscle would be ideal, i.e. if all the reactions and fiber motions would occur without any losses ($Ex_{dstrctn}$=0), then a maximum work of 3930.39 kJ would be produced by consuming one mole of glucose. A heat removal of 609.95 kJ/mol of glucose would accompany this work production.

Bartol et al. [47] measured the O_2 consumption by squid in slow swimming mode between 14.41- 40.71 μmol O_2/(h g). The most important parameters that affect the O_2 consumption rate is the body size and swimming velocity. A 65 g squid swimming at 0.5 mantle length per second, consumes about 21 μmol O_2/(h g). Under these conditions, glucose oxidization releases an enthalpy of 4.41 J/(kg s) and exergy of 3.82 J/(kg s). Aerobic metabolism produces 30-38 moles of ATP/mol of glucose. The case of 30 moles, e.g., 0.029 mol/(kg s), of ATP production is capable of doing 1.06 J/(kg s) of work, when all of the ATP is hydrolyzed. The ratio glucose oxidation exergy to the work can be extracted points 28 percent of the available chemical exergy is used to produce ATP. The variation of the Δg_{rxn} of the reactions SMR1 and SMR2 depending on the oxygen consumption rate is shown in Figure A.1.

During the jet escape, the metabolic pathway switches to anaerobic reactions and CMP fibers are engaged. Finke et al. [43] measured the change in metabolic concentrations during the jet escape. Their findings show that the squids switch to the anaerobic metabolism at speeds higher than ca. 2 mantle length s^{-1} and accumulate octopine, glucose-6-phosphate, and succinate.

It is worth noting that, these reaction schemes represent a simplified model for anaerobic metabolism. In the actual metabolism, hundreds of reactions occur simultaneously. For example, during the succinate production, the first oxaloacetate is formed from pyruvate, during which reaction one mole of ATP is consumed. Later, pyruvate and oxaloacetate react to form succinate, during which one mole of ATP is produced.

The 5 reactions were summarized as CMP4 in Table 4.1. The purpose of such a model is to describe the whole pathway with as few apparent reactions as possible. The model which is simple enough for through thermodynamic analysis, but also presents sufficient detail to account for the metabolite concentration changes measured *in vitro* [43].

Experimental data showed that squids performing jet escape for 15 minutes accumulate 0.09 mmol G6P, 0.95 mmol succinate and 9.16 mmol octopine per g of body mass [43]. Depending on these measurements, the rates of the reactions were calculated and listed in Table 4.1. Since mass accumulation occurs during the jet escape $\oint \frac{dE}{dT}$ and $\oint \frac{dEx}{dT}$terms are non-zero, the cyclic integral of the surroundings work$\oint P_0 \frac{dV}{dT}$ and $\oint \dot{Q}\left(1-\frac{T_0}{T}\right)$ terms are zero, as in the case of the slow-swimming mode. Multiplying the Δg_{rxn} values were listed in Table A.1 with the reaction rates showed us that 3.35 J/(kg s) of chemical exergy is released during the jet escape. In other words, the maximum reversible work that the squid can produce during a jet escape was 3.35 J/(kg s). Finke et al. [43] measured a decrease of the cellular ATP concentration $\left(\frac{dc_{ATP}}{dt} = -0.02\mu mol/gs\right)$, which means that during jet escape the amount of ATP produced via anaerobic respiration does not meet the demand for the muscular ATP consumption. The rate of ATP consumption is then calculated as:

$$r_{ATP} = 2r_{CMP2} - r_{CMP1} - \frac{dc_{ATP}}{dt} = 14.18\frac{\mu mol}{gs} \tag{4.1}$$

Hydrolyzing this ATP releases exergy of 0.51 J/(kg s), which is used up to perform work and overcome irreversibilities.

During swimming, a squid has to generate force in both vertical and horizontal directions, since squids are negatively buoyant. At high speeds, lift is generated via the kinetic energy difference on the upper and lower surfaces of the squid. However, at low swimming speeds, lift generation becomes a major issue and must be generated via the movement of fin and arms. Experimental observations state that at low speeds about 85 percent of the total muscle work is consumed for lift generation [47]. Squid's main mechanism to produce horizontal force is to eject water with a high momentum in the horizontal direction. The mantle cavity of a squid seems like a pressure vessel since the pressure in the mantle cavity can reach up to 25 kPa above the atmospheric pressure [40]. Water filled in the mantle cavity is

pressurized and ejected through squid's funnel. As the squid contracts the mantle cavity, both pressure and volume of the cavity change. A work of ∫PdV was applied to the water inside the mantle cavity. Figure 4.1a and Figure 4.1b showed that how the diameter and thickness of the mantle wall vary for a squid. It was realized that the initial diameter of the mantle cavity in jet escape mode was more significant than the initial diameter of the mantle cavity in slow swimming mode. However, the final diameter of the mantle cavity in jet escape mode was smaller than the final diameter of the mantle cavity in slow swimming mode (Figure 4.1). Diameter changes imply that a squid inflates her mantle cavity more in jet escape mode than slow swimming mode to draw a larger amount of water to be used for ejection later. Then the mantle cavity diameter in jet escape mode drops about 40 percent of its initial value implying that the amount of water driven in this mode appears to be maximized. Furthermore, it was noticed that the mantle thickness in jet escape mode is nearly 35 percent more than the mantle thickness in slow swimming mode because jet escape mode requires larger mantle wall thickness to sustain build up pressure inside the mantle cavity (Figure 4.1).

The mantle cavity dimensions for fast and slow swimming modes were given in Table A.2. Based on these data an in-house Matlab code was developed to calculate the work transferred to the water inside the mantle cavity.

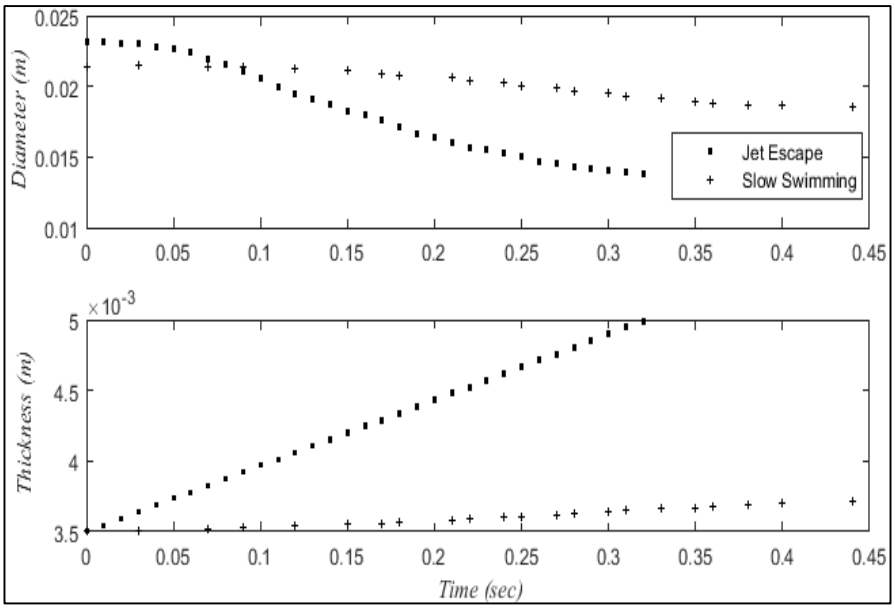

Figure 4.1. Change of a mantle cavity diameter and wall thickness with time during ejection of water.

Squid mantle cavity volume versus time was plotted in Figure 4.2a, for both fast and slow swimming modes. The volume of the mantle cavity was $V = \pi r^2 L$, where, r is the radius of the mantle cavity at any location and L is being the any length along the squid's dorsal mantle length. Volume change of the squid's mantle cavity was calculated with the formula below since radius (r) varies along the dorsal mantle length,

$$\int V = \int \pi[\sin\left(\frac{x\,\pi}{2L}\right) r_{max}]^2 dx \tag{4.2}$$

At the end of the water ejection, the volume decreased by about 35 percent in slow swimming and nearly 65 percent in the jet escape. Besides, the initial volume of the jet escape mode was approximately 20 percent more than the initial volume of the slow swimming mode, and the duration of ejection was about 40 percent longer in slow swimming than that of the jet escape. The volume change implies that the momentum of the jet escape, thus the applied horizontal force, was significantly higher than that of slow swimming. Variation of the pressure inside the mantle cavity with time during ejection of water was plotted in Figure 4.2, where it was demonstrated that pressure inside the mantle cavity could reach up to ten times higher value during jet escape than that attained during slow swimming. Pressure versus the volume of the mantle cavity was plotted in Figure A.3 Boundary work done by the mantle wall was evaluated for both fast and slow swimming modes by calculating the area under the P-V curve of Figure A.2c numerically with the integral ∫PdV. Total boundary work done by circumferential fibers was calculated as 1.6 x 10^{-4} J/(s g body mass) and 5.32 x 10^{-6} J/(s g body mass) for fast and slow swimming, respectively.

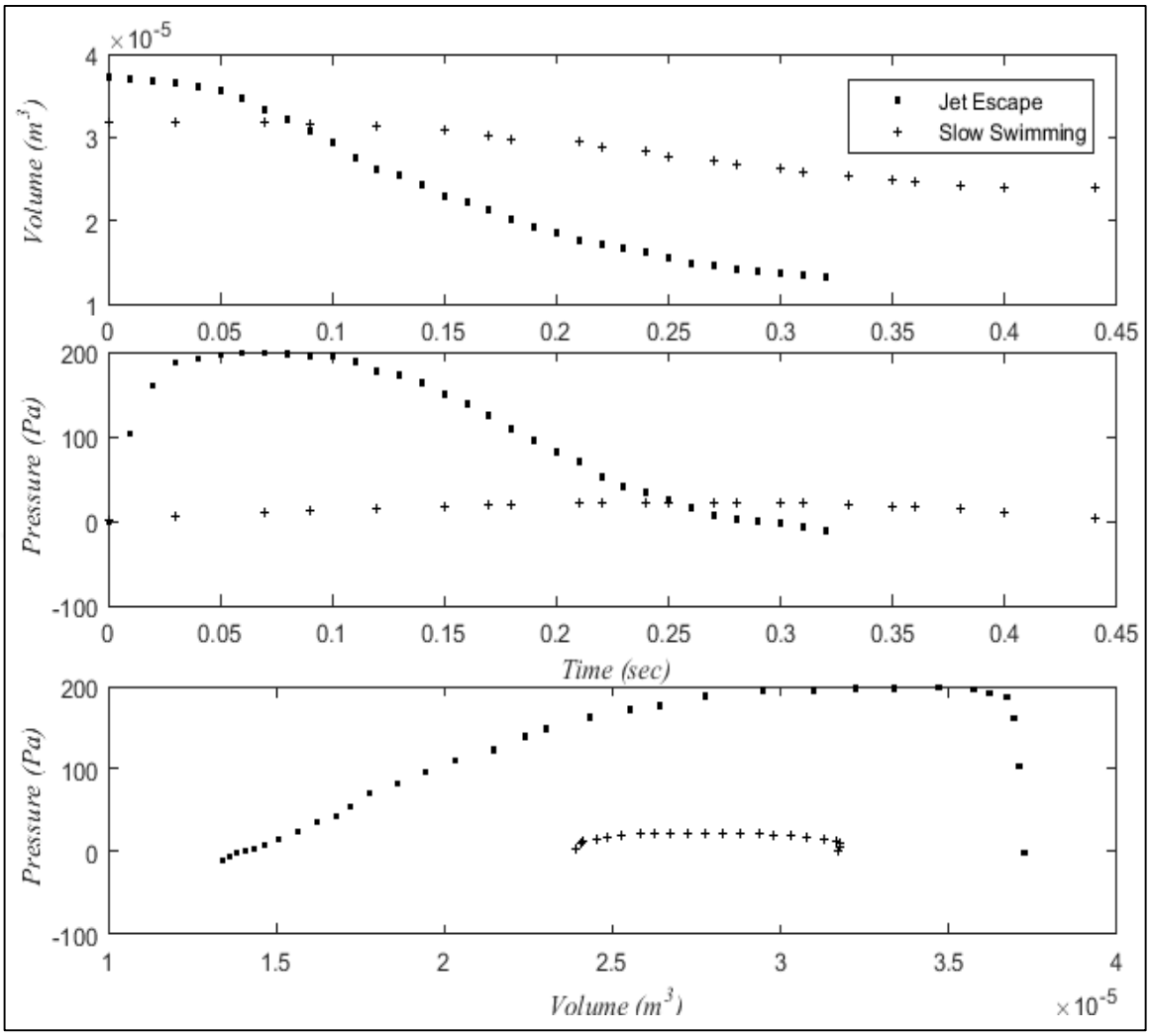

Figure 4.2. Variation of volume and pressure in the mantle cavity with time during ejection of water, and pressure versus the volume of the mantle cavity during ejection of water.

The muscle contraction work via muscle contraction was estimated with using force and displacement values. The total work done was calculated to be 4.35 x 10^{-4} J/(s g body mass) and 1.13 x 10^{-4} J/ (s g body mass) of fast and slow swimming modes, respectively. Summary of the main results of the muscle work models was given in Table 4.2 and Figure 4.3-4.

Table 4.2. Summary of the main results of the muscle work models [23].

	Slow swimming	Jet escape
Respiration Mode	Steady state aerobic respiration	Aerobic + anaerobic respiration accompanied with an accumulation of chemicals
Engaged muscle group	SMR fibers	CMP fibers
The rate of the exergy release due to aerobic respiration	3.82 J/(kg s)	6.55 J/(kg s)
The rate of the exergy release due to anaerobic respiration	0	3.35 J/(kg s)
The rate of the chemical exergy consumed from the cellular reserves	0	0.072 J/(kg s)
TOTAL EXERGY CONSUMED	3.82 J/(kg s)	9.97 J/(kg s)
The rate of the exergy release due to ATP hydrolysis	1.06 J/(kg s)	2.33 J/(kg s)
Respiration efficiency	27.7percent	Only aerobic: 27.7percent Only anaerobic: 13.2percent Overall: 23.37percent
Fin Power	0.27 J/(kg s)	0
Muscle contraction power	0.11 J/(kg s)	0.44 J/(kg s)
Power transferred to the ejected water	0.0053 J/(kg s)	0.16 J/(kg s)
TOTAL WORK OUTPUT	0.28 J/(kg s)	0.16 J/(kg s)
Percentage of the ATP exergy converted into work	26.41percent	6.87percent
Contraction efficiency	4.7percent	36.8percent
Exergy destruction rate	3.54 J/(kg s)	9.81 J/(kg s)
Entropy generation rate	0.01189 J/(kg s K)	0.03291 J/(kg s K)
Estimated life span	30.4 years	11.0 years

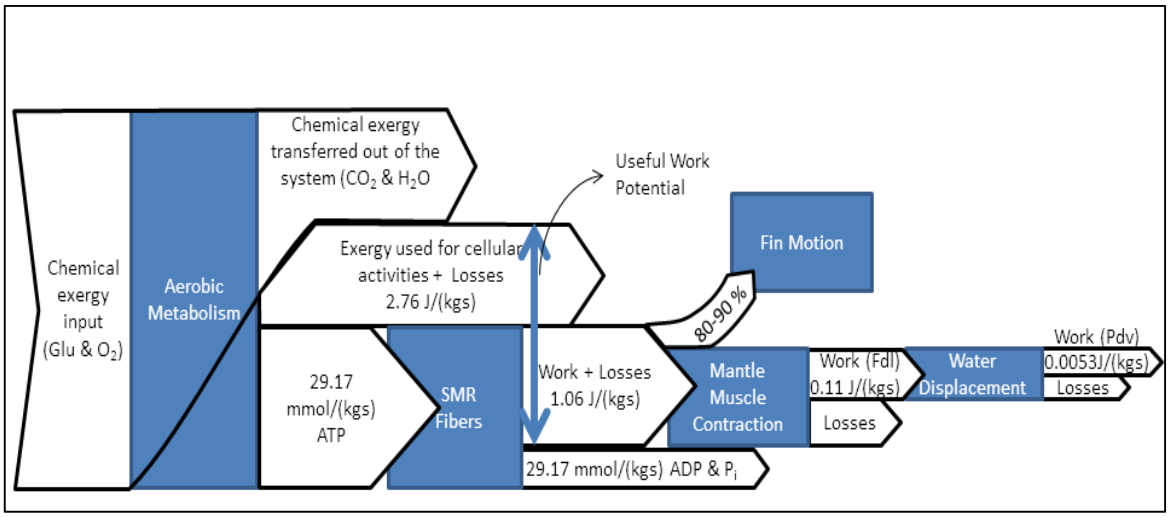

Figure 4.3. Exergy charts for the steady-state slow swimming of the squid [23].

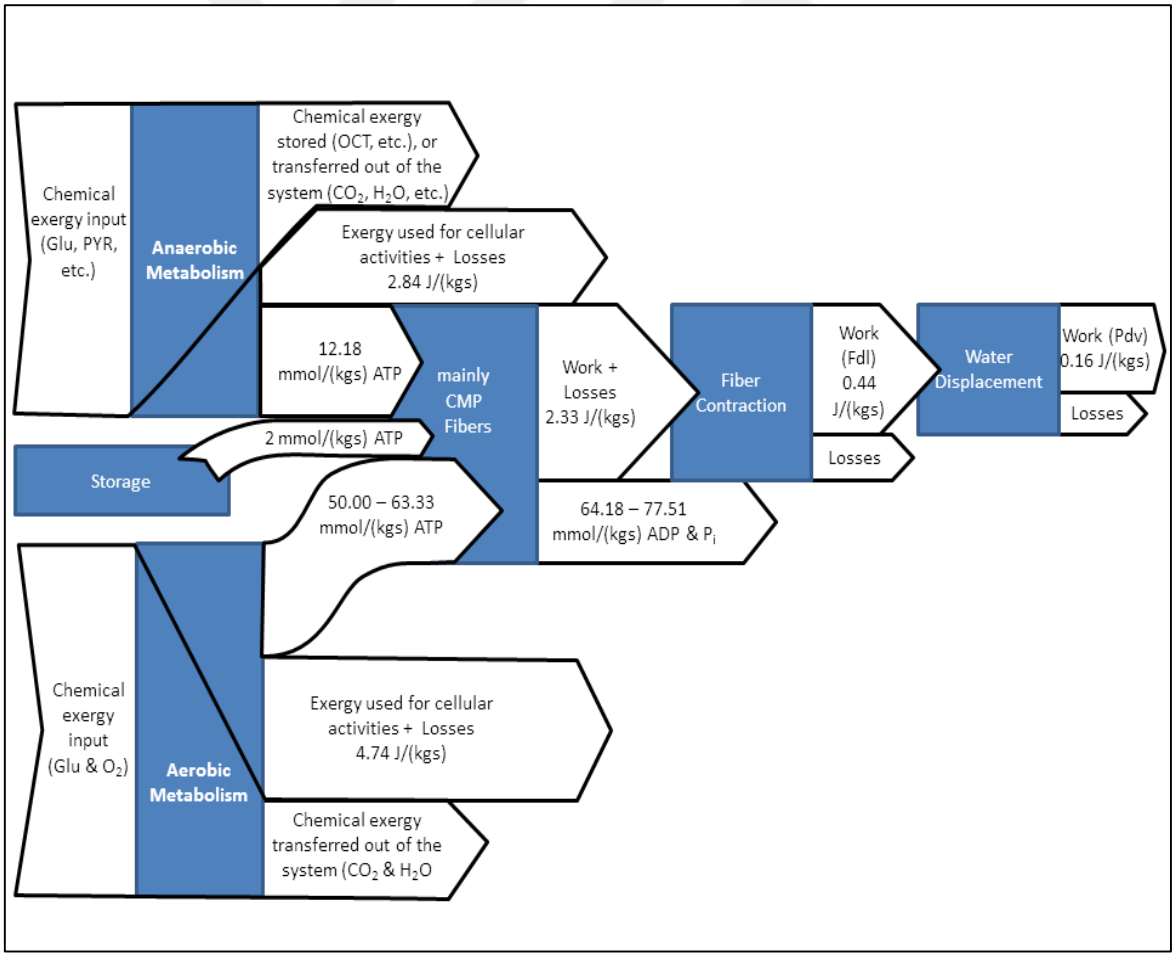

Figure 4.4. Exergy charts for the jet escape of the squid [23].

Note that during slow swimming only the SMR fibers are engaged. The CMP fibers, which make up ca. 95 percent of the mantle volume, are not activated (Figure 2.7) which means that during slow swimming, some of the muscle work generated by the SMR fibers has to be consumed to compress the passive mantle tissue. During slow motion 1.13 x 10^4 J/(s g) of work was generated due to muscle contractions. These muscle contractions are used to compress the mantle cavity and pressurize the water inside it. The work transferred to water via mantle compression was calculated in the previous section as 5.32 x 10^6 J/(s g), i.e. only 4.7 percent of the performed muscle work. During the jet escape, a larger volume of fibers was engaged and the passive part of the mantle tissue is only 5 percent (Figure 2.6). Therefore, a larger percentage (36.8 percent) of the generated muscle work was transferred to the water.

Thermodynamic analysis of the steady-state slow swimming showed that oxidation of glucose within the squid mantle releases exergy of 3.82 J/(kg s). Depending on whether 30 or 38 moles of ATP are produced per 1 mole of glucose, 0.029 to 0.037 mmol/(kg s) of ATP is produced. We assumed that during slow swimming, ATP concentration remains steady. Accordingly, exergy of 1.05 to 1.34 J/(kg s) was stored in the produced ATP, which can be converted into mechanical work via muscle fiber contraction (Fdl). Exergetic efficiency of the respiration was defined as:

$$\eta_{respiration} = \frac{exergy\ released\ via\ ATP\ hydrolysis}{exergy\ released\ during\ respiration} \tag{4.3}$$

Then, the exergetic efficiency of the squid aerobic respiration was:

$$28\ \% = \frac{1.05\,J/(kgs)}{3.82\,J/(kgs)} \leq \eta_{respiration,aero} \leq \frac{1.34\,\frac{J}{kgs}}{3.82\,\frac{J}{kgs}} = 35\ \% \tag{4.4}$$

Mantle muscle fiber contraction work (Fdl) was calculated as 0.11 J/(kg s) based on empirical data. Fiber contraction work result means that 8 to 11 percent of the exergy stored in ATP is used to perform mechanical work via the mantle SMR fibers. This result is in agreement with the previous observations [47,107], which state that during slow swimming approximately 85 percent of the muscle work is performed by the fin and the arms to generate

lift for the negatively buoyant squid. Lift generation is a major issue at low speeds. At high speeds, on the other hand, lift is generated via the kinetic energy difference on the upper and lower surfaces of the squid, and no special fin movement is necessary. If we assume that 85 percent of the ATP is consumed for the fin motion and that ATP chemical exergy is converted into useful work with a 30 percent efficiency then fin power was estimated as 0.27 J/(kg s) [108] (Table 4.2).

The work transferred to the ejected water (PdV) was calculated as 0.0053 J/(kg s). This means that about 0.5 percent of the exergy stored in ATP is transferred to the water ejected from the mantle cavity to the surrounding water. This is a negligible amount, proving that the squid does not use water jet momentum transfer as its primary mode of propulsion during slow swimming. The total work output during slow swimming was the sum of the Pdv and fin work, which is 0.28 J/(kg s). This means that 26.41 percent of the exergy stored in ATP is converted into useful work.

Contraction efficiency was defined as follows:

$$\eta_{contraction} = \frac{work\ transferred\ to\ ejected\ water\ (PdV)}{muscle\ contraction\ work\ (Fdl)} \tag{4.5}$$

$$\eta_{contraction} = \frac{0.0053}{0.11} = 4.7\ \% \tag{4.6}$$

The contraction efficiency during slow swimming was only ca. 5 percent. During the slow swimming, the SMR fibers are engaged, and the rest of the mantle tissue is passive. This result showed that about 95 percent of the work done by the SMR fibers is used up to compress the passive mantle tissue, and only about 5 percent can be employed to increase the cavity pressure.

During the jet escape, energy comes from both from the aerobic and anaerobic respiration. Oxygen consumption rate increases nearly linearly between 0.5-4 mantle length/s. Therefore, at a speed of 3 mantle length/s, squid consumes a large amount of oxygen; and about 6.55 J/(kg s) of exergy is released via aerobic respiration, which is near twice the amount of exergy as the previous case. The chemical exergy released via the anaerobic pathway was 3.35 J/(kg s). About 0.072 J/(kg s) of the chemical exergy comes via depleting the cellular ATP reserves.

The exergetic efficiency of the squid anaerobic respiration was:

$$\eta_{contraction} = \frac{0.44\ J/(kgs)}{3.35\ J/(kgs)} = 13.2\ \% \tag{4.7}$$

A squid swimming with a speed of 3 mantle length/s, produces exergy of 2.33 J/(kg s) via ATP hydrolysis. 0.44 J/(kg s) of this comes from ATP produced via anaerobic respiration, 0.07 J/(kg s) comes from the ATP used up from cellular reserves, and 1.82 J/(kg s) comes from ATP produced via aerobic respiration. Since the jet escape, swimming speed (3 mantle length/s) is very close to the critical speed (2 mantle length/s) at which anaerobic respiration begins; the squid still uses the aerobic pathway extensively to produce the required ATP. One can speculate that if the swimming speed would be higher, than the ATP production rate from the anaerobic pathway would increase dramatically so that a much higher percent of the consumed ATP would come from the anaerobic pathway. Here, at this low jet escape speed, still, 78 percent of the consumed ATP comes from the aerobic pathway. Therefore, the respiration efficiency of the overall system, which is 23.37 percent, is close to the aerobic respiration efficiency.

The animals in nature generally prefer to stay in steady state conditions. The squids also not depart from this rule. Squid generally prefers the steady-state swimming mechanism in their lifetime unless they are in danger or when they are hunting. The squid switches its swimming behavior for survival or to capture the prey. When the squid switches to the jet escape swimming mode, it means a drop in the respiration efficiency. At very high speeds, squids may be forced to use the anaerobic pathway exclusively, which would drop the respiration efficiency to 13.2 percent.

Mantle muscle fiber contraction work during the jet escape (Fdl) was calculated as 0.44 J/(kg s) based on empirical data which indicates 84 percent of the chemical exergy stored in ATP is converted into mechanical work by the mantle CMP muscles. Rest of this exergy may be used up as muscle work in other parts of the squid body, or to overcome the irreversibilities. The high ratio of contraction work to ATP hydrolysis exergy shows that during the jet escape, the squid consumes nearly all of its resources to contract the mantle.

The contraction efficiency during a jet escape is much higher than the slow speed contraction efficiency:

$$\eta_{contraction,jet} = \frac{0.16}{0.44} = 37\ \% \tag{4.8}$$

The volume of the engaged muscles during a jet escape is 20 times larger than the slow swimming. Thus, the passive volume in the mantle tissue during a jet escape is only about 11.8 percent (as opposed to 95.6 percent during slow swimming). Percentage of the passive tissue (tissue that is not activating during contraction) and contraction efficiency seems to be proportional. As the passive tissue decreases to $1/8^{th}$, contraction efficiency increases 8 times.

Calculations showed that a squid swimming slowly (0.5 mantle length/s) consumes exergy of 3.82 J/(kg s) and produces 0.28 J/(kg s). The difference between these values gives us an estimate of the exergy destruction rate, which was 3.54 J/(kg s). In addition to that, the squid destroys exergy of 0.034 J/(kg s) during the action potential propagation in the giant axon. The total exergy destruction rate during slow swimming is 3.57 J/(kg s). This corresponds to an entropy generation rate of 0.01198 J/(kg s K).

In the jet escape mode, anaerobic respiration begins. The extent of the anaerobic respiration depends on the swimming speed. As the swimming speed increases, ATP consumption rate increases. The overall system tries to generate ATP through the aerobic pathway as long as oxygen concentration allows; depletes the cellular ATP reserves, and generates the additional ATP through the inefficient anaerobic pathway. Even though the efficiency of the biochemical reactions drops, the mechanical efficiency during a jet escape is high. During the jet escape, a much larger volume of the muscle fibers are engaged, and the passive tissue, that the contracted fibers have to compress occupy a much smaller volume. The contraction efficiency during a jet escape is about eight times larger than that of the slow swimming.

During jet escape at three mantle length/s, the squid consumes chemical exergy of 9.97 J/(kg s), produces a work of 0.16 J/(kg s), which lead to an exergy destruction rate of 9.81 J/(kg s). The exergy destruction rate in the giant axon increases with respect to the slow swimming mode, because of two reasons: ATP production under hypoxic conditions is less exergy efficient, and a higher rate of signal emission is necessary. 0.101 J/(kg s) of exergy was

destroyed for the action potential propagation. The total exergy destruction rate was 9.91 J/(kg s) and the entropy generation rate is 0.03291 J/(kg s K).

Squids are able to swim at very high speeds, such as 25 mantle length/s during the jet escape. In such a case the respiration efficiency would approach to 13.2 percent, and the entropy generation would occur at a much higher rate.

Muscle work efficiency is widely studied with both analytical methods [108–110] and experiments [111,112]. In these studies, muscle efficiency is usually defined either via the first law efficiency, i.e. the ratio of the produced work to the chemical energy ($\eta_I = W/\Delta H$), or the second law efficiency, i.e., the ratio of the produced work to the maximum work ($\eta_{II} = W/W_{max} = W/\Delta G$). Sorgüven et al. [108] recently calculated the theoretically maximum first and second law efficiencies as 0.84 and 1.0, respectively, and compared these values to the experimentally measured muscle efficiencies, which ranged between 0.35 and 0.14 for the first law efficiencies, and between 0.42 and 0.17 for the second law efficiencies. These are efficiencies measured from isolated muscle groups. In this study, the ratio of the produced work to the ATP exergy was calculated for the fast and slow swimming modes as 0.26 and 0.069, respectively. These values are in agreement with the experimentally measured second law muscle efficiencies. Nevertheless, a direct comparison with the published muscle efficiencies should be made with caution. In this study, calculations were performed based on the measurements made from the whole body of the squid. Therefore, the consumed chemical exergy is not only used to generate muscle work, but also to perform basal metabolic activities. Hence, the calculated efficiencies are expected to be lower than the efficiencies of isolated muscle fibers.

4.2. THERMODYNAMIC ANALYSIS SQUID AXON ACTION POTENTIAL

The selected temperature effects on the Hodgkin and Huxley model was computed in squid giant axon after multiplying activation and inactivation gating variables with Equation 3.48-50. In Figure 4.3, by following the same approach as presented in the literature [98,100,113]. The Na^+ current curves showed that the Na^+ flux was the highest at 6.3ºC, and decreased as temperature increased to 12 and 18.5ºC (Figure 4.5).

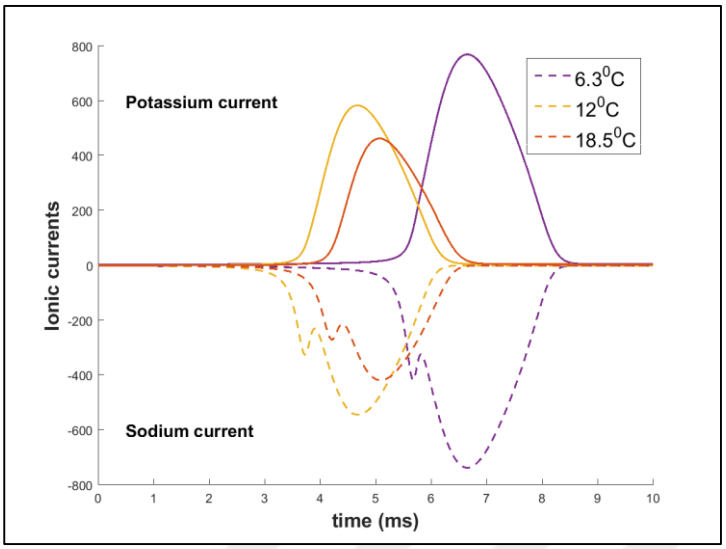

Figure 4.5. Sodium and potassium ionic currents during action potential (a) 6.3 ^{0}C, (b) 12 ^{0}C and (c) 18.5 ^{0}C.

Temperature effects on the Na^+ ion out flux through the cell membrane and the energy cost of this process were plotted versus the temperature in Figure 4.6., where, it was seen that the Na^+ ion flux became more energy efficient with the increase of the temperature, e.g., for a single action potential less ATP is employed than those of lower temperatures.

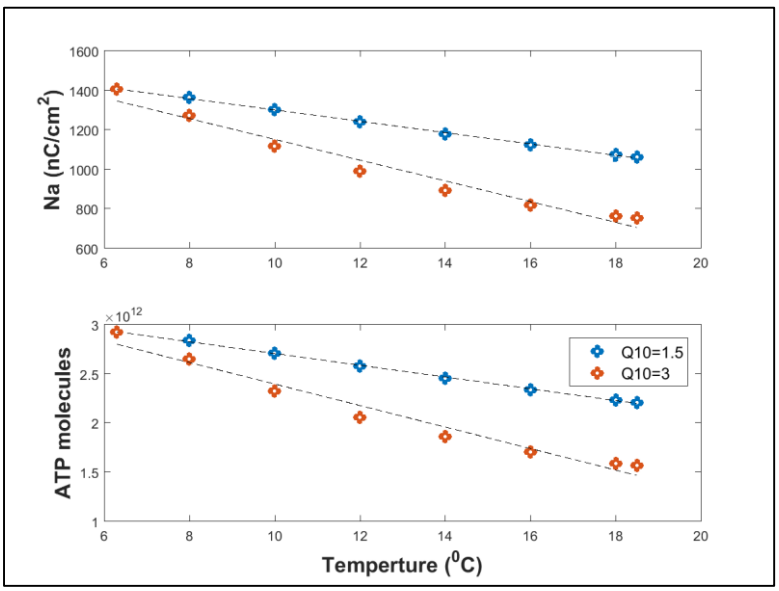

Figure 4.6. Sodium ion entry and related energy cost of the action potential in the temperature range of 6.3 to 18.5 ^{0}C.

The amount of the ATP molecules/cm^2 to produce action potential decreased by 1.87-fold with temperature increase. Na ion transfer loads decreased with temperature increase from 1407.2 nC/cm^2 to 990.75 nC/cm^2 and then 753.14 nC/cm^2 when temperature was 6.3 ^{o}C, 12 ^{o}C and 18.5 ^{o}C, respectively. ATP molecule requirement/cm^2, to supply sufficient energy to transfer Na^+ ions through the cell membrane varies from 2.93 x10^{12} at 6.3 ^{o}C to 1.57 x10^{12} at 18.5 ^{o}C at 6.3 ^{o}C. Wang et al. [99] estimated the demand as 4.94x10^{-12} mole/cm^2 while Sengupta et al. [98] estimated it as 2.3 x10^{12} ATP molecule /cm^2.

In an attempt to estimate the energy release of a single compartment, neuron action potential at different temperatures, the first step was examining the temperature effect on free energy released by ATP hydrolysis. In the previous publication [100] free energy of ATP hydrolysis release roughly, 50 kJ per mole of ATP. However, this free energy release has to be considered as a function of physiological conditions, ionic strength, pH and temperature which constructed as; $E_{ATP} = \Delta G^T{}_{ATP \rightarrow ADP}$. Here we used two approaches for the calculation of Gibbs free energy change of ATP hydrolysis in both simple and more realistic approaches are illustrated in Table 4.3. In the simple approach (R3), Gibbs energy change of a reaction is corrected with Alberty's method [89] for the effects of temperature, ionic strength, valance state and the pH to estimate the standard transformed Gibbs energy of formation of the biomolecules.

Table 4.3. Unit area action potential of sodium load and its thermodynamic cost at 6.3, 12.0 and 18.5 ^{0}C.

			Simple version		More realistic version	
Temperature (^{o}C)	Sodium ion load (nC)	ATP molecule	Energy Release by ATP (kJ)	Exergy destruction (kJ)	Energy Release by ATP (kJ)	Exergy destruction (kJ)
6.3	1407.2	2.93x10^{12}	1.71x10^{-10}	8.21x10^{-11}	1.77x10^{-10}	3.49x10^{-9}
12.0	990.75	2.06x10^{12}	1.21 x10^{-10}	5.48x10^{-11}	1.26x10^{-10}	2.46x10^{-9}
18.5	753.14	1.57x10^{12}	0.93x10^{-10}	4.17x10^{-11}	0.96 x10^{-10}	1.87x10^{-9}

In a more realistic approach, e.g., R4 in Table 4.3, for energy release via ATP hydrolysis the Na^+ and K^+ ion activity was also considered, where Gibbs free energy of each ion was estimated from the expression $\Delta G_{ion} = RTln(c) - 2.303RT(pH)$ as illustrated in Table 4.3. The intracellular and the extracellular concentration of the ions of the squid giant axon are described by Lodish and Zipursky [114]. While the numerical values of the biophysical

parameters were used in the model temperature effects were also taken into consideration. Energy release in the hydrolysis reactions reveals that the ions have a significant effect. The calculations showed that the energy change in a reaction of more realistic approach for 6.3 ^{0}C was -34.46 kJ/mol, where it has been estimated as -8 kcal/mol [115,116] for the squid giant axon. Also, regardless from the approach, temperature also affects the energy release, increasing the temperature increases the energy release of the hydrolysis reaction.

In a single compartment neuron action potential, energy cost was calculated by integrating Na^+ current curve with using equation 3.59 for the simple and more realistic approach. At 6.3 ^{0}C, energy supply to the squid giant axon was estimated as; 1.71x10^{-10} kJ cm^2 with the simple approach, while 1.77x10^{-11} kJ per cm^2 per area with the more realistic approach where Wang et al. [99] estimated the energy supply as 2.468x10^{-7} J/cm^2, where energy release assumed to be 50 kJ/mol, while Moujahid and d'Anjou [117] estimated it as 152 nJ/cm^2 with a non-ion counting approach. The energy release can be thought of as the work production potential of ATP, $W = NE_{ATP}$, where N is the ATP flux and E_{ATP} is the energy released by an ATP molecule. According to a more realistic approach, it is seen that with taking account ions energies, the energy release from ATP hydrolysis for Na^+/K^+ pump was approximately 0.96-fold more than that of the simple approach. Regardless from methods, the temperature has an effect on energy supply to an action potential, as temperature increases, the amount, of energy supply decreases, almost half of the energy is needed at 18.5 ^{0}C than what was calculated for 6.3 ^{0}C. Since the estimation of the energy of the reactions are affected by the physiological condition of the neurons, the concepts of the second law thermodynamics, such as entropy and exergy also depend on these factors. Standard Gibbs free energy of formation are affected by temperature, ionic strength, pH and concentration (Table B.1); H^+ ions are not conserved in biochemical reactions since the pH of the system acts as a buffer for these ions [118].

Exergy destruction when calculated with the simple approach (Table 4.3-R3) and the more realistic model (Table 4.3-R4) were substantially different, e.g., the simple approach predicts 8.21x10^{-11} kJ/cm^2 while the more realistic approach estimates 3.49x10^{-9} kJ/cm^2 (Table 4.3). The ratio of the exergy destruction, when calculated with the simple approach to the one

calculated with the more realistic model, was 0.02 at 6.3 ^{o}C. With the simple approach exergy destruction was 8.21 x10^{-11} kJ/mol cm^2 at 6.3 ^{0}C and with almost two-fold decrease 4.17 x10^{-11} kJ/mol cm^2 at 18.5 ^{0}C. In the simple approach, estimates of exergy destruction

during action potential did not change with temperature and fluctuated in the range of 16.80 squid giant axon exergy destruction at 0.17 kJ/mol cm^2 (Table 4.4).

Table 4.4. Metabolic reactions of energy supply via ATP hydrolysis in 1-mole basis at I=0.25 M and pH=7 at T=6.3, 12.0 and 18.5 ^{0}C.

Reactions		Energy release (kJ/mol)			Exergy destruction (kJ/mol)		
		6.3ºC	12.0ºC	18.5ºC	6.3ºC	12.0ºC	18.5ºC
R 1	$Glu + 6O_2 \rightarrow 6H_2O + 6CO_2$	-3929.18	-3916.66	-3902.45	4066.05	4056.32	4045.29
R 2	$Glu + 6O_2 + 30ADP + 30P_i \rightarrow 6H_2O + 6CO_2 + 30ATP + 30H_2O$	-2661.26	-2640.1	-2615.09	3457.93	3453.02	3446.55
R 3	$ATP + H_2O \rightarrow ADP + P_i$	-35.22	-35.46	-35.76	16.98	16.76	16.63
R 4	$3Na^+_{in} + 2K^+_{out} + ATP + H_2O \rightarrow 2K^+_{in} + 3Na^+_{out} + ADP + P_i$	-36.46	-36.72	-37.05	719.02	718.9	718.71

A detailed discussion of the energy budget for signaling in the grey matter of the brain was reviewed in detail by Attwell and Laughlin [58]. Work performance for pumping the ions is evoked by the signaling activity and energy needed for Na^+ extrusion is an item of energy expenditure. Work performance for pumping of the ions may be regarded as internal work, being performed within the system boundaries. Internal work performance is a fundamental source for energy utilization in the biological systems and includes every kind of work performed in the body to sustain life. Together with the mechanical work, other works that contribute the total work done can be summarized as; pumping of blood by the heart, for respiration by the lungs, the chemical activities carried out by the liver and re-absorption and secretion processes in the kidneys, along with the electrical work of the nervous system and the synthesis of the entire mass of muscles and the bones.

Based on the Hodgkin and Huxley model as applied to squid giant axon, the primary goal of this study was to emphasize the importance of thermodynamic aspects of the energy management in a single run of the action potential and illustrate the importance of temperature in single neuron model and thermodynamics. The main findings of this study were summarized in Table 4.3, where more efficient use of sodium entry was observed at higher temperatures. The values of Na^+ ion entry and energy cost of a single action potential

run, in terms of an ATP molecule at a temperature of 6.3 ºC agrees well with the values reported by Sengupta et al. [98] and Moujahid and d'Anjou [117]. For the calculation of work production potential of the flux of ATP, the energy of ATP is calculated as proposed, which considers the different valence states of an ATP molecule and the physiological conditions of the biological system; ionic strength, pH and the temperature. Data employed in this study were obtained in the experiments carried out at 6.3^0C and further correlated with temperature factor for 12 and 18.5 ^{0}C. Most of the longfin inshore squid catches occur at water temperatures of 10 to 13ºC, lesser amount of catch is also accounted between 8 to 16ºC [119], therefore experiments carried out at 12 ºC coincides with the most favored habitat temperature, and the other temperatures where the data was collected, e.g., 6.3 and 18.5 ºC, are beyond this range. To assess the temperature effects on the Hodgkin and Huxley model, conductance variables were multiplied Q_{10} the value which was selected as 3.0 [120], which might also be selected as 1.5 according to Chandler and Meves [121] in the temperature range of 6.3 to 18.5 ºC. The effect of $\phi(T)$ on the model was illustrated in Figure 4.4 by assessing the model at nine different temperatures in the range of 6.3 to 18.5 ºC. It was observed that $\phi(T)$ had s significant effect on Na^+ ion entry when $Q_{10} = 3.0$, this effect was even higher when $Q_{10} = 1.5$. Explaining the information flow in the neurons was previously suggested by Andersen et al. [122]. These researchers suggested regarding the proteins and lipids of the nerve membrane as an ensemble with thermodynamic properties and drawn attention to the similarity between the propagation of the sound waves and the nerve pulses, but did not suggest any mathematical models to simulate the phenomena. This study attempts to take a step beyond that of Andersen et al. [122] with calculating the thermodynamic cost of a single run of the action potential, which has never been studied before. Thermodynamic properties of each biomolecule that involve the energy cost is calculated and illustrated in Table B.1 for each physiological condition selected. Then, the thermodynamic cost of each reaction was estimated in terms of exergy destruction and entropy generation, per mole basis. To determine the thermodynamic concepts in a single action potential run, the calculation was based on Equations 59-61. While calculating these concepts two approaches were considered, a simple (Table 4.4-R3) and a more realistic (Table 4.4-R4) ATP hydrolysis, where Na^+ and K^+ ion concentration gradient across the cell membrane is considered to simulate the phenomena more realistically. It was shown that taking into account the entering Na^+ and the exiting K^+ ions had an effect on the thermodynamic concepts. Additionally, each approach was investigated under changing

temperatures. The results demonstrated a 0.96 fold difference in work production potential, changes in exergy destruction and entropy generation were even much higher, since the chemical exergies of the ions [92] were higher. Observations regarding the decreasing efficiency of the entry of Na^+ with temperature, agrees with the thermodynamic findings in terms of exergy and entropy values, where temperature increase lowers the thermodynamic cost of action potential run.

Hydrolysis efficiency of ATP at different temperatures was assessed based on aerobic respiration work production potential with glucose utilization. Under the presence of normal levels of oxygen, ATP production per mole of glucose utilization was assumed 30 moles [123]. Thermodynamic analysis of electric circuit analogy of neurons shows that energy supply is one of the most important limitations in the neuronal work performance. Subcellular processes parameters such as resting potential, action potential, post-synaptic transmission, pre-synaptic transmission and neurotransmitter recycling influence the energy demand. A fraction of the work performance ability of the glucose, e.g., the energy source is lost in the energy metabolism is due to exergy destruction. The exiting streams of the metabolism, e.g., CO_2, H_2O, and heat remove a considerable fraction of the exergy entering the process. ATP is a useful product of energy metabolism. Only a fraction of the work performance potential of the ATP is converted into work in the neuronal system.

Exergy destruction, heat generation, and current leak are the major thermodynamic events where the fractions of the exergy of the metabolic energy allocated for the neuronal work performance as presented in Figure 4.7. In the figure exergy input utilized and destroyed demonstrated at 6.3 ^{0}C on 1-mole basis via simplified ATP hydrolysis approach.

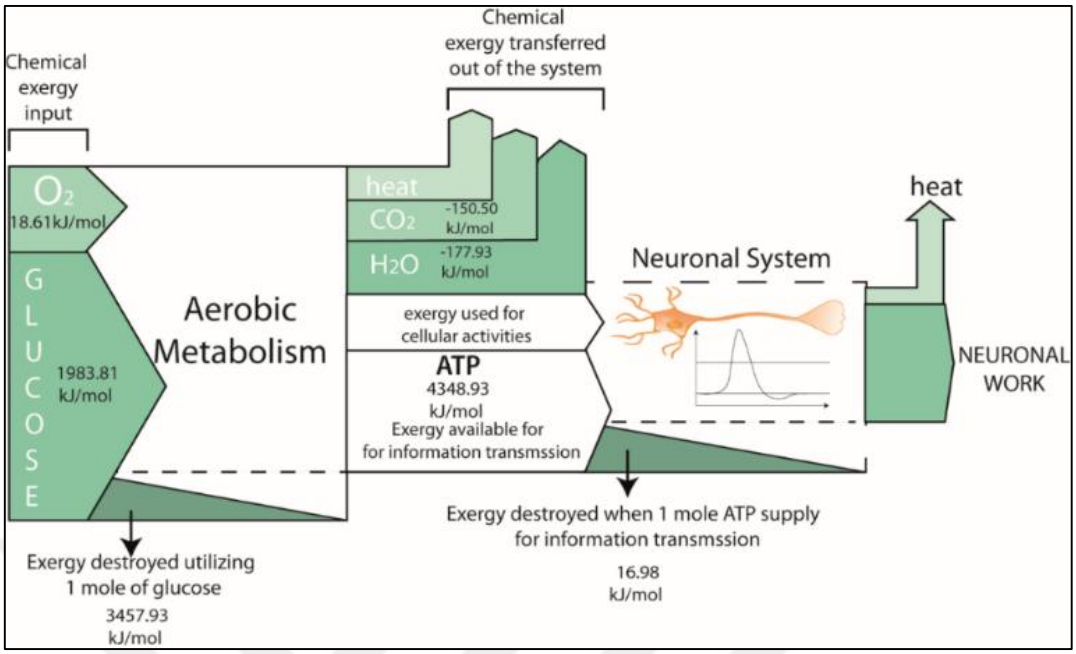

Figure 4.7. Exergy (Grassmann) chart. How and where the exergy input, e.g., exergy of the nutrients is utilized or destroyed.

ATP hydrolysis efficiency was assessed in Table 2 with both simple (R1) and more realistic (R2) reactions. The energetic metabolic efficiency was defined as:

$$\eta_{metabolic} = \frac{work\ production\ potential\ of\ ATP}{work\ production\ potential\ of\ glucose} \tag{4.9}$$

In Table 3, metabolic efficiencies were studied in accordance with different scenarios. When we consider the simple approach, $\eta_{metabolic}$ was calculated based on ATP hydrolysis (Table 4.4-R3) with a simplified version of aerobic respiration (Table 4.4-R1) and according to $\eta_{metabolic,1}$ was approximately equal to 27 percent with less than 1percent fluctuation. When we consider the more realistic approach of aerobic respiration (Table 4.4-R2) with more realistic ATP hydrolysis (Table 4.4-R4) $\eta_{metabolic,2}$ was 38 percent with less than 1 percent fluctuation. The metabolic efficiency calculations reveal that the closest scenario to biological system gave the highest efficiency.

In the 1950s, Hodgkin and Huxley experimented on the squid nerve membrane to establish a model to simulate the experimental data [70]. In the late 1960's Tsien and Noble [124] adapted the transition state theory to model kinetics of excitation of the membrane in terms

of thermodynamic concepts, such as the free energy difference, activation enthalpy, and activation entropy. They referred to Eyring's theory to estimate the energy of the excited state. In the present study, the effect of the temperature on the excitation of the membrane was assessed with the same method in the range of -100 to +100 mV (Figure 4.8).

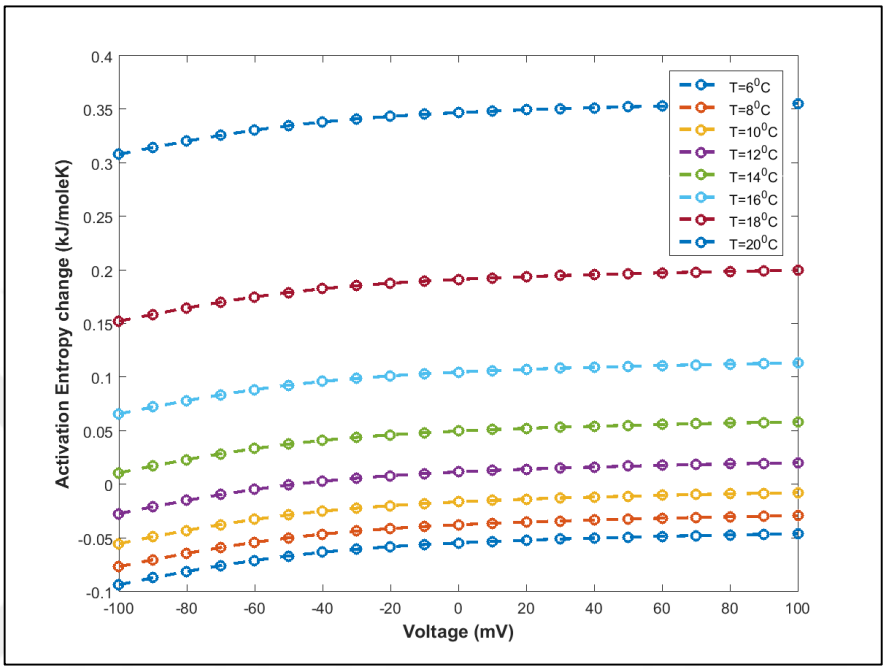

Figure 4.8. Variation of the activation entropy with voltage over temperatures range of 6.3 to 18.5^{0}C.

The thermodynamic Hodgkin and Huxley model does have explicit terms for temperature and requires Q_{10} factors to describe data at different temperatures. In the present study, each model constant is determined for Q_{10} = 3 as suggested by Fitzhugh at each temperature and their contribution to apparent activation entropy will be calculated from $\Delta G = \Delta H - T\Delta S$, while calculating the free energy change and activation enthalpy based on Tsien and Noble's article [124]. Figure 4.8 showed that the temperature effects on the activation entropy as a function of the voltage difference involving in the action potential. Temperature may affect the activation entropy via inducing changes in the excitable membrane structure. Activation enthalpy is generally larger than the free energy of activation and helps to assigns a positive value to activation entropy which states activated state is favorable. In the present study, at the lowest temperatures, the enthalpy of activation appeared to be smaller than the free energy change of activation and lead to a negative activation entropy. Such a behavior was

observed previously in the studies carried out with toad nerve [124–126]. Daniels and Alberty [127] draw attention to the point that the activation entropy has a negative value when rotational and vibrational freedom of the activated complex decreases. Eyring rate theory assumes that temperature has little or no effect on the relative energies of the states (Closed, Transition, and Open). Temperature changes probably affect the transition between the states but does not significantly change the states themselves [124]. Protein structure and membrane lipid structure are temperature dependent [128–130] and may change the ion channel structure especially kinetics of channels which may result in a different level of activation entropy.

Work done by moving a charge in an electric field was calculated as $W = \Delta V q$ where ΔV is the voltage difference in volts and q is the charge in Coulombs. In the present study, the charge was that of the sodium ion and the voltage difference was that of the excitable membrane. Initial voltage was taken as resting voltage, e.g., -65 mV, since the sodium influx is responsible for depolarization of membrane, and the final voltage was taken as the depolarization voltage +40 mV. Estimations of the work done by the moving charge in this field was illustrated in Figure 4.9, as a function of temperature, where it is observed that, as the amount of sodium ion influx decreased, the work needed to move the charge decreased, pointing that at the higher temperatures less work is needed to depolarize the membrane back to + 40 mV.

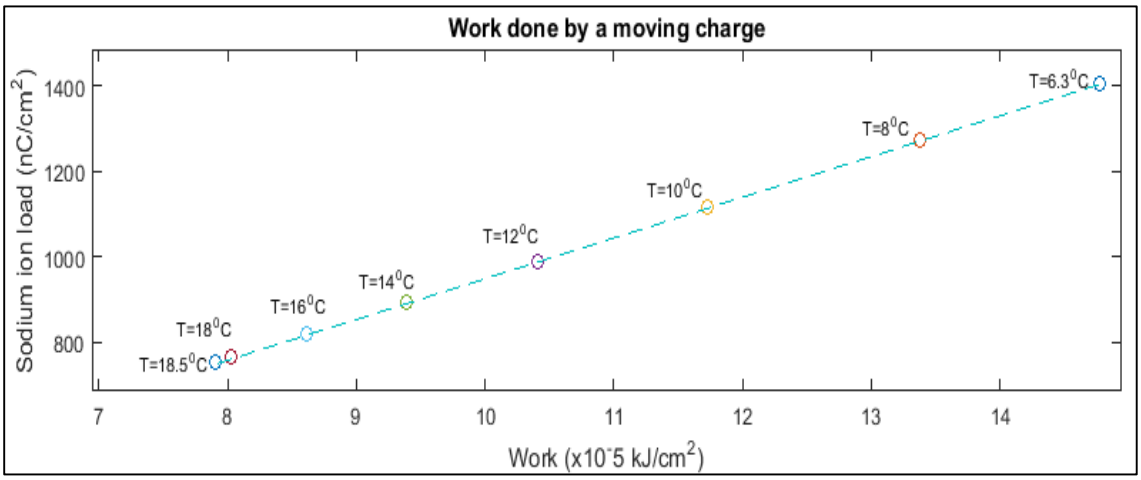

Figure 4.9. Work done by moving charge over 6.3 to 18.5 ^{0}C.

Energy efficiency may also be defined as:

$$\eta_{energy} = \frac{Work\ done\ by\ moving\ a\ charge\ in\ an\ electric\ field}{energy\ extracted\ for\ single\ run\ action\ potential} \quad (4.10)$$

In the temperature range of 6.3 to 18.5 ^{0}C, when we consider energy released via simple ATP hydrolysis the range of efficiency of the action potential, $\eta_{energy,1}$, may be calculated 85 percent with approximately ± 1 percent fluctuation. When we consider a more realistic approach of energy release from ATP hydrolysis, the range of energy efficiency of the action potential, $\eta_{energy,2}$, may appear to be 83 percent with approximately ± 1 percent fluctuation represented in Table 4.5.

Table 4.5. System efficiencies calculations and their corresponding result in 6.3, 12 and 18.5^{0}C.

	Efficiency (%)		
	6.3^{0}C	12^{0}C	18.5^{0}C
$\eta_{metabolic,1}$	26.9	27.2	27.5
$\eta_{metabolic,2}$	38.1	38.7	39.3
$\eta_{energy,1}$	86.3	85.7	84.9
$\eta_{energy,2}$	83.4	82.8	82.0
η_{exergy}	59.9	63.3	63.2

This result showed that, the squid neuron was able to transfer about 82 - 86 percent of the free energy released from ATP hydrolysis to work to run a single run of action potential, implying that 14 to 18 percent of the energy released from the hydrolysis of ATP cannot be used to produce work and may be converted into entropy following heat generation.
Exergy efficiency may also be defined as:

$$\eta_{exergy} = \frac{Work\ done\ by\ moving\ a\ charge\ in\ an\ electric\ field}{exergy\ destruction\ for\ single\ run\ action\ potential} \quad (4.11)$$

In this part, the exergetic efficiency was calculated for a temperature range of 6.3 to 18.5 ^{0}C where at 6.3^{0}C exergetic efficiency may appear as 59.9 percent with approximately 3.0

percent increase with temperatures increase to 12 and 18.5^{0}C while it did not give any significant increase between these temperatures. Therefore, the consumed chemical exergy is not only used to establish work done by moving charge, but also to perform basal metabolic activities.

In the squid giant axon at 6.3^{0}C capacitor generated 8.0 x10^{-13} kJ/cm^2 and stored 5.12x10^{-12} kJ of energy. At constant temperature T, heat generation causes $\Delta S = \frac{1}{2T} C_m {V_0}^2$ of entropy accumulation within the system [97] and estimated as 2.86 x10^{-15} kJ at 6.3 ^{0}C. While discharging the capacitor, as described in Figure B.1, current flows over the resistor and generates heat and entropy. In this process, it was assumed that the ions do not interact with each other and the quantum nature of the sodium ions. Contribution of the ion flow to entropy generation was calculated from the heat capacity model [131]. In this case, where the cell membrane behaves as a resistor and dissipates thermal energy entropy accumulates within the system depending on the charge, capacitance and temperature and calculated as; $\Delta S = \frac{{q_0}^2}{2C_m T}$. Lara et al. [132]. Theories of quantum mechanics [97] expresses the entropy change during the flow of the electrons between the plates of the capacitor as;

$$\Delta S = \frac{N k_B \pi^2}{2} \frac{k_B T}{\varepsilon_F} \tag{4.12}$$

where N is the number of the sodium ions passing thru the cell membrane and k_B is the Boltzmann's constant and ε_F is the Fermi energy. The Sommerfeld and Frank [133] approximation of equation (20) at Fermi temperature, T_F of the ions is:

$$\Delta S = \frac{N \pi^2}{2} \frac{k_B T}{T_F} \tag{4.13}$$

Since during depolarization the total discharging entropy depends directly on the number of sodium ions passing thru the cell membrane temperature increase causes a decrease in entropy as described in Figure 4.10. Entropy generation of the discharge causes 2-fold more entropy change than related entropy accumulation because of heat generation in the capacitor at 6.3 ^{0}C.

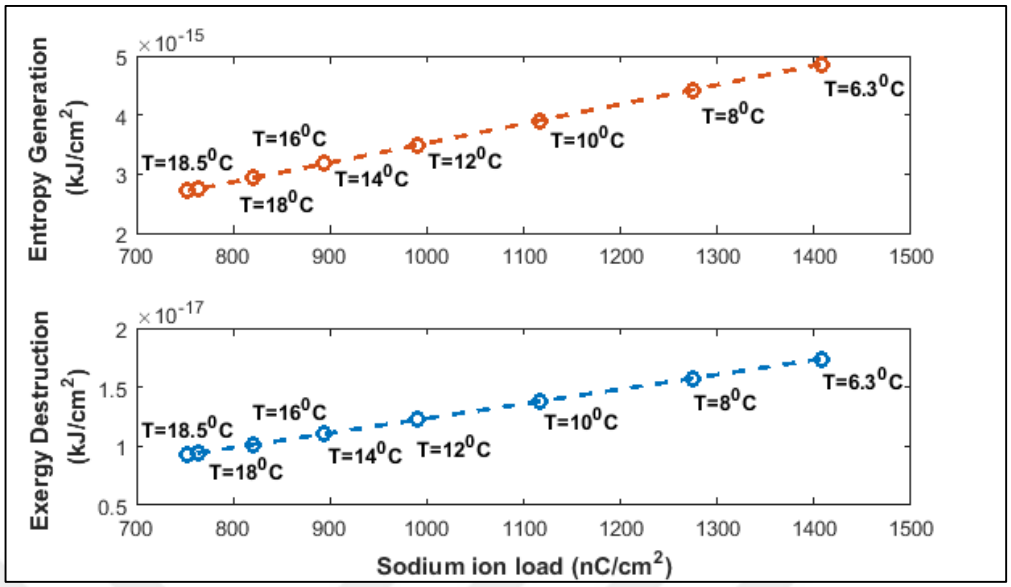

Figure 4.10. Entropy generation and exergy destruction. Depending on discharging over temperatures range of 6.3 to 18.5 ^{0}C.

Recently Yi et al. [134] studied the energy efficiency in cortical pyramidal cells under different dendrite properties. When the sodium load data adapt from the Matlab code provided in their study and carry out exergy analysis with the same method as described in the present study under the mammalian physiological conditions described by Genç et al. [12], e.g., I=0.18 M, pH=7 and T=37 ^{0}C. It is estimated that the exergy destruction of action potential energy allocation is $5.5x10^{-11} \pm 0.5$ kJ per cm^2 area in every model the original article discusses. Exergy destruction of cortical pyramidal cells gave a very similar result with that of squid giant axon assessed in the present study at T=12 ^{0}C. Different exergy destruction results may be obtained with the neurons of the other species depending on their sodium channel kinetics [135].

4.2.1. Thermodynamic Analysis of Dissipated Energy

Calculations showed that the entropy generation was directly proportioned with the electrotonic length (Figure 4.11).

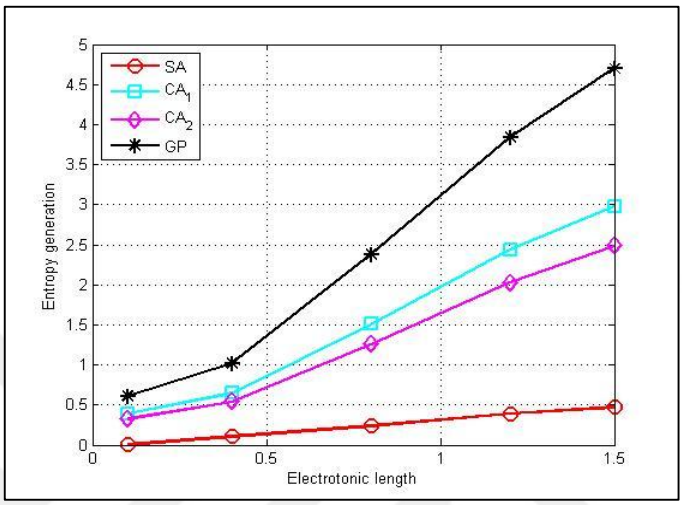

Figure 4.11. Entropy generation in a varying length for SA, CA_1, CA_2, and GP models.

Table 4.6 summarizes the main results of the thermodynamic analysis of the propagation entropy generation and exergy loss for unit electrotonic length where that the cat neuron models estimated nearly the same amounts of exergy loss while generating nearly the same amount of entropy. Exergy loss in the Guinea pig vagal motoneuron caused generation of almost twofold exergy when compared to the CA_2 model. Exergy loss and entropy generation with the squid motoneuron was nearly 10 percent of those of the guinea pig vagal motoneuron.

Table 4.6. Exergy destruction and entropy generation values when L=1.0.

Models	Exergy destruction (pJ)	Entropy generation (pJ)
SA	0.95	0.003
CA_1	6.19	0.020
CA_2	5.16	0.017
GP	9.75	0.031

The invertebrate (SA) entropy generation and exergy loss are lower than those of the vertebrate motoneurons (CA_1, CA_2, and GP), implying that may the electrical transmission from to input branch to other branches was more efficient in the invertebrate motoneuron than mammalian motoneurons. Figure 4.8 showed that the entropy generation was directly proportional to the electrotonic length. The electrotonic length was estimated as 1.5 for the spinal motoneurons [136] and 0.9 for the hippocampal pyramidal [137] and 1.2 for the granule cells [138]. Results showed that effective reduction in the electrotonic length in simple cylinder motoneurons reduces the propagation loss significantly. The results have shown that electrotonic length has great importance in the propagation loss and its thermodynamic costs and much more information lost during propagation in vertebrate motoneurons than those of the invertebrate.

4.3. PIG CARDIAC MUSCLE THERMODYNAMIC MODEL

In the kinetic model of pig heart, overall system cytoplasm, inner mitochondrial membrane and mitochondrial matrix where hexokinase, passive permeation, anti and co-transport, oxidative phosphorylation and TCA cycle fluxes investigated based on work provided by Wu et al. [105] for resting and active body. Since energy metabolism of mitochondria is the center of bulk production of energy via the TCA cycle and oxidative phosphorylation each reaction considered for the modeling represented Table C.1. Energy-rich compounds and their precursor produced and processed to contract and relax. This contraction and relaxation periods pumps blood through the where it is needed. Kinetic simulation conduct for the 30s where energy-rich compounds represented in Figure 4.12 for both states.

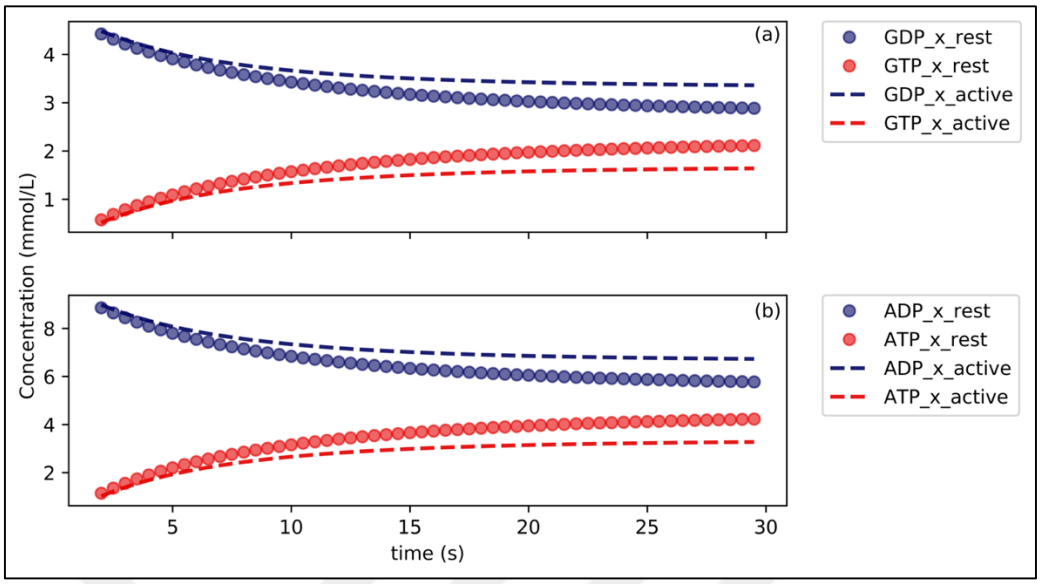

Figure 4.12. Resting and active modes of pig heart concentration of energy-rich compounds (mmol/l) as a function of time.

In both state of the body in cardiac muscle matrix, the concentration of energy-rich compounds, ATP and GTP, synthesized via TCA and oxidative phosphorylation. Due to higher intensity requirement of energy response to an active state the amount of energy-rich molecules in the mitochondrial matrix, ATP and GTP, lower than resting state thru simulation time since the produced energy-rich compounds allocated for corresponding active state or send to first inner membrane space via adenine nucleotide translocase than further send to its designated place. The unsteady-state model predicts mitochondrial matrix ATP concentration increase in resting and active via;

$$[\Delta c_{ATP}] = [c_{ATP}]_{final} - [c_{ATP}]_{initial} \tag{4.14}$$

where 3.08 and 2.25 mmol/L increase observed, respectively. It showed energy expand for power output and/or cellular activities that come from free energy released from ATP hydrolysis is lower in resting. Jeneson et al. [139] suggested that phosphate metabolite level within the cell is directly related to the level of ATP hydrolyzed which is linearly proportional to the power output of the muscle system. The phosphate metabolite concentration in the mitochondrial matrix and total intracellular phosphate concentrations as a function of time illustrated in Figure 4.13.

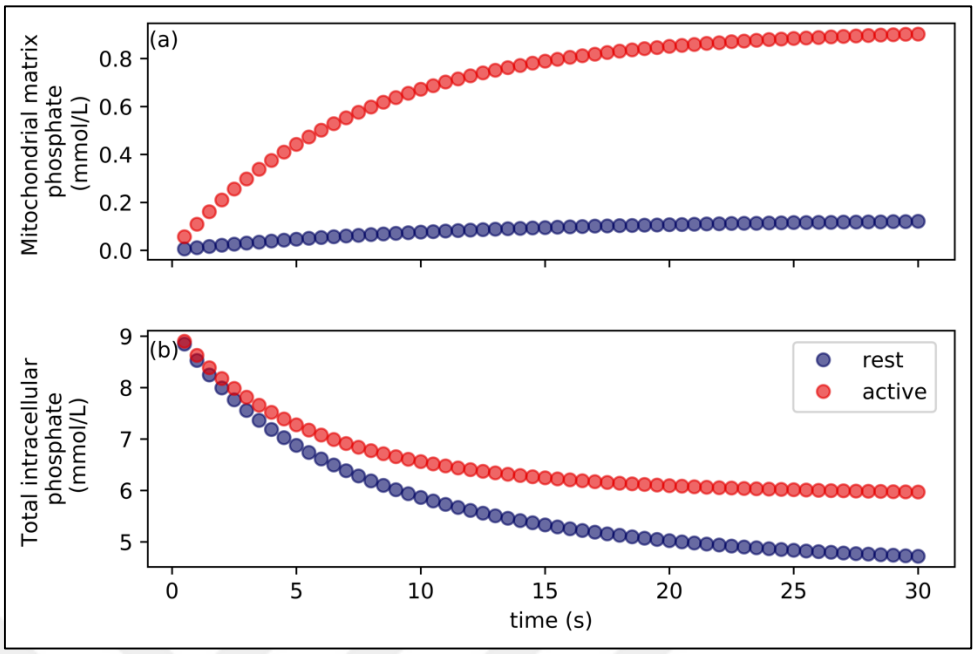

Figure 4.13. Phosphate concentrations (a) is mitochondrial matrix phosphate ion concentration (mmol/l) as a function of time in both resting and active modes of pig heart and (b) indicated total (cytoplasm and mitochondrial matrix) phosphate ion concentration (mmol/l) in the cell.

Mitochondrial matrix phosphate concentration increased as a function of time in both states of the body while cytoplasmic phosphate concentration decreases indicating more hexokinase activity and H/Pi cotransport activity from the cytoplasm to the matrix. As a result of these reaction fluxes, total concentration intracellular phosphate was decreased as a function of time since free phosphate in the cytoplasm is transported from cytoplasm to inner membrane via passive permeation and later used for F1-F0 ATPase activity in the mitochondrial matrix. The percent change of total intracellular phosphate concentration in resting showed variation 0.4 percent initial and final time of simulation while much higher variation occurs in the active state, 16 percent.

The heart model reactions (Table C.2), the nutrient catabolized into its minor precursors in the presence of oxygen while producing energy-rich compound's and then utilized for the contraction of cardiac muscle fibers. Table C.2. lists the ATP formation and transportation reactions and reaction Gibbs free energy change and enthalpy changes. Each of reactant of the model was calculated based on the method described under the biophysical condition,

pH=7.27, T=310.15 K and I=0.14 M to make the model physiologically more close the actual. Pig heart mitochondrial matrix pH was calculated via;

$$pH = -log[H^+] \tag{4.15}$$

where $[H^+] = 5.41x10^{-8}M$ assumed to be constant through simulation time and ionic strength estimated considering ionic gradient of a mitochondrial matrix of a pig heart.

Thermodynamic analysis biochemical reactant results indicate that if the system is ideal i.e. the system works under no losses ($Ex_{destruction} = 0$), the maximum work of 641.91 kJ of work can be extracted through utilization of one mole of pyruvate which accompanied by 277.34 kJ of heat removal from this work.

Mass, energy and exergy analysis was applied after kinetic simulation to the pig heart on the proposed model resting and active states. Upon the active state, to perform greater power more oxygen is required due to high-intensity metabolism. In Figure 4.14 complex IV reaction flux represented as overall oxygen flux of the system as a function of time where active state leads to a significant increase in oxygen usage. The physical active state of the body leads to more oxygen consumption to maintain sufficient external work to pump blood while producing more heat than resting in the heart (Figure 4.12).

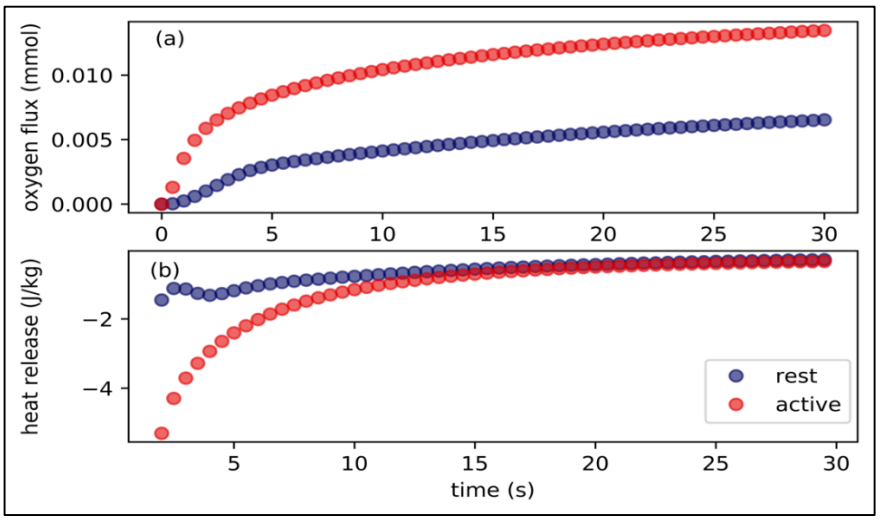

Figure 4.14. Oxygen flux and heat release (a) oxygen flux (complex IV reaction flux) (mmol/s) as a function of time in both resting and active modes of pig heart (b) heat release (J/kgs) from the system.

For the work output analysis the heart treated as a pump which consist of double pump system connected to each other, left and right, and its power to pump blood calculated via both exact method described methodology part with using data represented in [140] and via applying trapezoidal rule of data represented in [141] pig simultaneous bi-ventricular acute pressure-volume measurement (closed chest approach). In both estimations of left and right ventricle, cardiac power gave a very similar result with ±0.003-0.004 SD, respectively. The work output calculations from pressure-volume data showed that pig heart expands 0.033 J/kgs work in rest while 0.065 J/kgs in an active state. Since in the literature only resting pig heart data available, the active state pumping power was estimated assuming heart completes one cardiac cycle half of its time in active state. In each time step of simulation of both states, the work expanded by heart assumed to be the same.

The calculated power output prediction was further used for the thermodynamic analysis. Corresponding heat concept is calculated from energy balance (Equation 3.2) in response to resting and active state. Heat release, heat that is removed by the blood, was assumed to be heat generated that would accompany metabolism and the work output. The results revealed that heat is produced with the onset of metabolism than it is decreased after 5 seconds and reach steady state heat release in resting. In response to the active state, nearly 3.7 fold heat was generated, released onset of metabolism than its reach nearly the same steady-state value as resting behavior does. In prolonged activity cause a decline in heat production levels as a function of time may suggest the cardiovascular adaptations along with a total body that occurs to improve heat loss responses during activity-heat acclimation [142]. Heat generation can occur in any type of cell of the body via the conversion of metabolic energy into thermal and mechanical energy. The compensation of thermal regulation in muscle is inefficient. Up to 70 percent of liberated muscle energy can be thermal energy to sustain metabolism and power output [143–148]. Heat generation via muscle contraction shows an increase in the onset of exercise and plateau with continuing steady state activity while it does not level off in response to the increasing level of activity. Skeletal muscle studies demonstrate elevated heat production as a function of time through a contraction is highly coupled with heat liberated from energy metabolism to produce energy-rich compounds to maintain cardiac output [144,145,147,148]. This type of heat generation generally occurs in the liver, brain, skeletal muscle and heart [149]. The thermoregulation of homeostatic in the mammalian body has a crucial impact on living. The homeostatic balance of the biological

system is regulated via the cardiovascular system. Physical exercise increases heart rate and systolic blood pressure in response to cardiac muscle contraction coupled with more oxidation of chemical nutrient to provide sufficient blood flow where it is needed. The concurrent increase of metabolism leads to more heat production that transferred to the skin via blood flow where it is dissipated via convection. Inefficiencies of thermoregulation of metabolic heat lead to consequent excessive heat production in the corresponding body may lead to problems i.e. exercise-induced heat exhaustion.

Although the power consumed by heart was provided from dissociation of ATP calculated with respect to oxygen consumption rate, the power was correlated with the energy released by one mole of pyruvate and represented as;

$$P = \Delta G^{T}_{TCA} x \Omega_{O_2} \tag{4.16}$$

where ΔG^{T}_{TCA} is the Gibbs free energy of overall TCA cycle and Ω_{O_2} oxygen consumption flux. Efficiency of heart defined via the ratio of the external work done by the system to the power consumed by the system i.e. $\eta_{heart} = W_H/P$. Average heart efficiency in pumping blood to the vascular system gave statistically same result 0.23 in resting, 0.22 for active state. This result was expected since the active state of pig heart that is under investigation is not exercised state, it is the state that the pig body exposed to low level activity.

The energy is produced within the system and later expanded as external work. Since energy in the body is in the form of ATP, the required energy for cardiac output is supplied from free energy release ATP hydrolysis to ADP. Metabolic energy released by is the direct energy source for the heart, where, each mole of ATP roughly release 46 to 62 kJ of free energy previously estimated [100] but in physiological conditions of pig body it is estimated as free energy release 38.93 kJ per mole of ATP. The work potential that system can extract was modeled considering three reaction fluxes that produce and or exchange ATP molecule; Nucleoside diphosphokinase reaction and F_0-F_1 ATPase in the matrix and Adenylate kinase transport reaction calculated as;

$$J_{ATP} = J_{NDH} + J_{F_1F_0} - J_{ANT} \tag{4.17}$$

$$\dot{W}_{ATP} = J_{ATP}\, \Delta G^{T}_{ATP \leftrightarrow ADP} 30 \tag{4.18}$$

where J_{ATP} is in mol/s and constant value 30 is the amount of ATP molecule per 2 moles of pyruvate. The work production potential function of time calculation showed that until first 18 second simulation work production potential of a heart system in rest higher than active state since power output parallel with energy demand is lower that has a great effect on J_{ATP} fluxes. After the first 18 seconds, the work potential that system extract proceed in higher levels than resting in active state due to increment in the J_{ATP} fluxes which may demonstrate the level of adaptation to the active state of body.

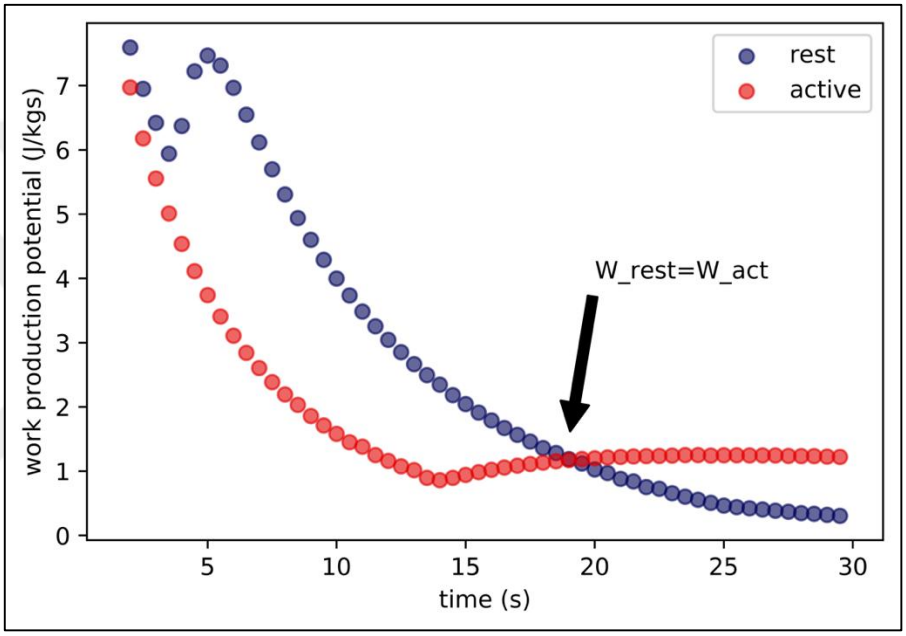

Figure 4.15. Heart work production potential.

In both rest and active states of the body cardiac demand of energy supplied via only aerobic respiration where oxygen consumption rate through simulation is showed different behavior. More oxygen consumed in response to an active state through the simulation period. Contraction efficiency in cardiac systems usually defined as the ratio of power output (external work) to total cellular energy transformed. In here we define the ratio of muscle contraction work (J/kgs) to free energy usage from ATP hydrolysis Due to the estimation of the ratio between considered as;

$$\eta_{contraction} = \frac{muscle\ contraction\ work\ (W_H)}{free\ energy\ release\ during\ respiration} \tag{4.19}$$

The estimated contraction efficiency from rest to the active state at time t=30s diverged from 0.14 to 0.12 indicated as;

$$0.14 = \frac{0.033\ J/(kgs)}{0.548\ J/(kgs)} \geq \eta_{contraction} \geq \frac{0.065\ J/(kgs)}{0.228\ J/(kgs)} = 0.12 \tag{4.20}$$

The contraction efficiency in resting and active state gave non-significant decrease (0.02) in active which was expected as it was demonstrated heart efficiency analysis. The efficiency values of contraction results are in agreement with previous observation where cardiac efficiency is defined as an analogy to that of motor efficiency is up to 25 percent [150] where economy of cardiac muscle contract is defined as energy, ATP, allocated for contraction.

Exergy analysis in a biological system is generally applied to assess energy conversion quality within the system that aims to understand indicators that affect the system in terms of exergy loss, exergy efficiency and exergy destruction rates.

Exergy losses of a system is a phenomenon that is described as irreversibility of a system, exergy transfer from the overall system to its surroundings that is no longer used in the system [151]. Internal exergy loss concept is calculated via subtraction exergy outflow, exergy that leaves from the system, from exergy inflow, the exergy amount that comes into the system [152]. In the case of biological systems, exergy loss is referred to as the amount of chemical exergy that cannot be captured and invested via metabolism. The internal exergy loss rate analysis of pig heart showed that active heart is invested upcoming chemical exergy more efficiently through its metabolism than resting. The amount of lost chemical exergy than cannot be further processed in higher values through the simulation time.

Energy conversion systems exergy analysis represent irreversibility's for each component of a system distinguishes this irreversibility's as endogenous and exogenous [153]. Upon this approach, endogenous exergy destruction occurs due to irreversibility's that particular component/sub-system while remaining parts operate in an ideal way where exogenous exergy destruction arises in the particular component/sub-system while remaining parts operate in not ideal.

In pig heart, unsteady state system exergy destruction calculation was contributed based on Equation 3.4 that may be thought as endogenous exergy destruction which is an internal

phenomenon where irreversibilities are caused due to chemical reaction, heat transfer. The exergy destruction was calculated with the aid of either entropy generation within the system ($\dot{X}_{dest} = \dot{S}_{gen} T_0$) or from analytical solving of exergy balance equation. This exergy balance equation allows to distinguish exergy loss from exergy destruction rate of a system. $\sum(\dot{m}ex)_{in} - \sum(\dot{m}ex)_{out}$ the term can be defined as the internal exergy loss which described detailed above and $\dot{X}_{dest}$ is the endogenous exergy destruction since all subsystems/components are assumed to be ideal.

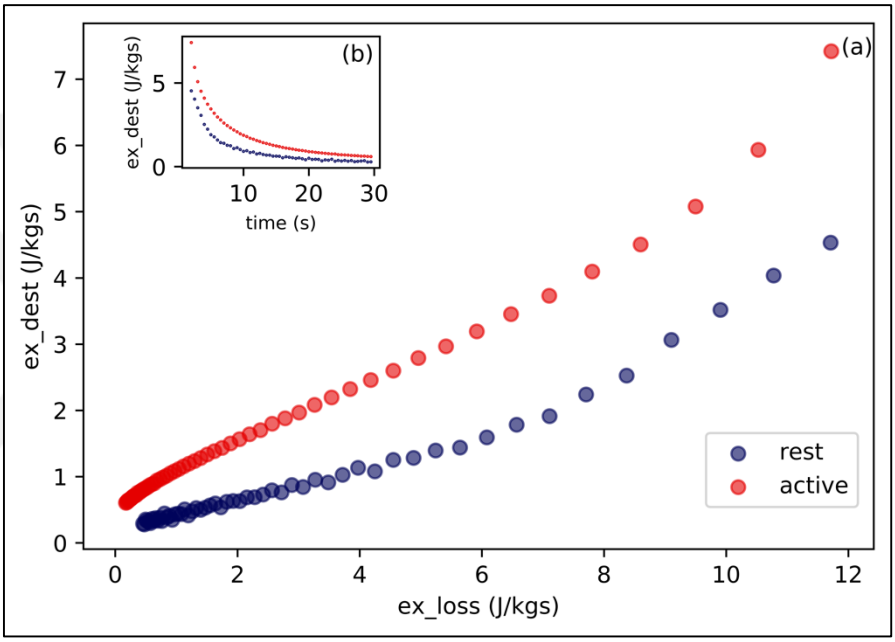

Figure 4.16. Exergy loss and exergy destruction (a) Heart exergy destruction as a function of time, (b) Exergy loss vs exergy destruction rate in pig resting and active state of heart.

Figure 4.16 showed the result of exergy destruction rate vs exergy loss analysis in cardiac muscle. In the active state exergy destruction rate is proceed in higher values throughout simulation time than resting indicating the effect of level of metabolism, power output, and heat generation. Upon the results, the decline in both exergy destruction rate and exergy loss through the simulation time were observed. In both systems, exergy loss and exergy destruction rate is positively proportional to each other. This results can be concluded as the system start to minimize its exergy loss and exergy destruction rate as a function of time.

That may be the product of adaptation since the generated heat is removed via blood through the simulation time to prevent temperature increase to establish homoeostatic balance.

Another efficiency term of the system was introduced that analyze respiration how efficiently energy coming from respiration corresponds to energy release via,

$$\eta_{energetic} = \frac{energy\ released\ via\ ATP\ hydrolysis}{energy\ released\ during\ respiration} \tag{4.21}$$

In the metabolism, the intensity of aerobic respiration depends on the state and the level of active state of the body. As the active state intensity level increase or system switch its behavior resting to active, the metabolism increase and ATP consumption rate increases. This efficiency analysis showed that the system behavior change rest to active has an effect on systems energetic efficiency in biomolecular reaction level where in rest 0.40 and in active state 0.47 leaving system more efficient in response to the active state.

To reveal how much exergy of respiration is invested in ATP synthesis during both states of pig heart the respiration efficiency defined as;

$$\eta_{exergetic\_respriration} = \frac{exergy\ released\ via\ ATP\ sythesis}{exergy\ released\ during\ respiration} \tag{4.22}$$

Then, exergetic respiration efficiency of pig aerobic respiration is;

$$0.36 = \frac{0.23\ J/(kgs)}{0.63\ J/(kgs)} \leq \eta_{respriration} \leq \frac{0.55\ J/(kgs)}{1.31\ J/(kgs)} = 0.42 \tag{4.23}$$

In rest, to correspond work output pig heart system total exergy consumed due to aerobic respiration was $0.63\ J/(kgs)$ and $0.23\ J/(kgs)$ exergy was stored in synthesized ATP while in active state these values were $1.31\ J/(kgs)$, $0.55\ J/(kgs)$, respectively. These exergy increments in active state increases respiration efficiency in the active state. The respiration efficiency calculated at t=30s, at the end of the simulation, increase from 0.36 to 0.42 in response to the active state.

The corresponding thermodynamic analysis further contributed to revealing exergy destroyed for the production of energy-rich compounds when the pig body condition is

diverged from resting to active. Exergy destroyed for the production of ATP was investigated via taking ratio exergy destruction rate at t=ts with the flux of ATP synthesis at the same time point. The calculation showed approximately 3.7 fold more exergy is destroyed is needed for the production of 1 mole of ATP.

5. CONCLUSION

The first part of the thesis presented a thermodynamic evaluation of the fast and slow swimming modes of a squid [23]. Squid engages different types of muscle fibers and switches between aerobic and anaerobic respiration modes as its swimming speed changes. Main findings of this part are:

i. During fast swimming 9.97 J/ (kg s) of chemical exergy was consumed, which is ca. 2.6 times larger than the exergy consumption during slow swimming (3.82 J/(kg s)).
ii. Respiration efficiency decreases as more ATP is produced via anaerobic respiration.
iii. During slow swimming, most of the power is generated via fin and the power transferred to water inside the mantle cavity was only 0.0053 J/(kg s).
iv. During jet escape power transferred to water rises to 0.16 J/ (kg s).
v. Contraction efficiency decreased from 36.8 percent to 4.7 percent as the volume of the passive tissue increases from 5 percent to 95 percent.
vi. The ratio of the produced work to the available ATP exergy was 26.41 percent for the slow and 6.87 percent for the fast swimming modes.

All of these conclusions point that slow swimming was exergetically more efficient and leads to about 3 times less exergy destruction. ATP consumption calculations during neural action potential propagation showed that during jet escape the giant axon destroyed nearly 3 times neuron exergy as that of slow swimming, suggesting another clue why squid prefers slow swimming under non-emergency conditions.

The second part of the thesis focused on Hodgkin and Huxley's conductance-based model which is a helpful theoretical–experimental approach to understand how action potential initiate and propagate in single neurons. This mathematical model is a very useful tool to quantify Na^+ entry and energy efficiency of axonal action potentials and their related metabolic thermodynamic costs. The primary object of this study was to use a Hodgkin and Huxley model to assess energy efficiency and investigate thermodynamic costs of the axonal action potential and preparing grounds for the further analysis in complex systems of mammalian neurons. The metabolic energy cost of action potential was assessed for different temperatures and related thermodynamic costs calculated based on this energy allocation in

neuron and investigated under different metabolism models. Our results emphasized that the energy cost of the action potential in squid giant axon is a function of physiological conditions of system and its energy and exergy utilization decreases as temperature increases. As the model employed to simulate the metabolic activity gets closer to the real biological system described in terms of the reactions employed, energy efficiency for effective use of the ATP increased.

In addition, Eyring's activated complex theory adapted to Hodgkin and Huxley squid giant axon kinetics (rate coefficients; α and β) to describe excitable membranes ionic current kinetics in terms of activation entropy and further emphasize the effect of temperature. Voltage-dependent activation entropy increased with respect to increasing temperature since rate coefficients of Hodgkin and Huxley's model changing with temperature.

Our models and predictions can be used to examine how other physiological conditions and kinetics of the neurons affect energy and thermodynamic efficiencies of spikes. Such examinations are essential for deeply understand neurons information processing and their metabolic efficiencies.

At 6.3 ^{o}C, energy cost of the action potential was $1.77x10^{-11}$ kJ /cm^2, exergy destruction and entropy generation were $3.49x10^{-9}$, $1.25\ x10^{-11}$ kJ/cm^2, respectively. The almost two-fold decrease is estimated in entropy generation was calculated as temperature increased from 6.3 to 18.5 ^{0}C decreases, almost by half and entropy generation decreased agreeing with the previous reports that the squids and the octopuses population thrive with global warming [10].

This third final part of the thesis was a comprehensive thermodynamic evaluation of resting and active modes of a pig heart. It was assumed that during both modes the heart is sufficient enough generate to cardiac output without anaerobic metabolism involved. Many studies were contributed to relate the mechanical performance of heart to cardiac energy metabolism. Although it is extremely difficult to analyze energetic behavior of the cardiovascular system in human and animals due to the presence of many regulatory systems that have an effect on cardiac related disease, isolated cardiac muscle studies can provide dependable metabolism data. Consequently, in this present study kinetic model was constructed using COPASI using isolated muscle experimental data [104] and detailed computer simulation and parameterization approach [105]. After the modeling kinetic

behavior of pig heart in both states, thermodynamic law equations were contributed to the energetic and exergetic analysis of cardiac muscle. From the analysis, the main findings of this study are:

i. Metabolism, aerobic respiration, increased in response to an active state where oxygen fluxes are significantly higher than resting;
ii. As it was suggested [140] that phosphate metabolite concentrations (mmol/L) level indicates more ATP hydrolyzed for the corresponding power output of the muscle system in an active state.
iii. Heart muscle fiber contraction work calculation based on empirical data showed that 3.5-6.5 percent of the exergy stored in ATP is used to perform mechanical work in resting in the active state, respectively.
iv. Since energy production, work output, of cardiac muscle must be interpreted in terms of the major ATPase's underwriting cardiac contraction, work production potential of a system analyzed and the result concluded as prolonged active state cause increment in that chemical potential that system can convert as mechanical work is proceeding increase over time after t=19s while it decreases without any change in basal resting state.
v. Upon the first law of thermodynamics, it was revealed that generated heat (-sign) is directly released through blood flow where 3.7 fold more generated heat is released in the active state at the onset of analysis.
vi. When the pig exposed to an active state, pig heart transfer energy that coming from respiration 7 percent more efficiently.
vii. At t=30s, during active state 1.31 $J/(kgs)$ of chemical exergy was consumed, which ca. 3.6 times larger than exergy consumed during resting (0.36 $J/(kgs)$) where active state 6percent more exergetically efficient than basal the resting state. Exergetic destruction rate to 1 mole of ATP synthesize nearly 2.7 more efficient in the active state. These all conclusion points demonstrate that although cardiac and contraction efficiencies are the statistically same in both states, the active state of the body leads to exergetically more efficient heart system in biochemical reactions consideration level.

Thermodynamic assessment in any system gives a mathematical framework to understand how energy transduces within the system and energy transfer from the system

to the environment. Hence, help us to design, predict and calculate the energy efficiency and feasibility of better systems.

6. FUTURE PROSPECTS

Assessing the comfort of the biological systems in terms of entropy generation and exergy destruction, exergy efficiency of the competing metabolic pathways in the brain, exergy efficiency of the muscle work, lifespan entropy generation understanding and finding ways to postpone symptoms of aging, heart attacks were among the areas where recent bioenergy conversion studies made a significant contribution to our knowledge. The discussion presented in this thesis clearly shows that thermodynamic evaluation of the biological systems has the potential to contribute to understanding diseases and aging. Future research may, therefore, focus on maintaining the health of the metabolism and making it generate energy for an as long period as possible.

REFERENCES

1. Xu J, Murphy SL, Kenneth BS, Kochanek D, Bastian B, Arias E. Deaths: final data for 2016. *National vital statistics reports: from the Centers for Disease Control and Prevention, National Center for Health Statistics, National Vital Statistics System*. 2018;67(5):1.

2. Mariūnas M, Daunoravičienė K, Griškevicius J, Andrašiutė J. Research of relation between muscle biosignal and systolic blood pressure, and application of its characteristics for evaluation of efficiency. *Journal of Vibroengineering*. 2008;10(3):329–335.

3. Ribeiro JP, Chiappa GR, Callegaro CC. The contribution of inspiratory muscles function to exercise limitation in heart failure: pathophysiological mechanisms. *Brazilian Journal of Physical Therapy*. 2012;16(4):261–267.

4. Barclay CJ. Getting energy to where it is required is a problem in the failing heart. *The Journal of Physiology*. 2008;586(21):5037–5038.

5. Kiriazis H, Gibbs CL. Effects of aging on the work output and efficiency of rat papillary muscle. *Cardiovascular Research*. 2000;48(1):111–119.

6. Carmeli E, Coleman R, Reznick AZ. The biochemistry of aging muscle. *Experimental Gerontology*. 2002;37(4):477–489.

7. Wolff E, Fun I, Hoskins B, Mitchell J, Palmer T, Santer B, et al. Climate Change Evidence & Causes. *National Acedemy of Sciences*. 2014;36.

8. Karl TR, Melillo JM, Peterson TC, Hassol SJ. Global climate change impacts in the Cambridge. Cambridge University Press; 2009.

9. UNFCCC. Clımate change: ımpacts, vulnerabilities and adaptation in developing countries. Bonn, Germany; 2007. [cited 2019 February 10]. Available from: https://unfccc.int/resource/docs/publications/impacts.pdf

10. Doubleday ZA, Prowse TAA, Arkhipkin A, Pierce GJ, Semmens J, Steer M, et al.

Global proliferation of cephalopods. *Current Biology*. 2016;26(10):406–407.

11. NASA. Global climate change vital sign of our planet; 2018. [cited 2019 February 10]. Available from: https://climate.nasa.gov/evidence/

12. Demirel Y, Sandler SI. Thermodynamics and bioenergetics. *Biophysical Chemistry*. 2002;97(2):87–111.

13. Demirel Y. Exergy use in bioenergetics. *International Journal of Exergy*. 2004;1(1):128–146.

14. Demirel Y. Nonequilibrium thermodynamics modeling of coupled biochemical cycles in living cells. *Journal of Non-Newtonian Fluid Mechanics*. 2010;165(17):953–972.

15. Demirel Y. Information in biological systems and the fluctuation theorem. *Entropy*. 2014;16(4):1931–1948.

16. Dincer I, Cengel YA. Energy, entropy and exergy concepts and their roles in thermal engineering. *Entropy*. 2001;3(3):116–149.

17. Jubrias SA, Vollestad NK, Gronka RK, Kushmerick MJ. Contraction coupling efficiency of human first dorsal interosseous muscle. *The Journal of Physiology*. 2008;586(7):1993–2002.

18. Mady CEK, Ferreira MS, Yanagihara JI, Saldiva PHN, de Oliveira Junior S. Modeling the exergy behavior of human body. *Energy*. 2012;45(1):546–553.

19. Mady CEK, Albuquerque C, Fernandes TL, Hernandez AJ, Saldiva PHN, Yanagihara JI, et al. Exergy performance of human body under physical activities. *Energy*. 2013;62(1):370–378.

20. Genc S, Sorguven E, Ozilgen M, Kurnaz IA. Unsteady exergy destruction of the neuron under dynamic stress conditions. *Energy*. 2013;59(1):422–431.

21. Genc S, Sorguven E, Kurnaz IA, Ozilgen M. Exergetic efficiency of ATP production in neuronal glucose metabolism. *International Journal of Exergy*. 2013;13(1):60–84.

22. Çatak J, Develi AÇ, Sorguven E, Özilgen M, İnal HS. Lifespan entropy generated by the masseter muscles during chewing: an indicator of the life expectancy? *International Journal of Exergy*, 2018;25(1):1-33.

23. Yalçınkaya BH, Erikli Ş, Özilgen BA, Olcay AB, Sorgüven E, Özilgen M. Thermodynamic analysis of the squid mantle muscles and giant axon during slow swimming and jet escape propulsion. *Energy*. 2016;102(1):537–549.

24. Semerciöz AS, Özilgen M, Yılmaz B. Entropy generation behavior of lean and obese rats when fed with butter fat or soybean oil diet. *International Journal of Exergy*, 2018;26(3):359-391

25. Shukuya M, Saito M, Isawa K, Iwamatsu T, Asada H. Human-body exergy balance and thermal comfort. *Report submitted for the final report of the IEA ECBCS Annex*. 2009:49(5):732-743.

26. Silva C, Annamalai K. Entropy generation and human aging: lifespan entropy and effect of physical activity level. *Entropy*. 2008;10(2):100–123.

27. Demirel Y, Sandler SI. Nonequilibrium thermodynamics in engineering and science. *The Journal of Physical Chemistry B*. 2004;108(1):31–43.

28. Schrodinger E, *What Is Life? the physical aspect of the living cell and mind*. Cambridge: Cambridge University Press, 1944.

29. Prigogine I. Dissipative structures in chemical systems. *Fast reactions and primary processes in chemical kinetics*. 1967;1(1)371–382.

30. Prigogine I, Wiame J-M. Biologie et thermodynamique des phénomènes irréversibles. *Experientia*. 1946;2(11):451–453.

31. Balmer RT. Entropy and aging in biological systems. *Chemical Engineering Communications*. 1982;17(6):171–181.

32. Von Stockar U, Liu J-S. Does microbial life always feed on negative entropy? Thermodynamic analysis of microbial growth. *Biochimica et Biophysica Acta (BBA)-Bioenergetics*. 1999;1412(3):191–211.

33. Matsushita S, Matsushita M, Itoh H, Hagiwara K, Takahashi R, Ozawa T, et al. Multiple pathology and tails of disability: space–time structure of disability in longevity. *Geriatrics & Gerontology International*. 2003;3(4):189–199.

34. Hayflick L. Entropy explains aging, genetic determinism explains longevity, and undefined terminology explains misunderstanding both. *PLoS Genetics*. 2007;3(12):2351-2354.

35. Salminen A, Kaarniranta K. Genetics vs. entropy: longevity factors suppress the NF-κB-driven entropic aging process. *Ageing Research Reviews*. 2010;9(3):298–314.

36. Casten TR, Schewe PF. Getting the Most from Energy: Recycling waste heat can keep carbon from going sky high. *American Scientist*. 2009;97(1):26–33.

37. Lewins J. Entropy pollution of the environment: a teaching approach to the Second Law. *International Journal of Mechanical Engineering Education*. 2011;39(1):60–67.

38. Yalçınkaya BH, Çatak J, Yılmaz B, Özilgen M. Mitochondrial Energy Conversion. *Comrehensive Energy Systems*. 2018:95-125.

39. Yalçınkaya BH, Çatak J, Yılmaz B, Özilgen M. Neuronal Energy Conversion. *Comprehensive Energy Systems*. 2018:638-672.

40. Gosline JM, DeMont ME. Jet-propelled swimming in squids. *Scientific American*. 1985;252(1):96–103.

41. Kier WM, Thompson JT. Muscle arrangement, function and specialization in recent coleoids. *Berliner Paläobiologische Abhandlungen*. 2003;3(1):141–162.

42. Young JZ. The functioning of the giant nerve fibres of the squid. *Journal of Experimental Biology*. 1938;15(2):170–185.

43. Finke E, Pörtner H-O, Lee PG, Webber DM. Squid (Lolliguncula brevis) life in shallow waters: oxygen limitation of metabolism and swimming performance. *The Journal of Experimental Biology*. 1996;199(4):911–921.

44. Moltschaniwskyj NA. Muscle tissue growth and muscle fibre dynamics in the tropical

loliginid squid Photololigo sp.(Cephalopoda: Loliginidae). *Canadian Journal of Fisheries and Aquatic Sciences*. 1994;51(4):8350–8355.

45. Bone Q, Pulsford A, Chubb AD. Squid mantle muscle. *Journal of the Marine Biological Association of the United Kingdom*. 1981;61(2):327–342.

46. Mommsen TP, Ballantyne J, MacDonald D, Gosline J, Hochachka PW. Analogues of red and white muscle in squid mantle. *Proceedings of the National Academy of Sciences*. 1981;78(5):3274–3278.

47. Bartol IK, Mann R, Patterson MR. Aerobic respiratory costs of swimming in the negatively buoyant brief squid Lolliguncula brevis. *Journal of Experimental Biology*. 2001;204(21):3639–653.

48. Drummond GI. Muscle metabolism. *Fortschritte der Zoologie*. 1967;18(3):359.

49. Hochachka PW. Oxygen efficient design of cephalopod muscle metabolism. *Marine and Freshwater Behaviour and Physiology*. 1995;25(3):61–67.

50. Portner HO, Finke E, Lee PG. Metabolic and energy correlates of intracellular pH in progressive fatigue of squid (L. brevis) mantle muscle. *American Journal of Physiology-Regulatory, Integrative and Comparative Physiology*. 1996;271(5):1403–1414.

51. Young JZ. The giant nerve fibres and epistellar body of cephalopods. *The Quarterly Journal of Microscopical Science*. 1936:78(1):367–86.

52. Albers RW, Siegel GJ. Basic Neurochemistry: Molecular, cellular and medical aspects. Philadelphia, PA: Lippincott Williams & Wilkins; 1999.

53. Magistretti PJ, Allaman I. Brain energy metabolism. *Neuroscience in the 21st Century*. Springer. 2013:1591–1620.

54. Aiello LC, Wheeler P. The expensive-tissue hypothesis: the brain and the digestive system in human and primate evolution. *Current Anthropology*. 1995;36(2):199–221.

55. Mitchison G. Axonal trees and cortical architecture. *Trends in Neurosciences*. 1992;15(4):122–126.

56. Koulakov AA, Chklovskii DB. Orientation preference patterns in mammalian visual cortex: a wire length minimization approach. *Neuron*. 2001:29(2):519–27.

57. Levy WB, Baxter RA. Energy efficient neural codes. *Neural Computation*. 1996;8(3):531–543.

58. Attwell D, Laughlin SB. An energy budget for signaling in the grey matter of the brain. *Journal of Cerebral Blood Flow & Metabolism*. 2001;21(10):1133–1145.

59. Lennie P. The cost of cortical computation. *Current Biology*. 2003;13(6):493–497.

60. Harris JJ, Jolivet R, Attwell D. Synaptic energy use and supply. *Neuron*. 2012;75(5):762–777.

61. Jolivet R, Allaman I, Pellerin L, Magistretti PJ, Weber B. Comment on recent modeling studies of astrocyte–neuron metabolic interactions. *Journal of Cerebral Blood Flow & Metabolism*. 2010;30(12):1982–1986.

62. Howarth C, Gleeson P, Attwell D. Updated energy budgets for neural computation in the neocortex and cerebellum. *Journal of Cerebral Blood Flow & Metabolism*. 2012;32(7):1222–1232.

63. Hodgkin AL, Huxley AF. Action potentials recorded from inside a nerve fibre. *Nature*. 1939;144(3651):710-711.

64. Hodgkin AL. Chance and design in electrophysiology: an informal account of certain experiments on nerve carried out between 1934 and 1952. *The Journal of Physiology*. 1976;263(1):1–21.

65. Brock LG, Coombs JS, Eccles JC. The recording of potentials from motoneurones with an intracellular electrode. *The Journal of Physiology*. 1952;117(4):431–460.

66. Tasaki I, Polley EH, Orrego F. Action potentials from individual elements in cat geniculate and striate cortex. *Journal of Neurophysiology*. 1954;17(5):454–474.

67. Phillips CG. Intracellular records from Betz cells in the cat. *Quarterly Journal of Experimental Physiology and Cognate Medical Sciences: Translation and Integration*. 1956;41(1):58–69.

68. Marmont G. Studies on the axon membrane. I. A new method. *Journal of Cellular and Comparative Physiology*. 1949;34(3):351–382.

69. Cole KS, Curtis HJ. Electric impedance of the squid giant axon during activity. *The Journal of General Physiology*. 1939;22(5):649–670.

70. Hodgkin AL, Huxley AF. A quantitative description of membrane current and its application to conduction and excitation in nerve. *The Journal of Physiology*. 1952;117(4):500–544.

71. Hodgkin AL, Katz B. The effect of sodium ions on the electrical activity of the giant axon of the squid. *The Journal of Physiology*. 1949;108(1):37–77.

72. Cole KS, Hodgkin AL. Membrane and protoplasm resistance in the squid giant axon. *The Journal of General Physiology*. 1939;22(5):671–687.

73. Hodgkin AL, Huxley AF, Katz B. Measurement of current-voltage relations in the membrane of the giant axon of Loligo. *The Journal of Physiology*. 1952;116(4):424–448.

74. Hodgkin AL, Huxley AF. Currents carried by sodium and potassium ions through the membrane of the giant axon of Loligo. *The Journal of Physiology*. 1952;116(4):449–472.

75. Hodgkin AL, Huxley AF. The dual effect of membrane potential on sodium conductance in the giant axon of Loligo. *The Journal of Physiology*. 1952;116(4):497–506.

76. Rall W. Membrane potential transients and membrane time constant of motoneurons. *Experimental Neurology*. 1960;2(5):503–532.

77. Rall W. Theory of physiological properties of dendrites. *Annals of the New York Academy of Sciences*. 1962;96(4):1071–1092.

78. Rall W. Theoretical significance of dendritic trees for neuronal input-output relations. *Neural Theory and Modeling*. 1969;73–97.

79. Rall W. Distinguishing theoretical synaptic potentials computed for different soma-

dendritic distributions of synaptic input. *Journal of Neurophysiology*, 1967;30(5): 1138-1168.

80. Rall W. Time constants and electrotonic length of membrane cylinders and neurons. *Biophysical Journal*. 1969;9(12):1483.

81. Rall W. Cable properties of dendrites and effects of synaptic location. *Excitatory synaptic mechanisms*. 1970;1:175–187.

82. Rall W. Core conductor theory and cable properties of neurons. *Comprehensive Physiology*. 2011;39-97.

83. Kameyama T, Asanoi H, Ishizaka S, Yamanishi K, Fujita M, Sasayama S. Energy conversion efficiency in human left ventricle. *Circulation*. 1992;85(3):988–96.

84. Dasi LP, Pekkan K, de Zelicourt D, Sundareswaran KS, Krishnankutty R, Delnido PJ, et al. Hemodynamic energy dissipation in the cardiovascular system: generalized theoretical analysis on disease states. *Annals of Biomedical Engineering*. 2009;37(4):661–73.

85. Gabr RE, El-Sharkawy A-MM, Schär M, Panjrath GS, Gerstenblith G, Weiss RG, et al. Cardiac work is related to creatine kinase energy supply in human heart failure: a cardiovascular magnetic resonance spectroscopy study. *Journal of Cardiovascular Magnetic Resonance*. 2018;20(1):81.

86. Muñoz-Diosdado A, Gálvez-Coyt G, Alonso Martínez A. Thermodynamic efficiency of the cardiac cycle and irreversibility in the interbeat interval time series. *Revista Mexicana de Ingeniería Biomédica*. 2010;31(2):103–10.

87. Henriques IB, Mady CEK, de Oliveira Junior S. Exergy model of the human heart. *Energy*. 2016;117(2):612-619.

88. Çatak J, Özilgen M, Olcay AB, Yılmaz B. Assessment of the work efficiency with exergy method in ageing muscles and healthy and enlarged hearts. *International Journal of Exergy*. 2018;25(1):1–33.

89. Alberty RA. Thermodynamics of biochemical reactions. New Jersey: John Wiley &

Sons; 2005.

90. Benson SW. III-Bond energies. *Journal of Chemical Education*. 1965;42(9):502.

91. Shieh JH, Fan LT. Estimation of energy (enthalpy) and exergy (availability) contents in structurally complicated materials. *Energy Sources*. 1982;6(1–2):1–46.

92. Szargut J, Morris DR, Steward FR. Exergy analysis of thermal, chemical, and metallurgical processes. New York: Hemisphere Publ. Corp, 1988.

93. Domalski ES, Hearing ED. Estimation of the thermodynamic properties of C-H-N-O-S-halogen compounds at 298.15 K. *Journal of Physical and Chemical Reference Data*. 1993;22(4):805–1159.

94. Marrero J, Gani R. Group-contribution based estimation of pure component properties. *Fluid Phase Equilibria*. 2001;183(1):183–208.

95. Gharagheizi F, Keshavarz MH, Ilani-Kashkouli P, Farahani N, Tumba K. A group contribution method for estimation of glass-transition temperature of 1, 3-dialkylimidazolium ionic liquids. *Journal of Thermal Analysis and Calorimetry*. 2013;114(3):1363–1382.

96. Lewandowski A, Jakobczyk P, Gnat M, Rudnicka E. Heat generated during electrochemical double-layer capacitor "self-discharge." *Journal of Applied Electrochemistry*. 2014;44(5):551–554.

97. Heinrich F. Entropy change when charging a capacitor: A demonstration experiment. *American Journal of Physics*. 1986;54(8):742–744.

98. Sengupta B, Stemmler M, Laughlin SB, Niven JE. Action potential energy efficiency varies among neuron types in vertebrates and invertebrates. *PLoS Computational Biology*. 2010:6(7):1-16.

99. Wang Y, Wang R, Xu X. Neural Energy Supply-Consumption Properties Based on Hodgkin-Huxley Model. *Neural Plasticity*. 2017;1(1)1-10.

100. Jansen MA, Shen H, Zhang L, Wolkowicz PE, Balschi JA. Energy requirements for the Na+ gradient in the oxygenated isolated heart: effect of changing the free energy

of ATP hydrolysis. *American Journal of Physiology-Heart and Circulatory Physiology*. 2003;285(6):2437–2445.

101. Rinzel J, Rall W. Transient response in a dendritic neuron model for current injected at one branch. *Biophysical Journal*. 1974;14(10):759.

102. Dodge FA, Cooley JW. Action potential of the motorneuron. *IBM Journal of Research and Development*. 1973;17(3):219–229.

103. Nitzan R, Segev I, Yarom Y. Voltage behavior along the irregular dendritic structure of morphologically and physiologically characterized vagal motoneurons in the guinea pig. *Journal of Neurophysiology*. 1990;63(2):333–346.

104. Bose S, French S, Evans FJ, Joubert F, Balaban RS. Metabolic network control of oxidative phosphorylation multiple roles of inorganic phosphate. *Journal of Biological Chemistry*. 2003;278(40):39155–39165.

105. Wu F, Yang F, Vinnakota KC, Beard DA. Computer modeling of mitochondrial tricarboxylic acid cycle, oxidative phosphorylation, metabolite transport, and electrophysiology. *Journal of Biological Chemistry*. 2007;282(34):24525–24537.

106. Blick EF, Stein PD. Work of the heart: A general thermodynamics analysis. *Journal of Biomechanics*. 1977;10(9):589–595.

107. Bartol IK, Patterson MR, Mann R. Swimming mechanics and behavior of the shallow-water brief squid Lolliguncula brevis. *Journal of Experimental Biology*. 2001;204(21):3655–3682.

108. Sorgüven E, Özilgen M. First and second law work production efficiency of a muscle cell. *International Journal of Exergy*. 2015;18(2):142-156

109. Holmes JW. Teaching from classic papers: Hill's model of muscle contraction. *Advances in Physiology Education*. 2006;0(2):67–72.

110. Reggiani C, Potma EJ, Bottinelli R, Canepari M, Pellegrino MA, Stienen GJM. Chemo-mechanical energy transduction in relation to myosin isoform composition in skeletal muscle fibres of the rat. *The Journal of Physiology*. 1997;502(2):449–640.

111. Gibbs CL, Chapman JB. Effects of stimulus conditions, temperature, and length on energy output of frog and toad sartorius. *American Journal of Physiology--Legacy Content*. 1974;227(4):964–791.

112. Smith NP, Barclay CJ, Loiselle DS. The efficiency of muscle contraction. *Progress in Biophysics and Molecular Biology*. 2005;88(1):1–58.

113. Moujahid A, d'Anjou A. Metabolic efficiency with fast spiking in the squid axon. *Frontiers in Computational Neuroscience*. 2012;6(95):1-8.

114. Lodish H, Zipursky SL. Molecular cell biology. *Biochemistry and Molecular Biology Education*. 2001;29(1):126–133.

115. Chapman JB. On the Reversibility of the Sodium Pump in Dialyzed Squid Axons: A Method for Determining the Free Energy of ATP Breakdown? *The Journal of General Physiology*. 1973;62(5):643.

116. Chapman JB, Johnson EA. The reversal potential for an electrogenic sodium pump: a method for determining the free energy of ATP breakdown? *The Journal of General Physiology*. 1978;72(3):403–408.

117. Moujahid A, d'Anjou A, Torrealdea FJ, Torrealdea F. Energy and information in Hodgkin-Huxley neurons. *Physical Review E*. 2011;83(3):31912.

118. Alberty RA. Standard transformed Gibbs energies of coenzyme A derivatives as functions of pH and ionic strength. *BiophysicalCchemistry*. 2003;104(1):327–334.

119. Lange AMT, Sissenwine MP. Squid resources of the Northwest Atlantic. *Advances in Assessment of World Cephalopod Resources*. 1983;21–54.

120. Fitzhugh R. Theoretical effect of temperature on threshold in the Hodgkin-Huxley nerve model. *The Journal of General Physiology*. 1966;49(5):989–1005.

121. Chandler WK, Meves H. Rate constants associated with changes in sodium conductance in axons perfused with sodium fluoride. *The Journal of Physiology*. 1970;211(3):679–705.

122. Andersen SSL, Jackson AD, Heimburg T. Towards a thermodynamic theory of nerve

pulse propagation. *Progress in Neurobiology*. 2009;88(2):104–113.

123. Berg JM, Tymoczko JL, Stryer L. Glycolysis and gluconeogenesis. *Biochemistry 5*. 2002:429-489.

124. Tsien RW, Noble D. A transition state theory approach to the kinetics of conductance changes in excitable membranes. *The Journal of Membrane Biology*. 1969;1(1):248–273.

125. Forrest MD. Can the Thermodynamic Hodgkin-Huxley Model of Voltage-Dependent Conductance Extrapolate for Temperature? *Computation*. 2014;2(2):47–60.

126. Frankenhaeuser B, Moore LE. The effect of temperature on the sodium and potassium permeability changes in myelinated nerve fibres of Xenopus laevis. *The Journal of Physiology*. 1963;169(2):431–437.

127. Daniels Alberty, Robert A F. Physical Chemistry. 4th ed. New Jersey: John Willey & Sons; 1975.

128. Creighton TE. Proteins: structures and molecular properties. New York: W. H. Freeman; 1993.

129. Alberts B. Molecular biology of the cell. New York: Garland science; 2017.

130. Stryer L. Biochemistry. New York: W.H. Freeman and Company; 1981.

131. Fetter AL, Walecka JD. Quantum theory of many-particle systems. New York: Courier Corporation; 2003.

132. Lara VOM, Lima AP, Costa A. Entropic considerations in the two-capacitor problem. *Revista Brasileira de Ensino de Física*. 2015;37(1):1306.

133. Sommerfeld A, Frank NH. The Statistical theory of thermoelectric, galvano-and thermomagnetic phenomena in metals. *Reviews of Modern Physics*. 1931;3(1):1-2.

134. Yi G, Wang J, Wei X, Deng B. Dendritic properties control energy efficiency of action potentials in Cortical pyramidal cells. *Frontiers in Cellular Neuroscience*. 2017;11:265.

135. Carter BC, Bean BP. Sodium entry during action potentials of mammalian neurons: incomplete inactivation and reduced metabolic efficiency in fast-spiking neurons. *Neuron*. 2009;64(6):898–909.

136. Glenn LL, Samojla BG, Whitney JF. Electrotonic parameters of cat spinal α-motoneurons evaluated with an equivalent cylinder model that incorporates non-uniform membrane resistivity. *Brain Research*. 1987;435(1–2):398–402.

137. Brown TH, Fricke RA, Perkel DH. Passive electrical constants in three classes of hippocampal neurons. *Journal of Neurophysiology*. 1981;46(4):812–27.

138. Glenn LL. Overestimation of the electrical length of neuron dendrites and synaptic electrotonic attenuation. *Neuroscience Letters*. 1988;91(1):112–9.

139. Jeneson JA, Westerhoff H V, Brown TR, Van Echteld CJ, Berger R. Quasi-linear relationship between Gibbs free energy of ATP hydrolysis and power output in human forearm muscle. *American Journal of Physiology-Cell Physiology*. 1995;268(6):1474–1484.

140. Weil B. Pig Simultaneous Bi-Ventricular Acute Pressure-Volume Measurement (Closed Chest Approach). In: Transonic, editor. The State University of NY: Institutional Animal Care and Use Committee of the University of Buffalo.

141. Lin H, Freed D, Lee TWR, Arora RC, Ali A, Almoustadi W, et al. Quantitative assessment of cardiac output and left ventricular function by noninvasive phase-contrast and cine MRI: Validation study with invasive pressure-volume loop analysis in a swine model. *Journal of Magnetic Resonance Imaging*. 2011;34(1):203–210.

142. Périard JD, Travers GJS, Racinais S, Sawka MN. Cardiovascular adaptations supporting human exercise-heat acclimation. *Autonomic Neuroscience*. 2016;196(2):52–62.

143. Edwards RH, Hill DK, Jones DA. Heat production and chemical changes during isometric contractions of the human quadriceps muscle. *The Journal of Physiology*. 1975;251(2):303–315.

144. González-Alonso J, Quistorff B, Krustrup P, Bangsbo J, Saltin B. Heat production in

human skeletal muscle at the onset of intense dynamic exercise. *The Journal of Physiology*. 2000;524(2):603–615.

145. Bangsbo J, Krustrup P, González-Alonso J, Saltin B. ATP production and efficiency of human skeletal muscle during intense exercise: effect of previous exercise. *American Journal of Physiology-Endocrinology and Metabolism*. 2001;280(6):956–964.

146. González-Alonso J. Human thermoregulation and the cardiovascular system. *Experimental Physiology*. 2012;97(3):340–346.

147. Krustrup P, González-Alonso J, Quistorff B, Bangsbo J. Muscle heat production and anaerobic energy turnover during repeated intense dynamic exercise in humans. *The Journal of Physiology*. 2001;536(3):947–956.

148. Krustrup P, Ferguson RA, Kjær M, Bangsbo J. ATP and heat production in human skeletal muscle during dynamic exercise: higher efficiency of anaerobic than aerobic ATP resynthesis. *The Journal of Physiology*. 2003;549(1):255–269.

149. Hall JE, Guyton AC. Guyton and Hall Textbook of medical physiology. 13th ed. Philadelphia: Elsevier; 2016.

150. Ten Velden GH, Elzinga G, Westerhof N. Left ventricular energetics. Heat loss and temperature distribution of canine myocardium. *Circulation Research*. 1982;50(1):63–73.

151. Torio H, Angelotti A, Schmidt D. Exergy analysis of renewable energy-based climatisation systems for buildings: A critical view. *Energy and Buildings*. 2009;41(3):248–271.

152. Stougie L, van der Kooi HJ. Possibilities and consequences of the total cumulative exergy loss method in improving the sustainability of power generation. *Energy Conversion and Management*. 2016;107:60–66.

153. Morosuk T, Tsatsaronis G. A new approach to the exergy analysis of absorption refrigeration machines. *Energy*. 2008;33(6):890–907.

APPENDIX A: THERMODYNAMIC ANALYSIS OF METABOLITES IN SQUID MANTLE MUSCLE CELL

Table A.1. Concentrations and thermodynamical properties of the metabolites under the physiological conditions (i.e. I=0.25M, T=298.15 K, and pH=7) in the squid mantle muscles.

Metabolite	Concentration (mM)	Δh (kJ/mol)	Δg (kJ/mol)	Ex_{ch} (kJ/mol)	RTln(c) (kJ/mol)	*Ex* (kJ/mol)
Glu	0.012	-1267.12	-426.71	2473.47	-10.96	2035.80
G6P	0.100	-2279.30	-1318.92	3343.03	-5.71	2018.40
ATP	0.360	-3616.92	-2292.50	6720.93	-2.53	4425.90
ADP	0.170	-2627.24	-1424.70	5851.38	-4.39	4422.29
NAD	0.0001	-41.83	1120.09	10372.87	-22.83	11470.13
NADH	0.00001	-10.26	1059.11	10372.87	-28.54	11403.44
P_i	1.890	-1299.36	-1059.49	871.54	1.58	-186.37
H_2O	1.000	-286.75	-155.66	1.99	0.00	-153.67
PYR	0.00001	-597.04	-350.79	1236.74	-28.54	857.41
ARG	29.370	-277.38	25.20	2466.91	8.38	2500.49
OCT	0.430	-608.52	-272.85	3701.63	-2.09	3426.69
SUC	0.065	-908.70	-530.64	1648.94	-6.78	1111.52
CO_2	0.026	-692.86	-547.10	414.32	-9.05	-141.83
O_2	0.960	-11.70	16.40	3.97	-0.10	20.27

Table A.2. Dimensions of mantle cavity at different swimming modes (adapted from Thompson et al. 2008).

	At rest	During slow swimming	During jet escape
DML (dorsal mantle length in mm)	150	150	150
r_i (initial mantle cavity radius in mm)	25	25	25
r_f (final mantle cavity radius in mm)	-	23.75	18.75
t_i (initial mantle wall thickness in mm)	3.5	3.5	3.5
t_f (final mantle wall thickness in mm)	-	3.71	5

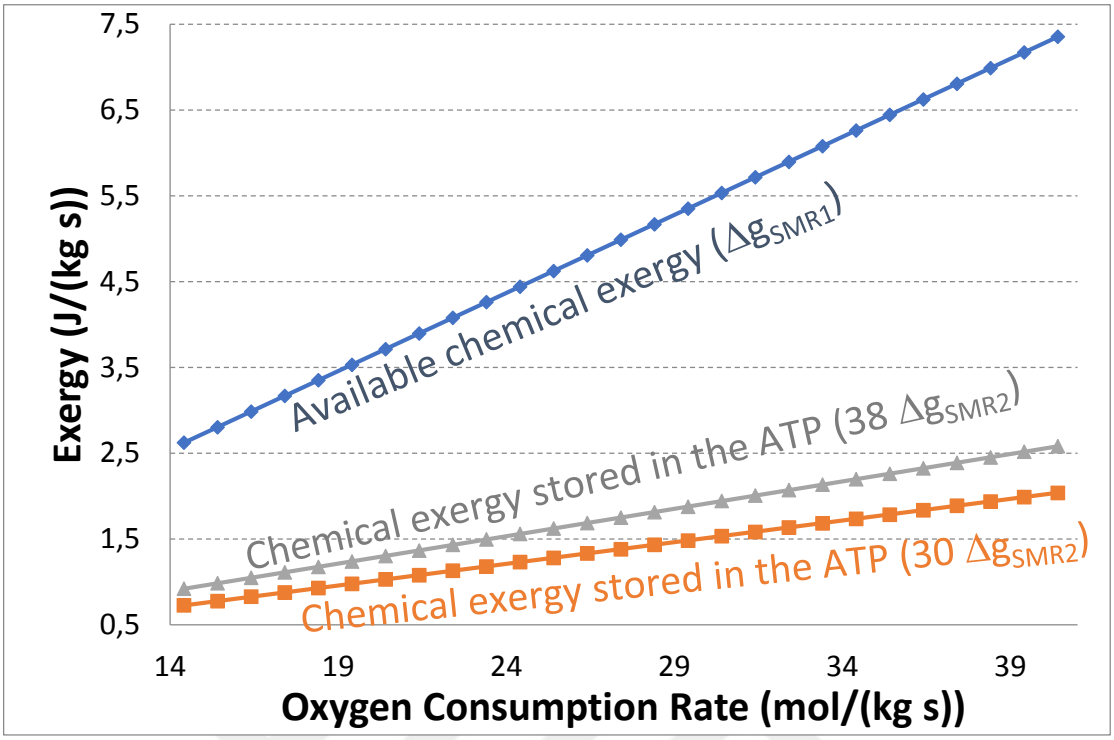

Figure A.1. Variation of the Δg_{rxn} of the reactions SMR1 and SMR2 depending on the oxygen consumption rate.

APPENDIX B: THERMODYNAMIC ANALYSIS OF METABOLITES IN SQUID NEURON CELL

Table B.1. Thermodynamic properties of the metabolites at 6.3, 12.0 and 18.5 ^{0}C when I=0.25 M and pH=7.

Molecule	ΔG (kJ/mol)			Ex_{total} (kJ/mol)		
	6.3 ºC	12.0 ºC	18.5 ºC	6.3 ºC	12.0 ºC	18.5 ºC
Glu	-479.38	-463.34	-445.03	1983.71	1999.64	2071.72
O_2	14.64	15.17	15.79	18.61	19.14	19.76
H_20	-163.87	-161.37	-158.51	-177.93	-175.76	-173.27
CO_2	-556.25	-553.46	-550.28	-150.50	-147.88	-144.90
ADP	-1500.11	-1477.13	-1450.92	4352.57	4375.58	4401.82
ATP	-2375.57	-2350.25	-2321.37	4348.93	4374.32	4403.28
Pi	-1074.55	-1069.95	-1064.72	-198.47	-193.77	-188.44

Table B.2. Cable parameters for cat spinal motoneuron, cat motoneuron, guinea pig vogal motoneuron, and squid giant axon.

		Representative values				
Parameters	Symbols	Units	Cat spinal motoneuron	Cat motoneuron	Guinea pig vogal motoneuron	Squid giant axon
Membrane resistivity	R_m	Ω/cm^2	2500	6000	5250	1000
Neuron input resistance	R_n	MΩ	1.5	1	67	5
Intracellular resisitivity	R_i	Ωcm	70	100	70	30
Membrane capacitance	C_m	μF/cm^2	2	1	1.8	1
Diameters of membrane cylinder	d	μm	251	-(assumed same as cat spinal motoneuron)	251	500
Dimensionless conductance ratio	rho		10	10	10	10

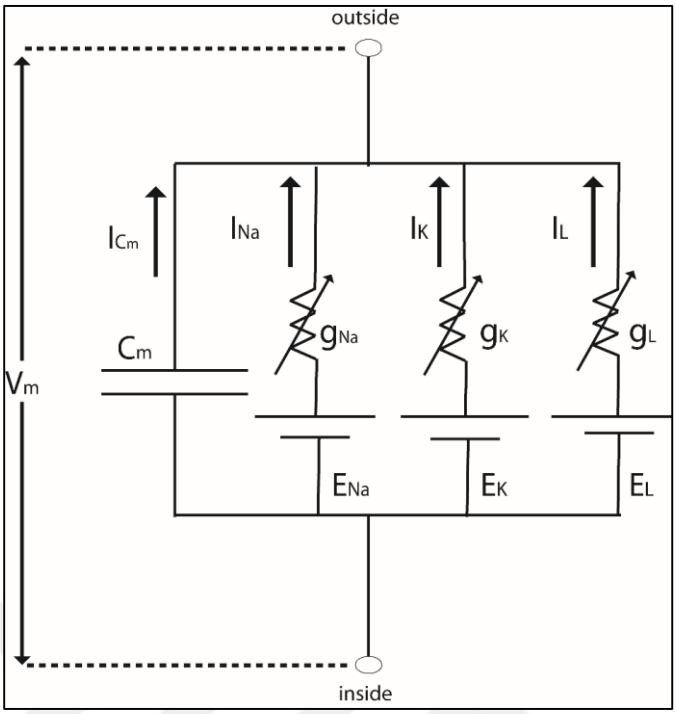

Figure B.1. Equivalent electrical circuit description of the axonal membrane in the Hodgkin-Huxley model. Neuron axonal membrane shows an analogy with an electrical circuit of constant capacitance C_m and parallel conductance elements (g_{Na}, g_K, g_{Cl}).

APPENDIX C: THERMODYNAMIC ANALYSIS OF PIG CARDIAC MUSCLE

Table C.1. Thermodynamic properties of the metabolites at T=37^{0}C, I=0.14 M, and pH=7 at rest.

Metabolites	ΔH (kJ/mol)	ΔG (kJ/mol)	Ex_ch (kJ/mol)	RTln_C (kJ/mol)		Ex_ch+ RTln_C + ΔG (kJ/mol)	
				T=0s	T=30s	T=0s	T=30s
CO2	-692.25	-543.72	414.23	-27.74	-27.74	-157.23	-157.23
COASH	-0.20	-4.59	11850.04	-33.72	-33.18	11811.73	11812.27
NAD	-8.65	1140.48	10372.87	-36.52	-39.65	11476.83	11473.70
NADH	-39.89	1204.85	10372.87	-53.47	-37.43	11524.25	11540.29
PYR	-596.91	-341.32	1236.74	-53.47	-62.44	841.95	832.98
SCOA	-1.04	-334.88	13497	-35.90	-37.92	13126.22	13124.20
ACCOA	-1.04	-48.68	12672.5	-65.08	-53.47	12558.74	12570.35
CIT	-1513.82	-949.79	2475.46	-53.76	-52.57	1471.91	1473.10
ICIT	1.35	-943.14	2475.46	-59.70	-62.53	1472.62	1469.79
OAA	0.87	-708.40	1650.97	-66.51	-61.97	876.06	880.60
AKG	0.00	-620.74	2061.23	-62.55	-47.43	1377.94	1393.06
GDP	-2627.26	-1386.14	5851.38	-31.49	-32.52	4433.75	4432.72
GTP	-3617.35	-2253.27	6720.93	-57.53	-34.37	4410.13	4433.29
Pi	-1298.71	-1055.47	871.54	-52.25	-35.91	-236.18	-219.84
SUC	-908.69	-517.78	1648.98	-57.82	-34.85	1073.38	1096.35
COQ	-31.12	3950.32	22734.82	-29.03	-31.64	26656.11	26653.50
FUM	-776.70	-516.99	1648.98	-51.36	-31.64	1080.63	1100.35
QH2	-31.81	3948.18	22734.82	-60.06	-36.04	26622.93	26646.95
MAL	-2245.67	-669.99	1650.97	-56.06	-30.19	924.92	950.79
ADP	-2627.26	-1386.14	5851.38	-29.70	-30.73	4435.54	4434.51
ATP	-3617.35	-2253.27	6720.93	-38.38	-32.58	4429.28	4435.08
ASP	-945.14	-433.25	1783.55	-41.02	-47.90	1309.28	1302.40
GLU	-982.31	-347.06	2653.41	-31.20	-32.03	2275.15	2274.32
Cred	1.38	-27.41	16352.69	-47.50	-36.97	16277.78	16288.31
Cox	3.11	-6.52	16352.69	-33.39	-34.11	16312.79	16312.06
GLC	-1266.34	-389.19	2473.47	-53.47	-53.47	2030.81	2030.81
G6P	-2278.85	-1277.03	3343.03	-71.29	-70.95	1994.71	1995.05
H2O (aq)	-191.86	-149.41	1.99	-41.58	-41.58	-189.00	-189.00
O2	-11.7	17.53	3.97	-42.70	-42.70	-21.20	-21.20

Table C.2. Thermodynamic properties of the reactions at T=37^{0}C, I=0.14 M, and pH=7.

Enzyme	Reactions	Δh_{rxn} (kJ/mol)	Δg_{rxn} (kJ/mol)	Ex_in (kJ/mol)	Ex_final (kJ/mol)
hexokinase	$Glu_c + ATP_c \rightarrow G6P_c + ADP_c + H_c$	-22.42	-20.71	20.73	38.19
Pyruvate dehydrogenase	$PYR_x + CoA_x + NAD_x \rightarrow ACoA_x + NADH_x + CO_{2x} + H_x$	-127.42	-182.12	204.74	165.53
Citrate synthase	$ACoA_x + OAA_x + H_20_x \rightarrow CIT_x + CoA_x + 2H_x$	-1321.99	-47.89	-37.83	-23.42
Acotinase	$CIT_x \rightarrow ISOCIT_x$	1515.17	6.65	-0.71	3.30
Isocitrate dehydrogenase	$ISOCIT_x + NAD_x + H_20_x \rightarrow \alpha KG_x + CO_{2x} + NADH_x + 2H_x$	-532.98	-7.54	15.47	-21.63
α-ketoglutarate dehydrogenase	$\alpha KG_x + CoA_x + NAD_x \rightarrow SCoA_x + CO_{2x} + NADH_x + H_x$	-724.33	-188.90	173.25	171.77
Succinyl-CoA synthetase	$SCoA_x + GDP_x + Pi_x \rightarrow SUC_x + CoA_x + GTP_x$	-599.23	0.85	28.55	-4.83
Succinate Deydrogenase	$SUC_x + COQ_x \rightarrow FUM_x + QH_{2x}$	131.30	-1.35	25.93	2.55
Fumarase	$FUM_x + H_2O_x \rightarrow MAL_x$	-1277.11	-3.59	-33.30	-39.44
Malate dehydrogenase	$MAL_x + NAD_x \rightarrow OAA_x + NADH_x + H_x$	2215.30	25.96	1.43	3.60
Glutamate oxaloacetate transaminase	$ASP_x + AKG_x \rightarrow OAA_x + GLU_x$	-27.65	-1762.69	9634.89	9621.18
Adenine nucleotide translocase	$ATP_x + ADP_i \rightarrow ATP_i + ADP_x$	0.00	0.00	9.12	0.00
Complex I	$NADH_x + COQ_x + 5H_x \rightarrow NAD_x + QH2_x + H_i$	30.55	-66.51	80.61	73.13
Complex III	$QH2_x + 2Cox_i + 2H_x \rightarrow COQ_x + 2Cred_i + 4H\_i$	-2.77	-39.64	36.83	40.96
Complex IV	$2Credi + 0.5\ O2x + 4H_x \rightarrow 2Cox_x + 2H_i + H2O$	-182.55	-116.40	108.40	130.90
F1F0-ATPase	$ADP_x + Pi_x + H_x + 3H_i \rightarrow ATP_x + H2O_x + 3H_x$	116.76	38.93	-40.92	-31.40
Overall TCA	$PYR + 4NAD + COQ + ADP + Pi + 5H2O \rightarrow 4NADH + QH2 + ATP + 3CO2 + 4H$	-212.61	-356.59	35480.77	35339.43